2021

CARBON CAPTURE AND UTILIZATION

Sriram Valluri
Michigan Technological University, skvallur@mtu.edu

https://doi.org/10.37099/mtu.dc.etdr/1227

CARBON CAPTURE AND UTILIZATION

By

Sriram Kumar Valluri

A DISSERTATION

Submitted in partial fulfillment of the requirements for the degree of

DOCTOR OF PHILOSOPHY

In Chemical Engineering

MICHIGAN TECHNOLOGICAL UNIVERSITY

2021

This dissertation has been approved in partial fulfillment of the requirements for the Degree of DOCTOR OF PHILOSOPHY in Chemical Engineering.

Department of Chemical Engineering

Dissertation Co-Advisor:	*Dr. S. Komar Kawatra*
Dissertation Co-Advisor:	*Dr. Timothy C. Eisele*
Committee Member:	*Dr. Tony N. Rogers*
Committee Member:	*Dr. Stephen A. Hackney*
Department Chair:	*Dr. Pradeep K. Agrawal*

Table of Contents

List of Figures:

List of Tables:

Preface

“Use of frothers to improve the absorption efficiency of dilute sodium carbonate slurry for post combustion CO_2 capture” was published in the journal *Fuel Processing Technology* in 2020. This article was slightly modified and used as Chapter 2. The first author performed all experiments and wrote the article. The second author aided in data interpretation and writing review.

“Simultaneous removal of CO_2, NOx and SOx using single stage absorption column” was published in the *Journal of Environmental Sciences* in 2021. This article was slightly modified and used as Chapter 3. The first author performed all experiments and wrote the article. The second author aided in data interpretation and writing review.

“Reduced reagent regeneration energy for CO_2 capture with bipolar membrane electrodialysis” was published in the journal *Fuel Processing Technology* in 2021. This article was slightly modified and used as Chapter 4. The first author performed all experiments and wrote the article. The second author aided in data interpretation and writing review.

Acknowledgements

I would like to acknowledge my advisor, Dr. S. Komar Kawatra for his patience and continued support for the last four years.

I would like to thank my Committee members for timely feedback and support. Also, I'd like to thank my family and friends for their unwavering support during my graduate studies. I would like to thank Sam Root for his help in conducting experiments for my research work. I would also like to extend my thanks to our machinists Jerry Norkol and Steve Wisniewski for their active support in building the experimental equipment required for my research.

I. Abstract

As the world moves towards clean energy initiative, carbon capture and utilization technologies are key to achieving net zero emissions. CO_2 capture with amines has many disadvantages and cannot be applied to commercial power plants. The current manuscript will address this issue as well as a solution that involves the use of low-cost alkali absorbent CO_2 capture solutions, combined with an electrochemical regeneration method that uses the least amount of energy available for capture and regeneration. This research will also further address the issue of how to deal with the captured CO_2. Several viable storage and utilization methods have been explored, as well as their technological readiness level.

The first chapter will introduce the subject and present various CO_2 utilization ideas. The second chapter will cover a novel topic: adding surfactants to improve the absorption performance of a low-cost sodium carbonate solution. The third chapter will focus on capturing NOx, SOx, and CO_2 using a single absorption column. In Chapter 4, we will look at how to reduce the reagent regeneration energy from 4MJ/Kg to 1.18MJ/Kg by switching from thermal regeneration to electrolysis. Chapter 5 will discuss an electrochemical approach for converting the capture CO_2 to Oxalic acid. Finally, in Chapter 5, we will present pilot scale experimental studies of CO_2 capture using our absorption columns at the MTU steam plant.

1. Opportunities and Challenges in CO_2 Utilization

1.1 Abstract

CO_2 utilizations are essential to curbing the greenhouse gas effect and managing the environmental pollutant in an energy-efficient and economically-sound manner. There have been several review papers on CO_2 utilization technologies including electrochemical reduction of CO_2, CO_2 enhanced oil recovery, mineral carbonation, and so on. However, there has not yet been a comprehensive overarching review of all of these technologies. This paper seeks to critically analyze these technologies in the context of each other, and highlight the most important utilization avenues available thus far. This review will introduce and analyze each major pathway, and discuss the overall applicability, potential extent, and major limitations of each of these pathways to utilizing CO_2. This will include the analysis of some previously underreported utilization avenues, including CO_2 utilization in industrial filtration and the processing of raw industrial materials such as iron and alumina. The core theme of this paper is to seek to treat CO_2 as a commodity instead of a liability.

1.2 Introduction

As carbon dioxide emissions rise, CO_2 capture and utilization technologies have been deemed necessary to reduce pollution and mitigate global warming (Edenhoffer, 2015). While the effects of global warming on Earth may never be as extreme as on, for example, Venus, there is little doubt that there will be drastic impacts on society and human wellbeing unless actions are taken to avoid that outcome. By current estimates, to achieve a 2 in 3 chance of limiting global temperature increase to less than 2°C by 2100 the emission of CO_2 must be decreased to less than 5GtCO_2/year before 2050. For comparison, present emissions total 48GtCO_2/yr (Rogelj, et al., 2016). Figure 1 shows the relative magnitudes of the sources and sinks of carbon dioxide on the Earth's surface.

The goal of CO_2 capture technology is to provide a method of isolating CO_2 and reducing its emissions to the environment. The methods of CO_2 capture have already been well-reviewed and we direct interested readers to (Spigarelli & Kawatra, 2013). A brief overview of these CO_2 capture technologies is provided in Figure 2. The ideal long-term goal of such emissions reduction is to reach net negative emissions, where human activities balance out or are result in the net removal of CO_2 from the atmosphere.

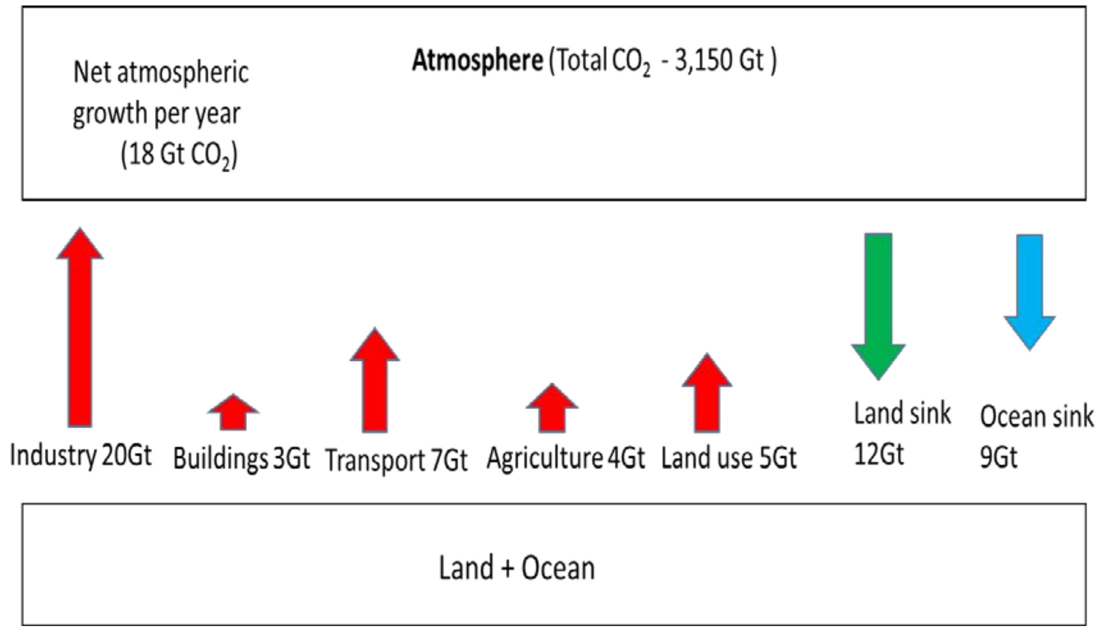

Figure 1: Annual CO_2 sources and sinks around Earth's atmosphere, in gigatons (Gt) (Hepburn, et al., 2019).

CO_2 utilization seeks to make this an economic and viable prospect by putting the CO_2 to work in stable and valuable tasks. Several avenues of CO_2 utilization are under investigation, including the transformation of CO_2 into valuable chemicals, high energy fuels, or directly into a plethora of working conditions. This paper will divide these into two major groupings: direct and indirect utilization.

Direct utilization uses the CO_2 as-is, without chemical conversion to other products. Widespread direct uses of CO_2 include use in food and beverages, fire extinguishers, concrete building materials, and CO_2 enhanced oil recovery.

Indirect utilization uses the CO_2 as a feedstock in creating a more complex final product. Indirect utilization techniques primarily include the conversion of CO_2 to useful chemicals or fuels. The conversion of CO_2 to high energy density fuels is an attractive option to meeting the energy storage demands facing renewable energy.

The major challenge associated with utilizing CO_2 from waste streams is the cost of capturing it from those streams as opposed to acquiring CO_2 from natural sources. Large amounts CO_2 can be obtained directly from natural gas reservoirs and industrial emissions, but in many cases the former has an economic advantage over the latter. However, CO_2 sourced from natural underground sources does not help reduce CO_2 emissions – rather, the CO_2 that is obtained from underground for these purposes is almost certain to end up, at least in part, as additional emissions. Currently, roughly 45 million metric tons of CO_2 per year are sourced from natural wells for use in enhanced oil recovery projects (Wilcox, 2012).

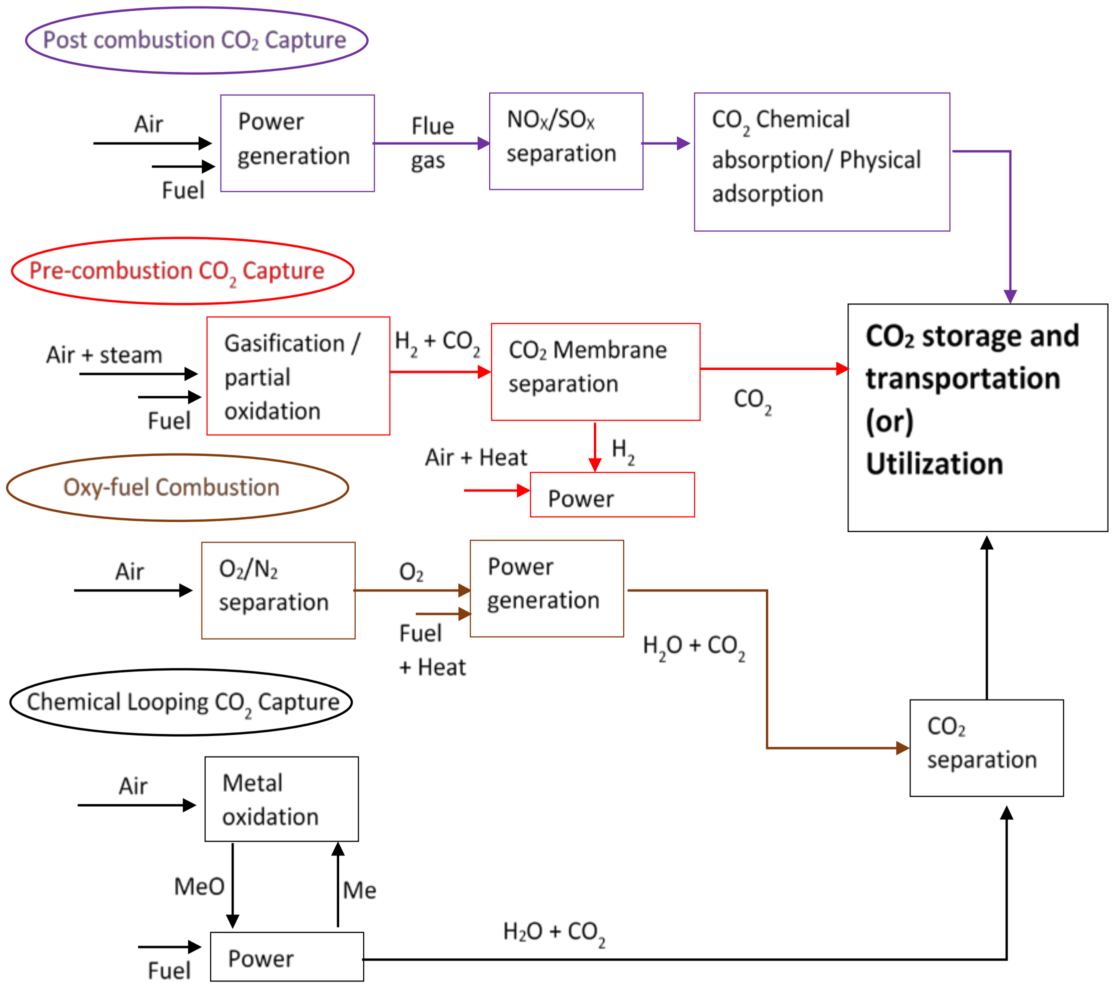

Figure 2: Integrated flow diagram of various CO_2 capture technologies available at the present time

(Spigarelli & Kawatra, 2013).

However, fossil fuels still represent a significant portion of power generation to date. The amount of CO_2 generated from these endeavors is considerable, and if it can be efficiently captured it can be used to replace some or all of those 45 million metric tons per year from natural sources. Figure 3 shows the expected fraction of power generation in the U.S. up to 2050, and fossil fuels are expected to maintain over 50% of the footprint of these activities through that point (EIA, 2020).

The main theme of this paper and the goal of CO_2 utilization in general are to show that **CO_2 should be treated as a commodity instead of a liability**. With the appropriate care and effort, the environmental responsible treatment of CO_2 can also be made to be economically viable.

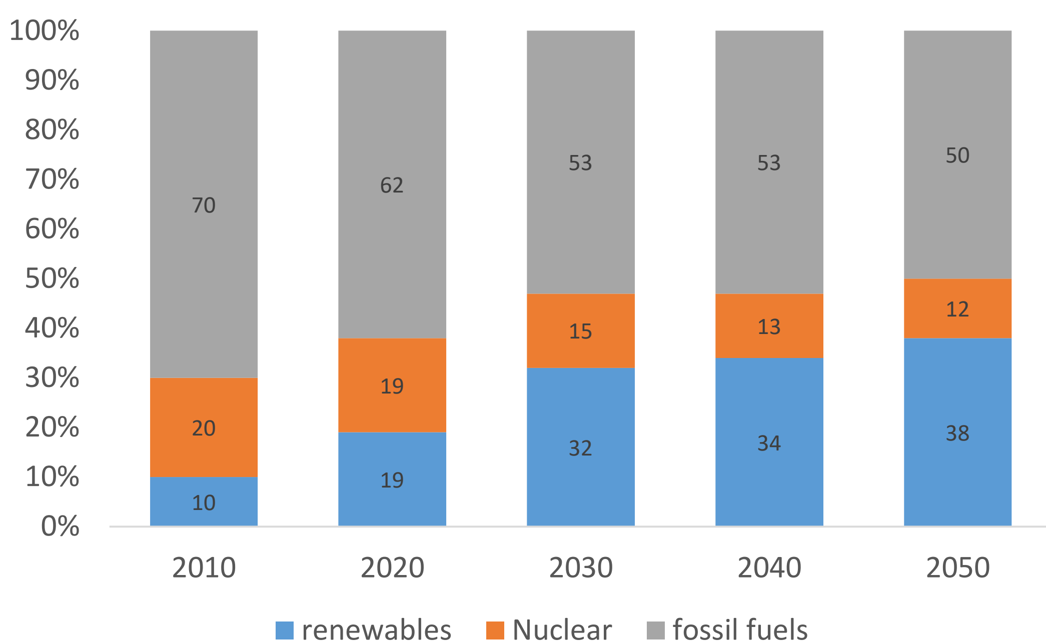

Figure 3: Fossil fuel usage trends as percentage contribution of different sources for energy production (EIA, 2020).

With regards to human sources of CO_2 emissions, the largest sectors are transportation and power generation. Unfortunately, capturing CO_2 from a typical transportation source is impractical with current technology, though research is continuing on that front. With current technology, the primary focus for capture should be on large stationary sources, such as fossil fuel power generation plants, steel plants, chemical plants, and so on. The most mature and widely used capture technology is post-combustion capture via chemical adsorption processes utilizing amines and other alkaline compounds. The primary challenge facing CO_2 capture in general is the necessity to compete with natural sources of CO_2 so that the ultimate goal of reducing CO_2 emissions is met with a commercial advantage. For post-combustion capture, the major costs are associated with regenerating the capture solution (roughly 70% of the total capture cost) and the initial costs of the reagent (roughly 10% of the total capture cost) (Knuutila, Svendsen, & Antilla, 2009). With recent advances of technology, reagent costs can be brought down by switching from amines to sodium carbonate solution (approximately 80% less expensive) enhanced with surfactants (Valluri & Kawatra, 2019).

Currently the cost of post-combustion capture is $52/ton, due largely to the energy required for regeneration (Rochelle, 2009). For comparison, natural sources are roughly $20-22/ton (Naims, 2016), so for post-combustion capture to be competitive there is still work to be done. One option for increasing the favorability of CO_2 capture is a carbon tax, wherein a tax is established on the emission of CO_2 and in turn requiring its capture and subsequent sequestration or utilization. Another option for post-combustion capture specifically, is investigate alternative regeneration routes. For sodium carbonate solutions, electrodialysis with bipolar membranes to generate acid for regenerating the capture solution may be practical. Theoretically, the regeneration energy for amine systems with thermal regeneration is around 4MJ/kg of CO_2, while the energy cost of the EDBM cycle could be as low as 2.1MJ/kg of CO_2 (Nagasawa, Yamasaki, Iizuka, Kumagai, & Yanagisawa, 2009; Eisaman, Alvarado, Larner, Wang, Garg, & Littau, 2011). Another potential process improvement is utilizing frothers to improve absorption rate for less expensive absorbents, such as sodium carbonate (Valluri and Kawatra, 2021a). Similarly, it may be possible to further reduce capture costs by combining the units for capturing CO_2, NO, and SO_2, as all of them can be captured using very similar equipment. Combined capture utilizing oxidizers such as sodium hypochlorite and hydrogen peroxide were effective in capturing a large fraction of NO and SO_2 while simultaneously improving CO_2 capture performance (Valluri and Kawatra, 2020).

With such process improvements, it should be possible to decrease post-combustion capture costs from \$52/ton to \$25-30/ton by 2030 (Valluri and Kawatra, 2021b). Assuming optimistic government policies, including carbon abatement costs and carbon tax, the cost that power plants are expect to have to pay for CO_2 emissions is roughly \$25/ton in 2020 and rising to about \$54/ton in 2030, as per (Luckow, et al., 2015). At such rates, it will become economically beneficial for power plants to capture CO_2 and sell it at a price competitive to natural sources rather than emitting it into the atmosphere. However, even at that point to reach net negative emissions in the whole atmosphere direct air capture will also need to be implemented.

1.3 Physical and Chemical Properties of CO_2

A clear understanding of CO_2's basic physical and chemical properties is vital to understanding and designing efficient utilization processes. As one example, it is important to understand that supercritical CO_2 has properties that allow it to be an excellent working fluid and solvent for many processes. This comes from the relatively accessible critical point of CO_2, allowing for relatively easy implementation of trans-critical processes. Supercritical CO_2 as such can be used for various applications, such as in power generation (as a working fluid), as a dyeing agent (as a clean solvent), and for food-safe chemical extractions (as a food-safe solvent).

It is also important to acknowledge the relative chemical stability of CO_2. Essentially all reactions involving CO_2 are some manner of reduction reaction, and require overcoming the highly negative enthalpy of formation of CO_2. Thus, efficient chemical processing of CO_2 is greatly assisted by the careful design and utilization of catalysts to ensure high selectivity and reaction efficiencies.

1.3.1 Physical Properties

CO_2 is a colorless and odorless gas at ambient temperature and pressure conditions. It absorbs infrared light near 15µm which results in its greenhouse gas potential, as these wavelengths have significant overlap with the radiative emissions from the Earth's surface. The triple point of CO_2 is -56.35°C and 5.1bar, and the critical point of CO_2 is 31.1°C and 73.8bar (Cabeza, de Gracia, Fernández, & Farid, 2017). Figure 4 presents this phase information graphically.

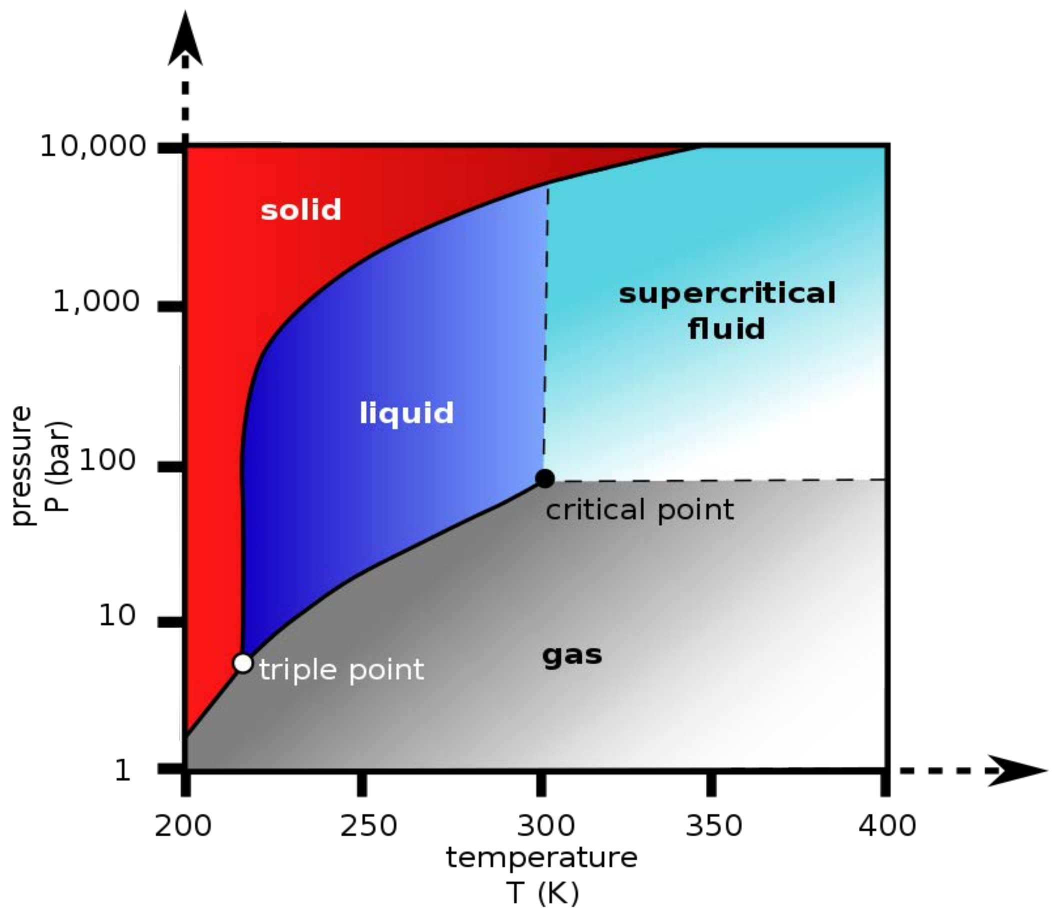

Figure 4: CO_2 Pressure-Temperature phase diagram.

The generally accessible critical point of CO_2 is particularly interesting, as it allows for the design of transcritical cycles at relatively modest working conditions. While this property is not strictly unique to CO_2, it is perhaps the most abundant material with a critical point so close to standard temperature and pressure.

It is also worth noting that CO_2 is soluble in water, and in that condition exists in equilibrium with carbonic acid. Since CO_2 is readily reduced, because it is capable of receiving an electron, and interacts with water as such, it is also known as an acid gas. It can be used as an inexpensive weak acid in most processes requiring pH control.

CO_2's widespread natural occurrence also makes its relative lack of acute toxicity in everyday quantities quite evident. While it poses an asphyxiation hazard if it displaces a significant amount of oxygen, it is largely harmless otherwise. Its supercritical and liquid phases are one of the most versatile food-safe aprotic solvents, and it is often used for pH control in food processing. There are concerns that the increasing atmospheric concentration of CO_2 has negative implications for human health in the long term, however.

1.4 CO_2 Utilization

There are several extant direct utilizations of CO_2, including in soft drinks, with foaming agents, in fire extinguishers, and as propellants. Some direct utilization methods, including CO_2 enhanced oil recovery and mineral carbonation inherently lend themselves to permanent storage of the CO_2 and proceed towards the goal of net negative emissions.

The alternative to direct utilization is to transform the CO_2 into something that is more useful overall. This is indirect utilization, such as electrochemical conversion, and is typically not expected to directly remove CO_2 from the atmosphere. The goal of indirect utilization is to establish a sort of anthropogenic carbon cycle, wherein CO_2 can be converted to useful chemicals which will in all likelihood eventually become CO_2 again. This CO_2 can be captured once more and transformed back into useful chemicals, without introducing new CO_2 into the atmosphere.

When discussing utilization as a whole, it is important to acknowledge that the conventional utilization pathways are ultimately insufficient to reach net negative emissions. The scale of enhanced oil recovery, storage in construction materials, and valuable mineral carbonation operations could plausibly be increased to a few billion $GtCO_2$/yr. However, as it is necessary to manage 45$GtCO_2$/yr, there is a need to develop additional CO_2 utilization techniques and to begin to close the loop on human CO_2 usage.

Similarly, due to the space and energy restrictions in the transportation sector, it simply will not be practical to attempt to capture all CO_2 directly from its emission sources. Direct air capture will also be a necessary part of reaching a net negative emissions goal. Thus, CO_2 capture and utilization from fossil fuel sources especially is more of a vital stopgap measure as utilization as a whole matures and direct air capture becomes more viable.

The goal of this review is thus to highlight potential avenues in which CO_2 utilization could come closer to the net negative emissions goal. Figure 5 provides an overview of the opportunities which will be discussed. These will be examined in terms common to other reviews (Chauvy, Meunier, Thomas, & De Weireld, 2019) on the subject, including: technology readiness level, geographical constraints, market size, economic returns, and CO_2 uptake capacity.

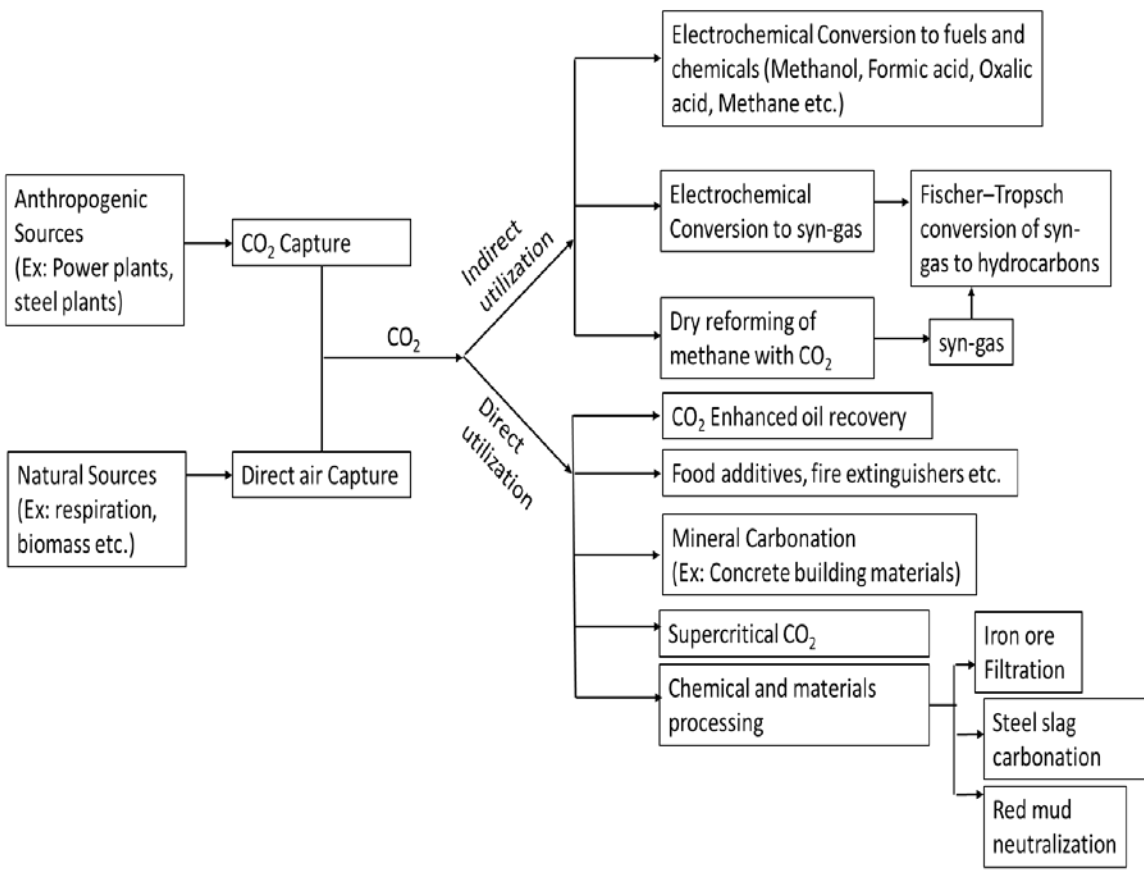

Figure 5: Overview of opportunities for CO_2 utilization.

1.5 CO_2 Use in Chemical and Materials Processing Industry

1.5.1 CO_2 Utilization in Iron and Steel Making

Steelmaking occurs in the following steps: after iron ore is mined, it is typically upgraded via flotation or magnetic separation, pelletized as preparation for transportation and feeding into the blast furnace, reduced into pig iron, and then refined into steel using a basic oxygen furnace or electric arc furnace. In each of these steps, the presence and behavior of CO_2 is an important aspect to be aware of.

CO_2 is emitted during the reduction of iron ore to metallic iron, shown in Equation 1, and the combustion of reducing materials like coke, shown in Equation 2. An average of 1.8 tons of CO_2 is emitted during the production of one ton of steel (Fischedick, Marzinkowski, Winzer, & Weigel, 2014).

$$\mathrm{Fe_2O_3 + 3CO \rightarrow 2Fe + 3CO_2} \qquad (1)$$

$$\mathrm{C + O_2 \rightarrow CO_2} \qquad (2)$$

CO_2 can play a crucial role in steel making by controlling the temperature of molten steel and inhibiting excess oxidation, allowing for the control of dust production in the basic oxygen furnace (Yi, Zhu, Chen, Wang, & Ke, 2009). China has also been exploring CO_2 utilization in various metallurgical processes since the 1980s (Wang, Zhu, Wang, & Li, 2017).

In the blast furnace CO_2 can be recirculated and utilized to control the temperature of the tuyere region, creating a stirring effect and increasing the carbon monoxide ratio by oxidizing coke. This technique would require around 50kgCO_2/t Fe. Overall, regardless of the amount of recycling performed, the CO_2 used in the blast furnace will eventually be released into the atmosphere.

Steel slag carbonation is another option to permanently sequester CO_2 in the steelmaking process. Carbonated steel slag is a useful construction material which can be used in concrete, asphalt, or as another coarse aggregate. Fine carbonated steel slag may also be suitable as a cement mortar or soil conditioner. This process flowchart is outlined in Figure 6.

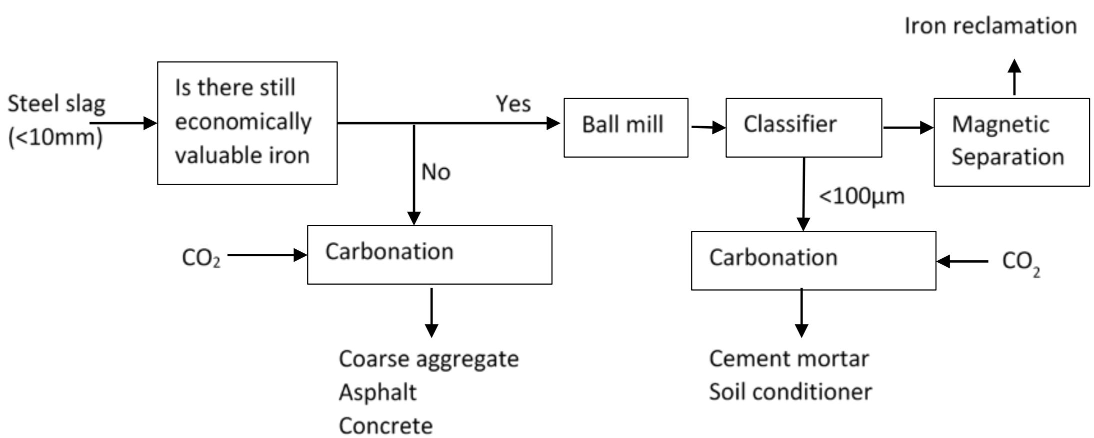

Figure 6: Steel slag carbonation flowchart

(Pan, Adhikari, Chen, Li, & Chiang, 2016).

Steel slag carbonation is estimated to be able to use about 268MtCO_2/yr (Myers, Nakagaki, & Akutsu, 2019). Over the course of 2020-2100, this is expected to allow for the sequestration of roughly 21.7Gt of CO_2, assuming a steady demand for steel. As steel demand is expected to continue to raise going into 2021, it is likely that this 21.7Gt number is ultimately an underestimate.

Earlier in the steelmaking process, the raw ore needs to be concentrated. A significant fraction of iron ores, especially hematite ores, are upgraded via flotation. In this process, the finely ground iron ore is dispersed in water at alkaline conditions, the valuable iron-bearing portions are depressed to the bottom, and the gangue silica is floated with the aid of a collector and air bubbles. This results in an iron-rich slurry which needs to be dewatered for further processing and transportation. This dewatering step often proceeds by filtration, but filtration benefits greatly from being performed under flocculating conditions. The dispersing conditions from flotation hinder the filtration step, and are maintained by the high pH value of the solution. CO_2 can be used as an acid gas to reduce the pH of the solution, which has been utilized to increase filtration rates in operating facilities by up to 23% (Kawatra & Claremboux, 2019). CO_2 utilization by this method is estimated to be about 0.54kgCO_2/t of ore (Ripke, Eisele, & Kawatra, 2004). The fraction of CO_2 which remains sequestered is likely to be low, as the material is later sintered and reduced in the blast furnace.

1.5.2 CO_2 Utilization in the Alumina Industry

Bauxite is the most common ore used for the production of alumina and subsequently aluminum. The Bayer process is the primary commercial process by which bauxite is converted to alumina (Al_2O_3). The Bayer process consists of digesting the bauxite ore in a concentrated sodium hydroxide solution and separating soluble aluminum oxides. The solid waste remaining after this digestion is known as red mud, which is highly caustic (typically pH>13) and is difficult to dispose of. The disposal of red mud is a technical challenge which poses significant environmental and societal risk, as shown in the Ajka red mud disaster where red mud spilled from a disposal pond in Hungary resulting in hundreds of injuries to chemical burns, several deaths, and significant property damage (Renforth, Mayes, Jarvis, Burke, Manning, & Gruiz, 2012).

Much of the danger of red mud stems purely from its caustic nature, which could be mitigated by neutralization with CO_2. The primary advantage of CO_2 over other acids in this role is its remarkable availability and low cost. The result of this neutralization would remain somewhat alkaline due to deeply embedded alkali species, but much of the caustic species could be converted to carbonates. Experiments have shown that the pH of red mud can be dropped to below 7 with this technique, but may bounce back to 9 within several hours as additional alkaline materials leach out from the red mud. This can be mitigated by exposing the red mud to CO_2 over multiple cycles of neutralization from 5 to 24hrs apart (Sahu, Patel, & Ray, 2010). It has also been found that the addition of extra Ca, e.g. in the form of gypsum, promotes additional CO_2 uptake due to the precipitation of $CaCO_3$ (Renforth, Mayes, Jarvis, Burke, Manning, & Gruiz, 2012; Han, Ji, Lee, & Oh, 2017).

Since red mud neutralization forms carbonates, if otherwise undisturbed the CO_2 will be captured permanently. As over 140 million tons of red mud are produced each year, and as roughly 83kgCO_2/t of red mud can be utilized in this way (Evans, 2016), the capacity for red mud utilization is roughly 0.33Gt of CO_2 from existing red mud stockpiles plus an additional 11.6Mt/yr. This neutralization can also lead to further utilization opportunities for the red mud itself, potentially including the extraction of rare earth materials which are often concentrated in red mud wastes. There are several recent articles discussing these neutralization and subsequent utilization routes in detail (Han, Ji, Lee, & Oh, 2017; Wang, Sun, Tang, & Sun, 2019; Mukiza, Zhang, Liu, & Zhang, 2019; Rivera, Ulenaers, Ounoughene, Binnemans, & Van Gerven, 2018).

1.5.3 CO_2 Use in Recovering Rare Earths from Acid Mine Drainage

Acid mine drainage (AMD) is generated by the weathering of sulfide minerals in the presence of oxygen, resulting in the nominal acidic discharge. AMD naturally contains the acidic component, but it also contains leached metals and often contains a considerable concentration of rare earth elements. The rare earth elements are used across all aspects of society, and are in turn a matter of national security and a significant trade opportunity for any country. In particular, the U.S. imports 80% of its rare earth resources from China. The rare earth element concentration of acid mine drainage varies per element from 30-1200ppm (Vass, Noble, & Ziemkiewicz, 2019). Between 700-3400 tons of rare earth elements may be recovered from AMD sites each year, representing a considerable source of these valuable elements.

The treatment of AMD wastes to recover rare earth elements is a bit complex. Typically, the AMD is neutralized using sodium hydroxide to form metal hydroxides, but the recovery of rare earths by this method is relatively limited. One alternative is to use carbonates, which due to more negative Gibbs free energy values will more strongly equilibriate to separate the rare earth elements as opposed to oxide or hydroxide species (Hassas, Rezaee, & Pisupati, 2020).

1.6 CO_2 Enhanced Oil Recovery

Enhanced oil recovery refers to techniques utilized to extract additional oil following the primary and secondary recovery stages (Lake, Johns, Rossen, & Pope, 2014). Enhanced oil recovery accounts for 30-60% or potentially even more of a reservoir's total oil recovery. Practically, enhanced oil recovery refers to 3 types of techniques: chemical, thermal, and gas injection. CO_2 enhanced oil recovery is an example of gas injection, where CO_2 is injected into the oil well to increase the pressure on the oil while decreasing its viscosity. CO_2 enhanced oil recovery accounts for more than 50% of gas injection enhanced oil recovery projects (Jiang, Rui, Hazlett, & Lu, 2019).

A large fraction of the CO_2 used for enhanced oil recovery is permanently trapped in reservoir as a result. However, the sourcing of CO_2 and the ultimate fate of the oil recovered are both important for determining whether or not this results in net negative emissions. As previously mentioned, natural CO_2 sources are presently less expensive than typically captured CO_2. But, as enhanced oil recovery is not 100% efficient in trapping the CO_2 utilized as such, using natural CO_2 sources will not lower emissions at all. Additionally, it is necessary to continue to capture and utilize CO_2 on the downstream consumers utilizing the oil if net negative emissions are to be achieved.

1.6.1 CO_2-Enhanced Oil Recovery at Offshore Oil Reserves

There are currently two large-scale projects utilizing CO_2 enhanced oil recovery in offshore oil fields, Sleipner and Snøhvit, both in Norway. In the U.S. there have also been past pilot projects undertaken to utilize CO_2 enhanced oil recovery in the Gulf of Mexico.

The challenges associated with offshore CO_2 enhanced oil recovery are significant. Notably (Sweatman, Crookshan, & Edman, 2011):

- Limited supplies of CO_2. As CO_2 must be sourced from somewhere, it decreases the likelihood that it could be sourced from a capture facility, and the transportation costs may impact the overall value of the enhanced oil recovery project overall.

- Higher capital and operational costs compared to onshore. This is in addition to the costs already mentioned prior; the lack of usable land infrastructure certainly adds an additional degree of challenge to offshore projects.

- Limited space for retrofitting new equipment and pipelines. Again, the lack of usable land infrastructure means that the equipment as designed today is likely to remain as designed today for the foreseeable future. The cost of adopting new technologies becomes much higher, as much more of the equipment may need to be replaced.

However, offshore projects do have lower initial capital costs, and are far from population centers which can ease certain regulatory burdens.

Geographic locality of CO_2 sources and sinks can come to particular light in these kinds of projects. As an example, the Gulf of Mexico enhanced oil recovery projects require about 10 million metric tons of CO_2 per year, but there are approximately 41 million metric tons of CO_2 emitted by fossil fuel power plants in the same region each year (Kuuskraa & Malone, CO2 Enhanced Oil Recovery for Offshore Oil Reservoirs, 2016). Thus, while CO_2 enhanced recovery cannot provide a sink for all of the CO_2 in the region, it is likely that with some appropriate economic incentives sufficient CO_2 could be acquired inexpensively from entirely manmade CO_2 sources.

1.6.2 Mechanism of CO_2 Enhanced Oil Recovery

In general, the concept of enhanced oil recovery is similar to the methodology for removing oil stains in everyday living. By using an appropriate solvent (e.g. ethanol, vinegar, engine degreasers, or so on) and mechanical action (whether vigorous scrubbing, simply gravity, or pressure), oil stains can be removed from everyday objects.

On the scale of enhanced oil recovery, however, these sorts of solvents are vastly more expensive than the oil that is sought to be removed from the reservoir. CO_2 on the other hand is relatively inexpensive, and is capable of lowering the viscosity of oil through partial miscibility and partial solvation. So long as the CO_2 can be acquired inexpensively, this can become a very profitable venture.

There are several requirements for CO_2 enhanced oil recovery to be successful: the depth of the original oil in place, the temperature, the available gas pressure, the oil's natural viscosity, and such (Bacchu, 2016). One particularly exciting recent advance in this technology is foam-assisted CO_2-EOR (Zhang, Li, & Liu, 2020). This process resolves issues related to the mobility of CO_2, resulting in a much better total sweep of the oil than gas-assisted recovery alone. Figure 7 below shows the CO_2-enhanced oil recovery (CO_2-EOR) cycle and the flow of CO_2 through the cycle.

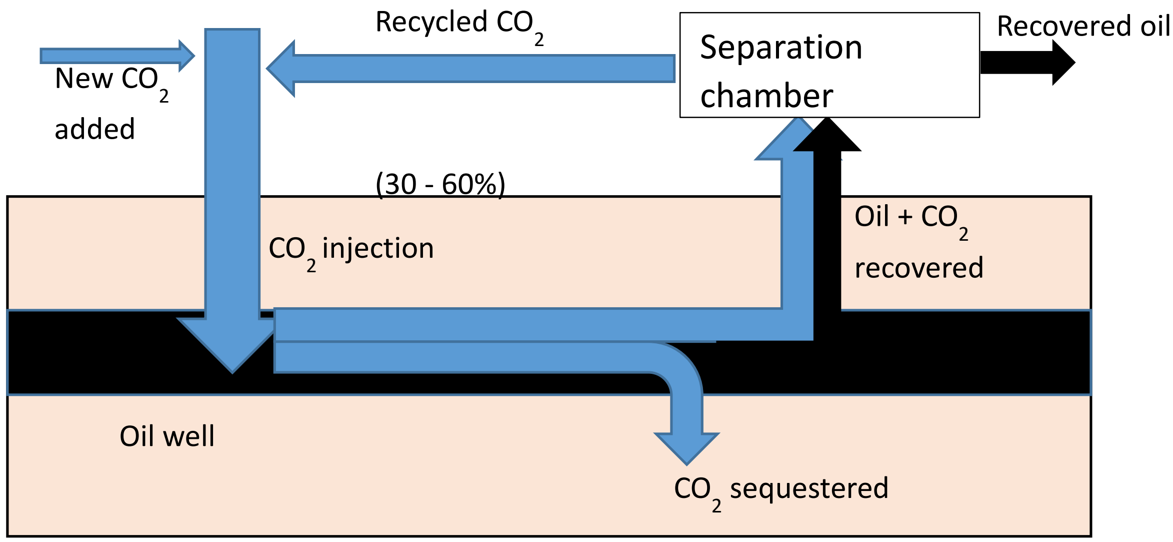

Figure 7: Overview of the CO2-EOR cycle.

1.6.3 Economic and Environmental Impact

With regards to CO_2, the primary goal of any oil field operator is to minimize the CO_2 loss into the reservoir and maximize the amount of CO_2 which can be recycled. To achieve maximum sequestration and in turn achieve the maximum contribution to a net negative emissions target, an economic incentive is required to justify storing CO_2 over recycling it. The use of anthropogenic CO_2 would also be necessary to achieve this end, which would again require an appropriate economic incentive to make it more practical than naturally sourced CO_2. CO_2 transportation costs are a major limiting factor in this, but integration carbon capture into the enhanced oil recovery project may be able to offset these expenses and help overcome the economic advantage of naturally sourced CO_2.

Several studies have approached the economics of CO_2 enhanced oil recovery hypothetically (Kwak & Kim, 2017; Wei, Li, Dahowski, Davidson, Liu, & Zha, 2015), but a particular highlight is the recent empirical techno-economic review by (Jiang, Rui, Hazlett, & Lu, 2019). This empirical review combines economic efficiency data from 40 active CO_2 enhanced oil recovery projects and estimates net present value (NPV) by Equation 3.

$$NPV = -C_{capital} + \sum_{t=1}^{T} (C_{revenue} - C_{O\&M} - C_{tax})/(1 + r_d)^t \qquad (3)$$

Where $C_{capital}$ is the capital cost (including CO_2 pipeline cost, equipment costs, and so on), $C_{revenue}$ is the revenue generated from selling the recovered oil, $C_{O\&M}$ is the cost of operation and maintenance, C_{tax} is the cost of any applicable taxes (e.g. carbon tax), r_d is the interest rate, t is time, and T is the final time of the evaluation period.

1.6.4 U.S. Perspective

With proper optimization of the operation of CO_2 enhanced oil recovery processes, it is feasible that net negative emissions can be locally achieved without discarding the profitability of the oil production (Núñez-López, Gil-Egui, & Hosseini, 2019). At that point, an increase in oil production is directly tied to a corresponding increase in CO_2 sequestration. It has been estimated that CO_2 enhanced oil recovery in the U.S. alone could generate \$1.2 trillion dollars of revenue to be used for CO_2 capture and transportation from fossil fuel fired power plants and industrial facilities (Kuuskraa, Godec, & Dipietro, CO2 utilization from "next generation" CO2 enhanced oil recovery technology, 2013). With the application of the next generation CO_2 enhanced oil recovery technologies described in this section over the next couple of decades, revenues of around \$8.5 trillion are expected in the U.S. domestic market (Kuuskraa, Godec, & Dipietro, CO2 utilization from "next generation" CO2 enhanced oil recovery technology, 2013; Wallace, Leewen, & Kuuskraa, 2011).

1.7 Use of CO_2 in Concrete Building Materials

The capacity for CO_2 utilization in concrete building materials has been estimated to be somewhere between 0.1-1.4GtCO_2/yr (Hepburn, et al., 2019). Concrete is a mixture of cement, water, and aggregates, and is widely used in all sorts of constructions.

Cement is composed of CaO (60-67%), SiO_2 (14-25%), Al_2O_3 (3-8%), Fe_2O_3 (0.1-5%), MgO (0.1-4%), Na_2O (0.1-1.3%), K_2O (0.1-0.3%), and SO_3 (0.5-3%) (Huntzinger, Gierke, Kawatra, Eisele, & Stutter, 2009; Jang, Kim, Kim, & Lee, 2016; Chi, Huang, & Yang, 2002; Zhang & Shao, 2016; Shao, Mirza, & Wu, 2006; Jang & Lee, Microstructural densification and CO2 uptake promoted by the carbonation curing of belite-rich Portland cement, 2016; Fang & Chang, 2015; Chang, Fang, & Shang, 2016; Rostami, Shao, Boyd, & He, Microstructure of cement paste subject to early carbonation curing, 2012; Rostami, Shao, & Boyd, Carbonation curing versus steam curing for precast concrete production, 2012). The two main components of Portland cement are dicalcium silicate ($2CaO \cdot SiO_2$) and tricalcium silicate ($3CaO \cdot SiO_2$), often abbreviated as C_2S and C_3S respectively. C_2S can also be found in steel slags in a variety of morphologies (α-C_2S, β-C_2S, and γ-C_2S). In Portland cement the calcium silicates become hydrated to a variety of phase chemistries to form compounds with the general formula of $xCaO \cdot ySiO_2 \cdot zH_2O$. Carbonation curing is an alternative to traditional water curing which forms carbonate minerals (usu. $CaCO_3$ or $MgCO_3$) instead of the calcium silicate hydrates. Many authors have studied the carbonation curing reactions (shown as Equations 4-10), but it cannot be said to be fully understood yet.

$$x\mathrm{CaO} \cdot y\mathrm{SiO_2} \cdot z\mathrm{H_2O} + x\mathrm{CO_2} \rightarrow x\mathrm{CaCO_3} + y(\mathrm{SiO_2} \cdot t\mathrm{H_2O}) + (z - yt)\mathrm{H_2O} \quad (4)$$

$$\mathrm{CaO} + \mathrm{H_2O} \rightarrow \mathrm{Ca(OH)_2} \quad (5)$$

$$\mathrm{Ca(OH)_2} + \mathrm{CO_2} \rightarrow \mathrm{CaCO_3} + \mathrm{H_2O} \quad (6)$$

$$3\mathrm{CaO} \cdot \mathrm{SiO_2} + 3\mathrm{CO_2} + n\mathrm{H_2O} \rightarrow \mathrm{SiO_2} + n\mathrm{H_2O} + 3\mathrm{CaCO_3} \quad (7)$$

$$2\mathrm{CaO} \cdot \mathrm{SiO_2} + 2\mathrm{CO_2} + n\mathrm{H_2O} \rightarrow \mathrm{SiO_2} \cdot n\mathrm{H_2O} + 2\mathrm{CaCO_3} \quad (8)$$

$$\mathrm{MgO} + \mathrm{H_2O} \rightarrow \mathrm{Mg(OH)_2} \quad (9)$$

$$\mathrm{Mg(OH)_2} + \mathrm{CO_2} \rightarrow \mathrm{MgCO_3} + \mathrm{H_2O} \quad (10)$$

The maximum theoretical storage capacity of cement based materials can be estimated from chemical composition according to Equation 11 (Huntzinger, Gierke, Kawatra, Eisele, & Stutter, 2009).

$$\%\mathrm{CO}_2 \text{ uptake} = 0.785(\%CaO - 0.56\ \%CaCO_3 - 0.7\ \%SO_3) + 1.091\ \%MgO + 0.71\ \%Na_2O + 0.468(\%K_2O - 0.632\%KCl) \quad (11)$$

The most important questions around the utilization of CO_2 in building materials are (Jang, Kim, Kim, & Lee, 2016):

1. What is the mechanism of the carbonation process?
2. What is the CO_2 storage capacity of the material?
3. How does the carbonation of the material affect its material properties?
4. What is the economic viability of the carbonation process as opposed to current industry practice?

1.7.1 Effect of Carbonation on Mechanical Properties of the Material

Carbonation can have both positive and negative effects on the durability and strength of a concrete-based material. Carbonation tends to increase the corrosion rate of reinforced steel, but it can also increase the compressive and splitting strength when the curing period is extend to 28 days (Chi, Huang, & Yang, 2002). The advanced corrosion of steel is believed to be caused by increased chloride penetration (Zhang & Shao, 2016). Several researchers have observed an increase in CO_2 uptake with increased CO_2 concentration and curing time.

It has also been observed that carbonation curing results in a decrease in pore volume within the material. Microstructure analysis via SEM found that calcite ($CaCO_3$) crystals occupied the pore spaces, resulting in a dense structure with increased compressive strength (Shao, Mirza, & Wu, 2006; Zhang & Shao, 2016; Fang & Chang, 2015; Chang, Fang, & Shang, 2016). 18hrs of air curing and 2hrs of accelerated carbonation reduced pore diameter within the cement by 74% due to precipitation of calcite into the original pore spaces (Fang & Chang, 2015). Early carbonation showed better durability than weathering carbonation due to lower chloride penetration in the early carbonation scenario (Rostami, Shao, Boyd, & He, Microstructure of cement paste subject to early carbonation curing, 2012; Zhang & Shao, 2016). With regards to β-C_2S and γ-C_2S, it has been found that β-C_2S responds more favorably to carbonation than γ-C_2S, displaying higher compressive strengths after 2hrs of carbonation (Chang, Fang, & Shang, 2016).

Table 1 summarizes the impact of carbonation on the strengths of various cement compositions and the resulting CO_2 uptake.

Table 1: Effect of carbonation on strength of cement-based materials (LOI = loss on ignition).

Reference	Chemical composition of the cement	CO_2 conc. used for carbonation	CO_2 uptake	Carbonation time	Increase in strength
(Shao, Mirza, & Wu, 2006)	CaO (63.9%), SiO_2 (20.2%), Al_2O_3 (2.32%), Fe_2O_3 (4.47%), MgO (3.54%), SO_3 (3.0%), LOI(0.85%)	99.5%	9-16%	2hr	9-30%
(Fang & Chang, 2015)	CaO (61.13%), SiO_2 (21.45%), Al_2O_3 (5.24%), Fe_2O_3 (2.89%), MgO (2.08%), SO_3 (2.5%)	99.9%	19.8%	2-4hr	25-30%

(Rostami, Shao, & Boyd, Carbonation curing versus steam curing for precast concrete production, 2012)	CaO (63.1%), SiO_2 (19.8%), Al_2O_3 (4.9%), Fe_2O_3 (2.0%), MgO (2.0%), SO_3 (3.8%), LOI(1.66%)	99.5%	7-8%	2hr[1]	17-69%
(Rostami, Shao, Boyd, & He, Microstructure of cement paste subject to early carbonation curing, 2012)	CaO (63.1%), SiO_2 (19.8%), Al_2O_3 (4.9%), Fe_2O_3 (2.0%), MgO (2.0%), SO_3 (3.8%), LOI(1.66%)	99.5%	7-19%	2hr[2]	34-162%
(Jang & Lee, Microstructural densification and CO2 uptake promoted by the	CaO (62.5%), SiO_2 (25.3%), Al_2O_3 (3.1%), Fe_2O_3 (3.6%), SO_3 (2.1%)	5%	13-16.9%	7-28days	120-197%

carbonation curing of belite-rich Portland cement, 2016)					

[1]Following 18hr air curing.

[2]Following steam curing.

1.7.2 Economic Feasibility and Environmental Impact

In recent years cement is pre-casted into blocks and transported to the construction site, so it could be advantageous from an environmental perspective to utilize carbonation curing if the CO_2 is sourced from anthropogenic sources (e.g. the stack emissions of the cement plant itself). Over a 100 year lifetime, assuming the service life of concrete is 70 years, CO_2 uptake is estimated to be about 0.3-0.39tCO_2/t of concrete, based on the experimental carbonation depth (Pade & Guimaraes, 2007; Meyer, 2004). Based on Equation 10, the theoretical maximum uptake capacity of cement-based materials could be as high 0.51tCO_2/t of concrete. The breakeven cost of storing 1t of CO_2 in concrete is estimated to be $25-56USD (Jang, Kim, Kim, & Lee, 2016).

The theoretical maximum sequestration potential of carbonation curing is approximately 3.9Gt/yr, assuming 0.39tCO_2/t concrete against the current global concrete production of roughly 10Gt/yr. However, assuming that all concrete can be carbonation cured is unrealistic – an optimistic estimate by (Hepburn, et al., 2019) suggests that a more realistic CO_2 storage capacity from concrete is roughly 0.1-1.4Gt/yr.

1.8 Fuels and Chemicals from CO_2

In reality, acquiring clean energy instantaneously is no longer a very difficult task. The major challenge remaining for renewable energy sources is not the acquisition of energy in the first place, but the storage required for maintaining its availability until it is actually needed. One appealing solution to this is to transform captured CO_2 into a fuel, thereby storing the energy until it is needed. This has the added advantage of creating a carbon neutral fuel, since the CO_2 that will be formed by its combustion was sourced from the atmosphere or fuel which had already been burned, as opposed to being fresh CO_2 from underground. With appropriate care, this can be used to form an anthropic carbon cycle, wherein only atmospheric CO_2 is sourced for fuels and thus eliminating new CO_2 emissions to the atmosphere entirely.

The process of converting CO_2 to useful chemicals is accomplished by reduction. This can be achieved by thermochemical means, supplying sufficient energy in the presence of a reducing agent, or more directly by the direct application of electricity as an electrochemical process. The thermochemical methods have the disadvantage of requiring comparatively high temperatures and pressures while simultaneously being more difficult to control with catalysts as the catalysts need to be stable at the conditions involved. Electrochemical processes on the other hand require catalysts to achieve useful selectivity, efficiency, and yield. In most cases, the lower temperature and pressure requirements of the electrochemical process are appealing, especially when trying to form more complex chemicals selectively. Table 2 shows the energy required to make different basic products from CO_2.

Table 2: Energy cost for producing various chemicals from CO2 (based on Gibbs free energy).

Product	**Overall Reaction**	**Energy (MJ/Kg)**
Oxalate	$2CO_2 \rightarrow C_2O_4^{2-}$	2.68
Formic acid	$2CO_2 + 2H_2O \rightarrow 2\mathrm{HCOO}H + O_2$	5.51
Carbon monoxide	$2CO_2 + H_2O \rightarrow 2CO + O_2 + H_2O$	9.19
Methanol	$CO_2 + 2H_2O \rightarrow 1.5O_2 + CH_3OH$	21.71
Ethanol	$2CO_2 + 3H_2O \rightarrow C_2H_5OH + 3O_2$	28.70
Propanol	$3CO_2 + 4H_2O \rightarrow C_3H_7OH + 4.5O_2$	29.53
Ethylene	$2CO_2 + 2H_2O \rightarrow C_2H_4 + 3O_2$	41.29
Methane	$CO_2 + 2H_2O \rightarrow 2O_2 + CH_4$	51.15

1.8.1 Thermochemical Conversion of CO_2

There are two primary paths for thermochemical conversion of CO_2. The earlier methodology is the dry reforming of methane. Methane reformation proceeds following a mixture of Equations 12-14 (Gangadharan, Kanchi, & Lou, 2012).

$$\mathrm{CH_4 + H_2O \rightarrow CO + 3H_2} \text{ (endothermic)} \tag{12}$$

$$\mathrm{CO + H_2O \rightarrow CO_2 + H_2} \text{ (exothermic)} \tag{13}$$

$$\mathrm{CH_4 + CO_2 \rightarrow 2CO + 2H_2} \text{ (endothermic)} \tag{14}$$

Due to the availability of methane (as natural gas), the reformation of methane is one of the least expensive methods of forming syngas, which is a feedstock for creating methanol and ethanol for commercial application. Steam reforming of methane is the current commercial leader for this sort of process, and proceeds as shown in Equation 12 in the presence of a heterogeneous catalyst at 600°C. Equation 13, known as the reverse water gas reaction, is competitive with Equation 12 at lower temperatures decreasing the CO yield but increasing the H_2 yield. Equation 14 is dry reforming of methane using CO_2 and CH_4 to form CO and H_2 directly, and typically proceeds in the presence of a Ni-based catalyst as shown in Figure 8 (Jing, Lou, Fei, Hou, & Zheng, 2004;

Buelens, Galvita, Poelman, Detavernier, & Marin, 2016; Pawelec, Damyanova, Arishtirova, Fierro, & Petrov, 2007; Juan-Juan, Román-Martínez, & Illan-Gomez, 2009; Chawl, George, Patel, & Patel, 2013).

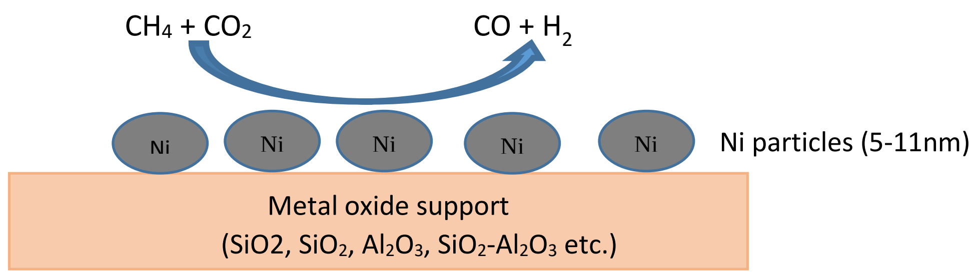

Figure 8: Dry reforming of methane over a Ni-based catalyst on a metal oxide support.

Ni-based catalysts are not ideal from a catalytic viewpoint, as they are subject to carbon deposition which fouls the catalyst via Equations 15 and 16 (Nikoo & Amin, 2011). This carbon deposition deactivates the catalyst, inhibiting further reactions. This fouling can be inhibited by having a wide size distribution of Ni particles and by interactions from the metal oxide surface (Kim, Suh, Park, & Kim, 2000; Juan-Juan, Román-Martínez, & Illan-Gomez, 2009). An appropriate choice of metal oxide surface can slow the formation of carbon deposits, such as with $MgAl_2O_4$ support materials (Kim, Suh, Park, & Kim, 2000; Guharoy, Le Saché, Cai, Reina, & Gu, 2018; Kaydouh, El Hassan, Davidson, Casale, El Zakhem, & Massiani, 2015; Sokolov, Kondratenko, Pohl, Barkschat, & Rodemerck, 2012; Damyanova, Pawelec, Arishtirova, & Fierro, 2012). Ni particle sizes below 7nm also help to inhibit carbon deposition (Kim, Suh, Park, & Kim, 2000). Ni can also be coupled into bimetallic complex to help reduce carbon deposition (Kaydouh, El

Hassan, Davidson, Casale, El Zakhem, & Massiani, 2015). Table 3 shows some experimental studies involving dry reforming under a variety of conditions. Although higher catalytic activity is observed with Rh, Pt, Ir, Pd, and other noble metals (Rezaei, Alavi, Sahebdelfar, & Yan, 2006), the considerable cost of these materials means that Ni remains the dominant catalyst choice in production.

$$CH_4 \rightarrow C + 2H_2 \tag{15}$$

$$2CO \rightarrow C + CO_2 \tag{16}$$

Table 3: Ni based catalyst combinations for high conversion ratios.

Ref	Catalyst	Experimental conditions	Yield				
			CH_4 conversion (%)	CO_2 conversion (%)	H_2 yield (%)	CO yield (%)	H_2/CO ratio
(Jing, Lou, Fei, Hou, & Zheng, 2004)	Ni/SrO-SiO_2	650°C, 1atm	65.3	71.4	38.7	56.5	0.70
(Pawelec, Damyanova	Pt1Ni/ZSM-5	599.8°C, 1atm	18.0	32.0	-	-	0.48

, Arishtirova, Fierro, & Petrov, 2007)	Pt3Ni/ZSM-5		26.7	68.2	-	-	0.73
	Pt6Ni/ZSM-5		29.9	71.4	-	-	0.93
	Pt12Ni/ZSM-5		53.8	98.5	-	-	1.0
(Damyanova, Pawelec, Arishtirova, & Fierro, 2012)	Ni/Al_2O_3	650°C, 1atm	67.5	76.5	41.3	58.5	0.70
	Ni/SiO_2-Al_2O_3		51.8	67.0	29.5	48.9	0.60
	Ni/$MgAl_2O_4$		75.3	81.2	46.5	66.3	0.70
	Ni/ZrO_2-Al_2O_3		66.8	78.7	42.6	59.3	0.70
(Chawl, George, Patel, & Patel, 2013)	Ni/CeO_2-γ-Al_2O_3	800°C, 1atm	71.08	-	65.4	88.9	0.73
	Ni/ K_2O-γ-Al_2O_3		75.09	-	76.2	83.0	0.91
	Ni/MgO-γ-Al_2O_3		74.78	-	74.6	82.5	0.90

(Kaydouh, El Hassan, Davidson, Casale, El Zakhem, & Massiani, 2015)	Ni-CeO_2 /Mesoporous SiO2 (SBA-15)	600°C, 1atm	100	90	-	-	0.96

For a detailed study on absorption mechanisms between the gas species and the catalyst along with the resulting conversion reactions, the reader is referred to the recent study conducted by (Guharoy, Le Saché, Cai, Reina, & Gu, 2018) utilizing density functional theory to interpret the molecular interactions between the gas species and the heterogeneous catalyst.

Another interesting thermochemical conversion method is a redox cycle over a metal oxide catalyst (e.g. ceria, CeO_2). This cycle consists of the metal oxide taking oxygen from the CO_2 to form CO, and then regenerating the original catalyst thermally and releasing the oxygen. With ceria catalysts, a corresponding reaction is also possible with water, forming H_2. The temperature ranges are roughly 900-1000°C, as at lower temperatures the reaction favors graphite formation (Chueh & Haile, 2010). Ceria is the most commonly used catalyst for this style of reaction, but overall this technology is less mature and has not yet seen commercial application (Chueh & Haile, 2010; Nair & Abanades, 2016; Bhosale & Takalkar, Nanostructured co-precipitated Ce0.9Ln0.1O2 (Ln = La, Pr, Sm, Nd, Gd, Tb, Dy, or Er) for thermochemical conversion of CO2, 2018; Bhosale, et al., 2015). Figure 9 shows this redox cycle visually.

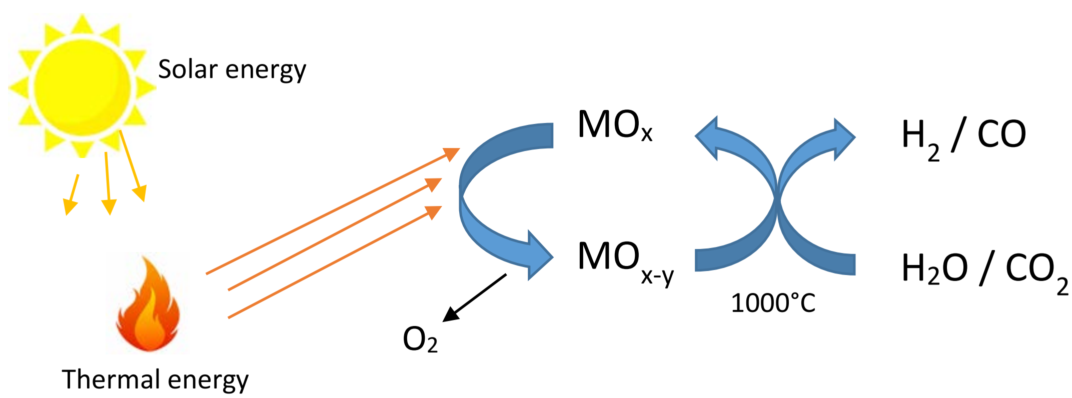

Figure 9: Thermochemical conversion of H_2O or CO_2 into H_2 or CO over a metal oxide catalyst (adapted from (Chueh & Haile, 2010)).

Economically speaking, the dry reforming of methane is quite attractive as it reduces CO_2 and methane emissions while creating a syngas stream which can be further processed into valuable chemicals. Dry reforming has not yet been introduced as a distinct operation on a commercial basis yet, it has been used in conjunction with steam reforming for quite a long time (Gangadharan, Kanchi, & Lou, 2012). Theoretical calculations show that dry reforming temperatures can be further reduced from current practice, perhaps to as low as 300°C, but it will require the development of a high efficiency heterogeneous catalyst (Nikoo & Amin, 2011). A Ni/La_2O_3-ZrO_2 catalyst has achieved good conversion at 400°C (Sokolov, Kondratenko, Pohl, Barkschat, & Rodemerck, 2012), representing a major step towards this goal. If the theoretical minimum could be achieved, the cost of pure dry reforming should be competitive with the cost of steam reforming. The key areas that seem most promising to achieve this goal are bi-metallic Ni-based catalysts, in-situ characterization for predicting and verifying the control of reaction mechanisms at low temperatures, and further understanding of gas diffusion kinetics in these scenarios.

1.8.2 Electrochemical Reduction of CO_2

The electrochemical reduction of CO_2 provides a method to create a variety of products besides carbon monoxide from CO_2. This includes methanol, ethanol, oxalic acid, formic acid, formaldehyde, methane, and a handful of others, based on the specific reaction pathway promoted by the available solvent and catalysts. The faradaic efficiency and selectivity of the reaction depends on a variety of parameters, including but not limited to catalyst, electrode potential, pH, and the electrolyte species.

One major challenge of converting CO_2 to valuable chemicals in aqueous electrolytes is the reaction of the water with the cathode, which tends to form hydrogen gas at a considerable energy cost. This can mitigated to an extent by choosing cathodes with minimal hydrogen overpotentials, or by using non-aqueous or aprotic solvents. Careful catalyst design can help improve the yields at the lower voltages required to avoid hydrogen formation.

In the last few years many authors have explored several novel electrocatalysts for increasing the selectivity and efficiency towards many products. Table 4 shows a variety of electrochemical reduction products with high faradaic efficiencies over highly selective electrocatalysts. Figure 10 shows the general scheme of converting CO_2 to various products in an electrolysis cell.

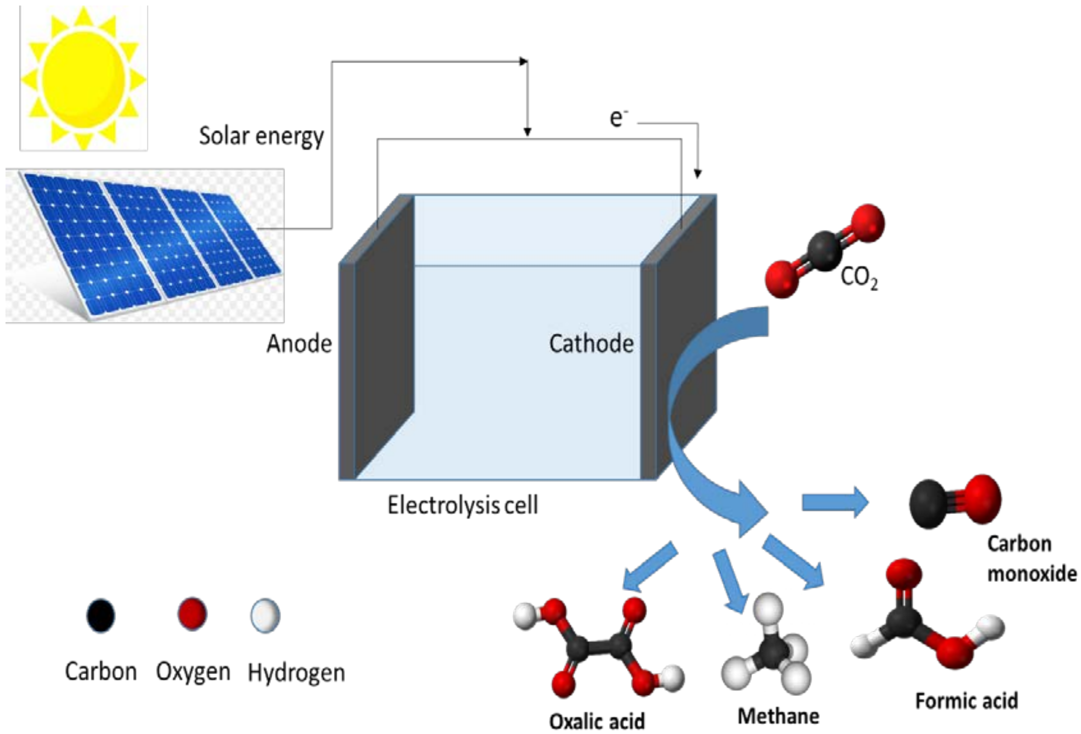

Figure 10: Electrochemical conversion of CO_2 to various products

Table 4: Selected CO_2 reduction products with high faradaic efficiencies over highly selective catalysts.

Ref	Electrocatalyst	Electrolyte	Temperature, pressure	Main Product (Faradaic efficiency %)
(Zhou, Liu, Yang, Wang, Alshammari, & Deng, 2014)	Silver	1-butyl-3-methylimidazolium Chloride in water	25°C, 1atm	CO (99%)
(Valluri & Kawatra, Electro catalytic reduction of CO2 to oxalic acid, 2019)	Zinc, o-tolunitrile	0.1M TEABR in DMF	25°C, 1atm	ZnC_2O_4 (91%)

(Chen, Handoko, Wan, Ma, Ren, & Yeo, 2015)	Copper meso crystals	0.1M $KHCO_3$	25°C, 1atm	CH_4 (1.47), C_2H_4 (27.2)
(Kaneco, Ueno, Katsumata, Suzuki, & Ohta, 2006)	Copper Nano particles	0.08M NaOH in 99% methanol	-30.15°C, 1atm	CO (60), CH_4 (12)
(Ren, Deng, Handoko, Chen, Malkhandi, & Yeo, 2015)	Copper oxide film	0.1M $KHCO_3$	25°C, 1atm	C_2H_4 (34–39%), C_2H_5OH (9–16%), CH_4 (<1%)
(Qu, Zhang, Wang, & Xie, 2005)	Platinum + RuO_2/TiO_2 nanotubes	0.5M $NaHCO_3$	25°C, 1atm	CH_3OH (60.5%)

(Yan, Zeitler, Gu, Hu, & Bocarsly, 2013)	Platinum	Pyridinium in DMF	25°C, 1atm	CH_3OH (30%)
(Yang, et al., 2018)	Atomically dispersed nickel on graphene	0.5M $KHCO_3$	25°C, 1atm	CO (>80%)
(Wang et al., 2017)	Spongy nickel-organic photocatalyst	2.5 mmol $Ru(bpy)_3Cl_2 \cdot 6H_2O$ in CH_3CN/H_2O = 8/2	20°C, 1atm	CO (100%)
(Weng, Jiang, Wang, & Xiao, 2020)	Carbon paper	GeO_2 in NaCl-$CaCl_2$ molten electrolyte	750°C, 1atm	Ge-carbon nanotube composites (80%)

(Dai, et al., 2017)	Cu/Ni(OH)$_2$ Nanosheets	0.5 M $NaHCO_3$	20°C, 1atm	CO (92%)
(Wang, et al., 2017)	ZnO-ZrO_2 solid solution	NA	320°C, 49.3atm	CH_3OH (86-91%)
(Tarek, et al., 2019)	CdS-$CuFe_2O_4$ nanocomposite	0.1M $NaHCO_3$	25°C, 1atm	CH_3OH (72%)
(Albo, Beobide, Castaño, & Irabien, 2017)	2-methylpyridine	0.5 M $KHCO_3$	25°C, 1atm	CH_3OH (25.6%)
(Pardal, et al., 2017)	Cu-Zn bimetallic coating on Cu foil	1-ethyl-3-methyl-imidazolium triflate + 10% H_2O	45°C, 29.6atm	CO/H_2 (100%)*

*The CO/H2 ratio in this case is tunable based on the catalyst surface coating ratio of Cu-Zn. NA-Not available.

The activity of the electrocatalyst is primarily at the cathode surface. The CO_2 molecules adsorb to the cathode as they are being reduced to the active anion radical form, as was shown by Chandrasekaran and Bockris (1987) using polarization modulation Fourier transform infrared spectroscopy (Chandrasekaran & Bockris, 1987). The reduction potential for formation of the CO_2 anion radical is approximately -1.9V vs. SHE at 25°C and 1atm pressure. It is evident from the literature that the reduction of CO_2 happens directly at the cathode (Gao, et al., 2015; Liu, Tao, Zeng, Liu, & Luo, 2017; Reuillard, Ly, Rosser, Kuehnel, Zebger, & Reisner, 2017). Figure 11 outlines the possible reaction schemes and common cathode choices to achieve them. Because the catalyst activity is almost universally at the surface of the electrode, the presence of catalyst, or even electrolyte, elsewhere in the system is irrelevant so long as the CO_2 can be adsorbed to the cathode and reacted.

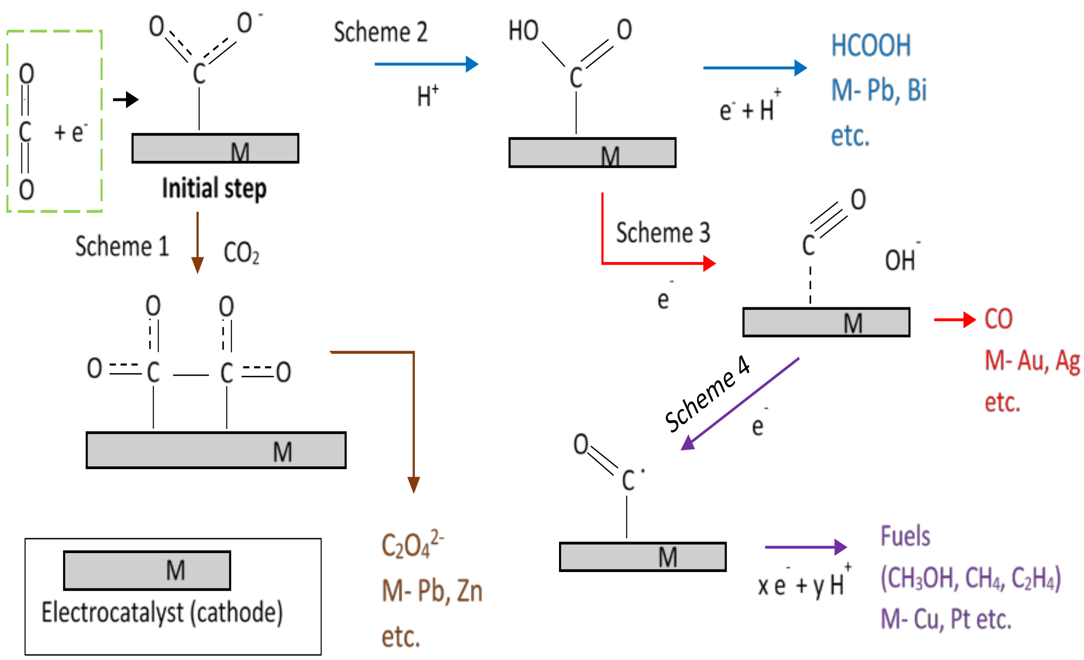

Figure 11: CO2 adsorption and reaction mechanism on heterogeneous electrocatalyst surfaces

(Valluri & Kawatra, Electro catalytic reduction of CO2 to oxalic acid, 2019; Ren, Deng, Handoko, Chen, Malkhandi, & Yeo, 2015; Birdja, Pérez-Gallent, Figueiredo, Göttle, Calle-Vallejo, & Koper, 2019; Jones, Prakash, & Olah, 2014).

Scheme 1 is preferred in an aprotic solvent (absence of H^+) and the other schemes are preferred in aqueous electrolytes. The design of the electrolysis cell controls the amount of electrolyte required and the options available for introducing and extracting CO_2 and product respectively. The cell design should be chosen to allow for efficient gas diffusion, an acceptably small amount of electrolyte required, sufficiently high cathode surface area, and other parameters as appropriate to ensure high reaction rates at minimal cost. Depending on the reaction scheme targeted and products desired, the cell design and material may be influenced. Between aprotic electrolytes and aqueous electrolytes, different hazards and material compatibility restrictions will present themselves.

In recent studies and reviews (Liang, Altaf, Huang, Gao, & Wang, 2020), the primary cell designs observed were microfluidic cells (Whipple, Finke, & Kenis, 2010), solid oxide cells (Uhm & Kim, 2014; Graves, Ebbesen, & Mogensen, 2011), and membrane electrolysis cells. An overview of these cell types is diagrammed in Figure 12.

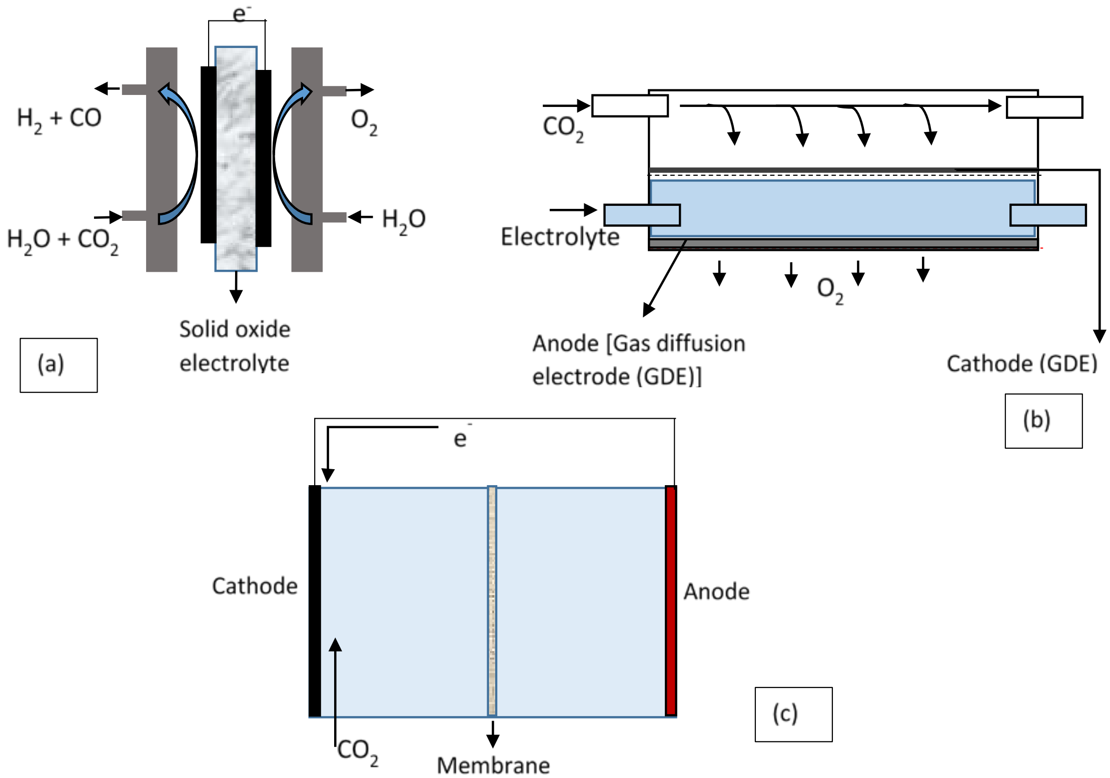

Figure 12: Electrochemical reduction cell design: (a) Solid oxide electrolysis cell (b) Microfluidic cell (c) Membrane electrolysis cell

(Uhm & Kim, 2014; Whipple, Finke, & Kenis, 2010).

The microfluidic cell shown is essentially optimal in minimizing the volume of electrolyte required for the electrolysis. Since aprotic electrolytes in particular are typically expensive compared to any of the possible products of the conversion, minimizing the volume required can represent a significant cost savings. However, the microfluidic cell tends to have a limited capacity for scale-up, making high throughput designs more difficult to manage.

The specific choice of catalyst in the design of an electrochemical process for converting CO_2 remains a relatively tricky problem. Though many catalyst options are listed in Table 4, it is not clear how many of them are suitable for large scale production. To narrow down the optimal operating parameters and to assist in the design of new catalysts, one potential option is machine learning or neural network approaches. These techniques allow for the correlation of existing experimental data to find interesting points within the parameter space, allowing the number of experiments required to find or deny interesting results to be minimized. Combined with effective calculation techniques for predicting catalyst behavior, such as density function theory, machine learning models combined with experimental evidence provides an interesting avenue to decrease the experimental work and researcher time required to develop new catalysts. There have already been some studies which apply this style of approach successfully, including for the prediction of the reaction mechanism of syngas on an Rh(111) catalyst (Ulissi, Medford, Bligaard, & Nørskov, 2017).

1.8.3 Other Reduction Products and Economic Impact

Multi-carbon products (C2+) have higher energy density than typical CO_2 reduction products, so producing these products has gained popularity as of late. The major products for energy density are methane, methanol, ethylene, and ethanol. Ethanol and ethylene both require form a C-C bond. Copper cathodes commonly increase the faradaic efficiency of this C-C coupling (Birdja, Pérez-Gallent, Figueiredo, Göttle, Calle-Vallejo, & Koper, 2019). Selectivity towards specific C2+ products is then achieved by tuning the surface of the copper cathode. Unfortunately, faradaic efficiencies for this process remain low, around 25-40%, because the CO_2 molecule typically detaches during the intermediate steps (Chen, Handoko, Wan, Ma, Ren, & Yeo, 2015; Ren, Deng, Handoko, Chen, Malkhandi, & Yeo, 2015).

Syngas has also been frequently mentioned thus far. Syngas is a precursor to methane and methanol formation, along with the feedstock for the Fischer-Tropsch process which is used to produce higher order hydrocarbons. While hydrogen evolution during electrolysis is usually undesirable due to the high energy cost of electrolyzing water, in the reduction of CO_2 this can be used to control the ratio of hydrogen to CO in the syngas being produced. One research group was able to achieve different ratios for CO/H_2 in an ionic liquid electrolyte (Pardal, et al., 2017). Typically fixed CO/H_2 ratios have been observed (Zhou, Liu, Yang, Wang, Alshammari, & Deng, 2014; Kaneco, Ueno, Katsumata, Suzuki, & Ohta, 2006; Yang, et al., 2018; Niu, et al., 2017; Dai, et al., 2017).

The electrochemical reduction of CO_2 is important for achieving a closed carbon cycle, and has good economic promise. However, as shown from Table 2, the energy cost of forming many of these products is considerable. If the goal is to achieve net negative emissions, then it is important to acknowledge the source of the energy used for these reactions. Using fossil fuels to create methanol is counterproductive, as due to the limited efficiency of the original conversion combined with the high energy density of methanol, more CO_2 will be generated by burning the fossil fuels for energy than will actually be captured in the methanol. This is due not only to the inefficiencies of the process, but also simply due to the energy requirements of forming the chemicals in the first place. Coal simply does not contain the energy to create methanol in a 1:1 carbon ratio. Natural gas does suffer the inefficiencies, as though it technically contains enough energy to be converted to methanol, doing so would require an energetic efficiency of around 90%. Instead, it is highly recommended that attempts to form fuel compounds from CO_2 source their energy from renewable supplies.

As a worked example, assume a typical coal-fired power plant efficiency of approximately 34% burning a high quality coal comparable to graphite. In this scenario, to form one mole of oxalic acid requires two moles of CO_2 and 243 kJ of energy. Burning 2 moles of graphite at 34% efficiency produces 267.6 kJ which is sufficient to provide all of the energy necessary to form oxalic acid. There are 24.6 kJ of electrical energy remaining, and 494.8 kJ of thermal energy remaining. However, if one is to form one mole of ethanol, this requires two moles of CO_2, 3 moles of H_2O, and 1366.2 kJ of electrical energy. Acquiring this electrical energy requires burning 10.21 mol of graphite, or 5.11 mol per mole of carbon sequestered (Kawatra, Advanced Coal Preparation and Beyond: CO2 Capture and Utilization, 2020). It is worth repeating that renewable energy sources such as solar and wind power do not encounter this issue.

Urea is another major product formed from CO_2 using ammonia, via Equations 17 and 18. Urea is currently one of the most profitable pathways for CO_2 utilization. Currently 140 million metric tons of CO_2 are used each year to make urea (Jarvis & Samsatli, 2018), which is by far the highest in the conversion pathway at present. However, over the urea lifecycle, 98% of the stored carbon will be emitted back into the atmosphere (Aresta, 2010). As such, if the goal is to reduce emissions overall, the CO_2 sourced for urea production must be sourced from direct air capture or otherwise recycled CO_2.

$$2NH_3 + CO_2 \rightleftharpoons H_2N - COONH_4 \tag{17}$$

$$H_2N - COONH_4 \rightleftharpoons (NH_2)_2CO + H_2O \tag{18}$$

Other products which have immediate potential for utilization include: oxalic acid, which can be used to leach rare earth metals; syngas for the production of various industrial chemicals; methanol, as a solvent, fuel, or chemical feedstock; or ethylene, for polymer production. Methanol and ethylene stand out particularly well due to their consistent and stable market applications. Methanol's market size is expected to reach $38 billion by 2025, with a global demand of 140Mt/yr and growing. Ethylene is widely used in the chemical industry overall, and much of it is processed into polyethylene plastics. The ethylene market is expected to reach about $160 billion by 2027, and it is currently produced primarily by steam cracking of hydrocarbons at 750-950°C. Both of these applications can be well-addressed by CO_2 reduction if high faradaic efficiencies and throughput can be achieved. For ethylene in particular, the present cost of production is around $1000-1500/t of ethylene, which CO_2 reduction could become competitive with at a faradaic efficiency of greater than 60%.

1.9 Supercritical CO_2 (s-CO_2)

The supercritical phase of CO_2 is when the temperature and pressure of the fluid exceed the critical temperature and pressure and as a result the fluid behaves as a gas and a liquid simultaneously. Supercritical fluids are gas-like in that they are essentially inviscid and expand to fill their containers, while they are liquid-like in that they have large heat capacities and conductivities and are capable solvents. Supercritical CO_2 in particular has several applications which stem from its solvent properties, its heat transfer properties, and its accessible critical point. The primary uses of supercritical CO_2 include as a working fluid, refrigerant, polymerization, textile dyeing, electrochemical solvent, decaffeination, and lipid extraction. In many of these applications s-CO_2 is uniquely suitable to overcome existing challenges, such as in refrigeration where the existing competitors (primarily chlorofluorocarbons and hydrochlorofluorocarbons) have significantly more drastic environmental consequences due to ozone depletion (Ehsan, Guan, & Klimenko, 2018). Non-polar organic compounds tend to be highly soluble in s-CO_2, making it an effective solvent for otherwise complex extractions (Noyori, 1999). Supercritical CO_2 is also an effective dry etching agent used in semiconductor fabrication, an oft-overlooked aspect in discussions on CO_2 utilization (Bessel, et al., 2003).

Textile dyeing is a particularly interesting application, as every year 0.7 million metric tons of synthetic dyes are generated in the textile industry and roughly 5-10% of them make it to wastewater streams (Kong & Wu, 2008). These dyes are a considerable environmental issue, and have considerable associated water treatment costs. In addition to these costs, however, even obtaining a water source for this purpose can represent a significant capital investment (Ramsey, Qiubai, Zhang, Zhang, & Wei, 2009). Using s-CO_2 as the solvent could save on these capital costs, as well as simplifying the drying step (since the CO_2 can be removed simply by decreasing the pressure) and the resulting separation of solvent from the dye. Supercritical CO_2 also effectively diffuses into many textile materials, potentially shortening the overall processing times required. The use of s-CO_2 in dyeing has been successful in synthetic materials (polyethylene terephthalate and polyamide), but further research is needed to develop methodologies for dyeing polypropylene fabrics (Abou Elmaaty & Abd El-Aziz, 2018).

Supercritical CO_2 also deserves significant attention in power generation. The conventional steam cycle suffers from low efficiencies (30-34%) due to high compression work combined with low turbine inlet temperatures and pressures. A supercritical steam cycle overcomes part of the problem by allowing for higher energy transfers within the fluid and higher turbine temperatures and pressures. However, supercritical steam has significant associated material requirements, and designing the process for these adverse conditions represents a considerable capital expense. Supercritical CO_2 is significantly easier to design materials for due to its low critical temperature and pressure, while also having a low compressibility factor (Z: 0.2 – 0.5) (Ahn, et al., 2015). Due to the improved heat transfer properties, the physical scale of a supercritical CO_2 turbine can be an order of magnitude smaller than a conventional gas and steam turbine. This decreased size is particularly helpful for benchtop and pilot scale research, as significantly more capable turbomachinery can be designed in the same footprint. Table 5 shows a variety of operational pilot-scale testing facilities for s-CO_2 power cycle units.

Table 5: Pilot scale S-CO_2 power generation research.

(Koytsoumpa, Bergins, & Kakaras, 2018)

Research Institute	Power output	sCO_2 cycle efficiency
NREL (National lab, Golden, CO)	5-10MW	38.3%
Sandia (National Lab, Livermore, CA)	200MW	45-50%
KAIST (South Korea)	300MW	40%
EPRI (Palo Alto, CA)	400-800MW	-

1.10 Summary and Conclusions

The utilization technologies mentioned prior are, for the most part, potentially attractive from an economic viewpoint. However, few of them have a significant potential to contribute to a net negative emissions goal. Primarily those technologies which simultaneously sequester the CO_2 as it is used beneficially are effective for reducing emissions overall. This would include acid mine drainage carbonation, steel slag carbonation, red mud neutralization, enhanced oil recovery, and use in building materials. These technologies are of the foremost interest for decreasing emissions overall, especially as carbon capture is becoming cheaper. Even if all of these net negative emissions technologies take root however, geological sequestration will still be necessary.

In 2018, federal carbon storage and utilization tax credits were updated. At present, there is a \$60/tCO_2 tax credit for carbon capture and storage. This is an especially attractive option for facilities which can capture CO_2 with minimal cost, such as ethanol plants (\$25-40/tCO_2 captured).

To summarize the technologies discussed so far, the concept of technology readiness level can be helpful. By assigning an index of 1 to 10 to each technology, where 1 means that the technology is fundamentally still in the idea stage, 5 means it has seen significant laboratory work and is ready for pilot scale implementation, and 10 meaning that the technology has achieved widespread commercial adoption, it is possible to get a sense for which technologies are presently most exciting. Table 7 below lists the technology readiness levels, in the author's estimation, of the technologies discussed prior.

Table 6: Technology readiness levels of various CO_2 utilization technologies.

Division	**Application**	**Impact**	**CO_2 uptake capacity**	**Technology readiness level**	**Breakeven cost (\$/ton)**

			(Gt CO_2/yr)		
Fuels and chemicals	Fuels (methanol, ethanol, syngas, methane) Chemicals (formic acid, oxalic acid) Urea production	High	-	5-6	-
Food	Dry Ice Drinks carbonation Baking soda (bicarbonate) Food preservative	Medium	-	10	-
Chemical and materials processing industry	[empty cell?]	Medium	0.2-0.3	6-8	-20 to 50

Oil and gas	Enhanced oil recovery	Very high	0.1-1	10	-45 to -60
Mineral carbonation	Concrete building materials Red-mud (Bauxite residue) Neutralization	Medium	3-4	7-8	-30 to 70
Power sector	Working fluid in power cycle	Medium	-	3-4	-
Other	Solvent (Supercritical CO_2) Refrigerant Dry cleaning	Low	-	6	-

Mineral carbonation technologies seem particularly promising in the short term, especially concrete building materials. This is primarily because of the combined advantage of increasing material strength while sequestering CO_2 for a considerable length of time, combined with the tremendous and continued demand for concrete. Enhanced oil recovery is perhaps less exciting, as the permanent storage of CO_2 is not its primary goal and it is driven by costs to try to use naturally sourced CO_2 where possible.

While there is certainly tremendous capacity for CO_2 available in enhanced oil recovery sequestration sites, it is not so clear that it is viable to increase CO_2 storage in those sites to their very limit any time soon.

CO_2 conversion to chemicals and fuels is likely to be the key to reaching a carbon neutral future. It is essentially unthinkable that carbon products will disappear entirely, so the responsible management of the CO_2 that is already in the atmosphere and the formation of a human carbon cycle will be key to minimizing the environmental risks of continuing in this fashion. In this area, research should continue in the direction of understanding and optimizing catalyst development, so that long-lived, highly-effective, and low-cost catalysts can be developed to create useful chemicals from CO_2.

1.11 References

- Abou Elmaaty, T., & Abd El-Aziz, E. (2018). Supercritical carbon dioxide as a green media in textile dyeing: a review. *Textile Research Journal, 88*(10), 1184-1212.
- Ahn, Y., Bae, S., Kim, M., Cho, S., Baik, S., Lee, J., et al. (2015). Review of supercritical CO2 power cycle technology and current status of research and development. *Nuclear Engineering and Technology, 47*(6), 647-661.
- Albo, J., Beobide, G., Castaño, P., & Irabien, A. (2017). Methanol electrosynthesis from CO2 at Cu2O/ZnO prompted by pyridine-based aqueous solutions. *Journal of CO2 Utilization, 18*, 164-172.
- Aresta, M. (2010). *Carbon dioxide as chemical feedstock.* Weinheim: Wiley-VCH.

- Bacchu, S. (2016). Identification of oil reservoirs suitable for CO2-EOR and CO2 storage (CCUS) using reserves databases, with application to Alberta, Canada. *International Journal of Greenhouse Gas Control, 44*, 152-165.
- Bessel, C., Denison, G., DeSimone, J., DeYoung, J., Gross, S., Schauer, C., et al. (2003). Etchant solutions for the removal of Cu (0) in a supercritical CO2-based "dry" chemical mechanical planarization process for device fabrication. *Journal of the American Chemical Society, 125*(17), 4980-4981.
- Bhosale, R., & Takalkar, G. (2018). Nanostructured co-precipitated Ce0.9Ln0.1O2 (Ln = La, Pr, Sm, Nd, Gd, Tb, Dy, or Er) for thermochemical conversion of CO2. *Ceramics International, 44*(14), 16688-16697.
- Bhosale, R., Dardor, D., Gharbia, S., Folady, J., Jilani, M., Kumar, A., et al. (2015). Thermochemical conversion of CO2 into solar fuels using ferrite nanomaterials. *Proceedings of the 4th International Gas Processing Symposium* (pp. 141-148). Qatar: Elsevier.
- Birdja, Y., Pérez-Gallent, E., Figueiredo, M., Göttle, A., Calle-Vallejo, F., & Koper, M. (2019). Advances and challenges in understanding the electrocatalytic conversion of carbon dioxide to fuels. *Nature Energy, 4*(9), 732-745.
- Buelens, L., Galvita, V., Poelman, H., Detavernier, C., & Marin, G. (2016). Super-dry reforming of methane intensifies CO2 utilization via Le Chatelier's principle. *Science, 354*(6311), 449-452.

- Cabeza, L., de Gracia, A., Fernández, A., & Farid, M. (2017). Supercritical CO2 as heat transfer fluid: A review. *Applied thermal engineering, 125*, 799-810.
- Chandrasekaran, K., & Bockris, L. (1987). In-situ spectroscopic investigation of adsorbed intermediate radicals in electrochemical reactions: CO2- on platinum. *Surface Science, 185*(3), 495-514.
- Chang, J., Fang, Y., & Shang, X. (2016). The role of β-C 2 S and γ-C 2 S in carbon capture and strength development. *Materials and Structures, 49*(10), 4417-4424.
- Chauvy, R., Meunier, N., Thomas, D., & De Weireld, G. (2019). Selecting emerging CO2 utilization products for short-to mid-term. *Applied Energy, 236*, 662-680.
- Chawl, S., George, M., Patel, F., & Patel, S. (2013). Production of synthesis gas by carbon dioxide reforming of methane over nickel based and perovskite catalysts. *Procedia Engineering, 355*(1-2), 461-466.
- Chen, C., Handoko, A., Wan, J., Ma, L., Ren, D., & Yeo, B. (2015). Stable and selective electrochemical reduction of carbon dioxide to ethylene on copper mesocrystals. *Catalysis Science & Technology, 5*(1), 161-168.
- Chi, J., Huang, R., & Yang, C. (2002). Effects of carbonation on mechanical properties and durability of concrete using accelerated testing method. *Journal of Marine Science and Technology, 10*(1), 14-20.
- Chueh, W., & Haile, S. (2010). A thermochemical study of ceria: exploiting an old material for new modes of energy conversion and CO2 mitigation. *Philosophical*

Transactions of the Royal Society A: Mathematical, Physical and Engineering Sciences, 368(1923), 3269-3294.

- Dai, L., Qin, Q., Wang, P., Zhao, X., Hu, C., Liu, P., et al. (2017). Ultrastable atomic copper nanosheets for electrochemical reduction of carbon dioxide. *Science Advances, 3*(9), 1-9.
- Damyanova, S., Pawelec, B., Arishtirova, K., & Fierro, J. (2012). Ni-based catalysts for reforming of methane with CO2. *International Journal of Hydrogen Energy, 37*(21), 15966-15975.
- Edenhoffer, O. (2015). *Climate change 2014: mitigation of climate change* (Vol. 3). Cambridge University Press.
- Ehsan, M., Guan, Z., & Klimenko, A. (2018). A comprehensive review on heat transfer and pressure drop characteristics with supercritical CO2 under heating and cooling applications. *Renewable and Sustainable Energy Reviews, 92*, 658-675.
- EIA. (2020). *Annual Energy Outlook 2020.*
- Eisaman, M., Alvarado, L., Larner, D., Wang, P., Garg, B., & Littau, K. (2011). CO2 separation using bipolar membrane electrodialysis. *Energy & Environmental Science, 4*(4), 1319-1328.
- Evans, K. (2016). The history, challenges, and new developments in the management and use of bauxite residue. *Journal of Sustainable Metallurgy, 2*(4), 316-331.

- Fang, Y., & Chang, J. (2015). Microstructure changes of waste hydrated cement paste induced by accelerated carbonation. *Construction and Building Materials, 76*, 360-365.
- Fischedick, M., Marzinkowski, J., Winzer, P., & Weigel, M. (2014). Techno-economic evaluation of innovative steel production technologies. *Journal of Cleaner Production, 84*, 563-580.
- Gangadharan, P., Kanchi, K., & Lou, H. (2012). Evaluation of the economic and environmental impact of combining dry reforming with steam reforming of methane. *Chemical Engineering Research and Design, 90*(11), 1956-1968.
- Gao, D., Zhou, H., Wang, J., Miao, S., Yang, F., Wang, G., et al. (2015). Size-dependent electrocatalytic reduction of CO2 over Pd nanoparticles. *Journal of the American Chemical Society, 137*(13), 4288-4291.
- Graves, C., Ebbesen, S., & Mogensen, M. (2011). Co-electrolysis of CO2 and H2O in solid oxide cells: performance and durability. *Solid State Ionics, 192*(1), 398-403.
- Guharoy, U., Le Saché, E., Cai, Q., Reina, T., & Gu, S. (2018). Understanding the role of Ni-Sn interaction to design highly effective CO2 conversion catalysts for dry reforming of methane. *Journal of CO2 Utilization, 27*, 1-10.
- Han, Y., Ji, S., Lee, P., & Oh, C. (2017). Bauxite residue neutralization with simultaneous mineral carbonation using atmospheric CO2. *Journal of hazardous materials, 326*, 87-93.

- Hassas, B., Rezaee, M., & Pisupati, S. (2020). Precipitation of rare earth elements from acid mine drainage by CO2 mineralization process. *Chemical Engineering Journal, 399*, 125716.
- Hepburn, C., Adlen, E., Beddington, J., Carter, E., Fuss, S., Mac Dowell, N., et al. (2019). The technological and economic prospects for CO 2 utilization and removal. *Nature, 575*(7781), 87-97.
- Huntzinger, D., Gierke, J., Kawatra, S., Eisele, T., & Stutter, L. (2009). Carbon dioxide sequestration in cement kiln dust through mineral carbonation. *Environmental Science & Technology, 43*(6), 1986-1992.
- Jang, J., & Lee, H. (2016). Microstructural densification and CO2 uptake promoted by the carbonation curing of belite-rich Portland cement. *Cement and Concrete Research, 76*, 50-57.
- Jang, J., Kim, G., Kim, H., & Lee, H. (2016). Review on recent advances in CO2 utilization and sequestration technologies in cement-based materials. *Construction and Building Materials, 127*, 762-773.
- Jarvis, S., & Samsatli, S. (2018). Technologies and infrastructures underpinning future CO2 value chains: A comprehensive review and comparative analysis. *Renewable and Sustainable Energy Reviews, 85*, 46-68.
- Jiang, J., Rui, Z., Hazlett, R., & Lu, J. (2019). An integrated technical-economic model for evaluating CO2 enhanced oil recovery development. *Applied Energy, 247*, 190-211.

- Jing, Q., Lou, H., Fei, J., Hou, Z., & Zheng, X. (2004). Syngas production from reforming of methane with CO2 and O2 over Ni/SrO-SiO2 catalysts in fluidized bed reactor. *International Journal of Hydrogen Energy, 29*(12), 1245-1251.
- Jones, J., Prakash, G., & Olah, G. (2014). Electrochemical CO2 reduction: recent advances and current trends. *Israel Journal of Chemistry, 54*(10), 1451-1466.
- Juan-Juan, J., Román-Martínez, M., & Illan-Gomez, M. (2009). Nickel catalyst activation in the carbon dioxide reforming of methane: effect of pretreatments. *Applied Catalysis A: General, 197*(2), 27-32.
- Kaneco, S., Ueno, Y., Katsumata, H., Suzuki, T., & Ohta, K. (2006). Electrochemical reduction of CO2 in copper particle-suspended methanol. *Chemical Engineering Journal, 119*(2-3), 107-112.
- Kawatra, S. (2020). *Advanced Coal Preparation and Beyond: CO2 Capture and Utilization.* Boca Raton, FL: CRC Press.
- Kawatra, S., & Claremboux, V. (2019). Application of surface chemical fundamentals to improving industrial filtration rates. *Mineral Processing and Extractive Metallurgy Review, 40*(4), 292-297.
- Kaydouh, M., El Hassan, N., Davidson, A., Casale, S., El Zakhem, H., & Massiani, P. (2015). Effect of the order of Ni and Ce addition in SBA-15 on the activity in dry reforming of methane. *Comptes Rendus Chimie, 18*(3), 293-301.

- Kim, J., Suh, D., Park, T., & Kim, K. (2000). Effect of metal particle size on coking during CO2 reforming of CH4 over Ni-alumina aerogel catalysts. *Applied Catalysis A: General, 197*(2), 191-200.
- Knuutila, H., Svendsen, H. F., & Antilla, M. (2009). CO2 capture from coal-fired power plants based on sodium carbonate slurry; a systems feasibility nad sensitivity study. *International Journal of Greenhouse Gas Control, 3*(2), 143-151.
- Kong, H., & Wu, H. (2008). Pretreatment of textile dyeing wastewater using an anoxic baffled reactor. *Bioresource Technology, 99*(16), 7886-7891.
- Koytsoumpa, E., Bergins, C., & Kakaras, E. (2018). The CO2 economy: Review of CO2 capture and reuse technologies. *The Journal of Supercritical Fluids, 132*, 3-16.
- Kuuskraa, V., & Malone, T. (2016). CO2 Enhanced Oil Recovery for Offshore Oil Reservoirs. *Offshore Technology Conference.* Houston, TX: Offshore Technology Conference.
- Kuuskraa, V., Godec, M., & Dipietro, P. (2013). CO2 utilization from "next generation" CO2 enhanced oil recovery technology. *Energy Procedia, 37*(1), 6854-6866.
- Kwak, D., & Kim, J. (2017). Techno-economic evaluation of CO2 enhanced oil recovery (EOR) with the optimization of CO2 supply. *International Journal of Greenhouse Gas Control, 58*, 169-184.

- Lake, L., Johns, R., Rossen, W., & Pope, G. (2014). *Fundamentals of enhanced oil recovery.* Richardson: SPE.
- Liang, S., Altaf, N., Huang, L., Gao, Y., & Wang, Q. (2020). Electrolytic cell design for electrochemical CO2 reduction. *Journal of CO2 Utilization, 35*, 90-105.
- Liu, S., Tao, H., Zeng, L., Liu, Q., & Luo, J. (2017). Shape-dependent electrocatalytic reduction of CO2 to CO on triangular silver nanoplates. *Journal of the American Chemical Society, 139*(6), 2160-2163.
- Luckow, P., Stanton, E., Fields, S., Biewald, B., Jackson, S., Fisher, J., et al. (2015). *2015 carbon dioxide price forecast.* Cambridge, MA: Synapse Energy Economics, Inc.
- Meyer, C. (2004). Concrete materials and sustainable development in the USA. *Structural Engineering International, 14*(3), 1348-1356.
- Mukiza, E., Zhang, L., Liu, X., & Zhang, N. (2019). Utilization of red mud in road base and subgrade materials: A review. *Resources, Conversation, and Recycling, 141*, 187-199.
- Myers, C., Nakagaki, T., & Akutsu, K. (2019). Quantification of the CO2 mineralization potential of ironmaking and steelmaking slags under direct gas-solid reactions in flue gas. *International Journal of Greenhouse Gas Control, 87*, 100-111.

- Nagasawa, H., Yamasaki, A., Iizuka, A., Kumagai, K., & Yanagisawa, Y. (2009). A new recovery process of carbon dioxide from alkaline carbonate solution via electrodialysis. *AIChE Journal, 55*(12), 3286-3293.
- Naims, H. (2016). Economics of carbon dioxide capture and utilization -- a supply and demand perspective. *Environmental Science and Pollution Research, 23*(22), 22226-22241.
- Nair, M., & Abanades, S. (2016). Tailoring hybrid nonstoichiometric ceria redox cycle for combined solar methane reforming and thermochemical conversion of H2O/CO2. *Energy & Fuels, 30*(7), 6050-6058.
- Nikoo, M., & Amin, N. (2011). Thermodynamic analysis of carbon dioxide reforming of methane in view of solid carbon formation. *Fuel Processing Technology, 92*(3), 678-691.
- Niu, K., Xu, Y., Wang, H., Ye, R., Xin, H., Lin, F., et al. (2017). A spongy nickel-organic CO2 reduction photocatalyst for nearly 100% selective CO production. *Science Advances, 3*(7), 1-9.
- Noyori, R. (1999). Supercritical fluids: Introduction. *Chemical Reviews, 99*(2), 353-354.
- Núñez-López, V., Gil-Egui, R., & Hosseini, S. (2019). Environmental and operational performance of CO2-EOR as a CCUS technology: A Cranfield example with dynamic LCA considerations. *Energies, 12*(3), 448.

- Pade, C., & Guimaraes, M. (2007). The CO_2 uptake of concrete in a 100-year perspective. *Cement and Concrete Research, 37*(9), 1348-1356.
- Pan, S., Adhikari, R., Chen, Y., Li, P., & Chiang, P. (2016). Integrated and innovative steel slag utilization for iron reclamation, green material production and CO_2 fixation via accelerated carbonation. *Journal of Cleaner Production, 137*, 617-631.
- Pardal, T., Messias, S., Sousa, M., Machado, A., Rangel, C., Nunes, D., et al. (2017). Syngas production by electrochemical CO_2 reduction in an ionic liquid based-electrolyte. *Journal of CO2 Utilization, 18*, 62-72.
- Pawelec, B., Damyanova, S., Arishtirova, K., Fierro, J., & Petrov, L. (2007). Structural and surface features of PtNi catalysts for reforming of methane with CO_2. *Applied Catalysis A: General, 323*, 188-201.
- Qu, J., Zhang, X., Wang, Y., & Xie, C. (2005). Electrochemical reduction of CO_2 on RuO_2/TiO_2 nanotubes composite modified Pt electrode. *Electrochimica Acta, 50*(16-17), 3576-3580.
- Ramsey, E., Qiubai, S., Zhang, Z., Zhang, C., & Wei, G. (2009). Mini-Review: Green sustainable processes using supercritical fluid carbon dioxide. *Journal of Environmental Sciences, 21*(6), 720-726.
- Ren, D., Deng, Y., Handoko, A., Chen, C., Malkhandi, S., & Yeo, B. (2015). Selective electrochemical reduction of carbon dioxide to ethylene and ethanol on copper (I) oxide catalysts. *ACS Catalysis, 5*(5), 2814-2821.

- Renforth, P., Mayes, W., Jarvis, A., Burke, I., Manning, D., & Gruiz, K. (2012). Contaminant mobility and carbon sequestration downstream of the Ajka (Hungary) red mud spill: the effects of gypsum dosing. *Science of the Total Environment, 421*, 253-259.
- Reuillard, B., Ly, K., Rosser, T., Kuehnel, M., Zebger, I., & Reisner, E. (2017). Tuning product selectivity for aqueous CO2 reduction with a Mn (bipyridine)-pyrene catalyst immobilized on a carbon nanotube electrode. *Journal of the American Chemical Society, 139*(41), 14425-14435.
- Rezaei, M., Alavi, S., Sahebdelfar, S., & Yan, Z. (2006). Syngas production by methane reforming with carbon dioxide on noble metal catalysts. *Journal of Natural Gas Chemistry, 15*(4), 327-334.
- Ripke, S., Eisele, T., & Kawatra, S. (2004). Effects of retained calcium ions in iron ore filtration and pelletization performance. In Laskowski (Ed.), *Particle Size Enlargement in Mineral Processing-Proc. 5th UBC-McGill Int. Symposium* (pp. 384-391). Hamilton: Metallurgical Society of Canadian Institute of Mining and Metallurgy.
- Rivera, R., Ulenaers, B., Ounoughene, G., Binnemans, K., & Van Gerven, T. (2018). Extraction of rare earths from bauxite residue (red mud) by dry digestion followed by water leaching. *Minerals Engineering, 119*, 82-92.
- Rochelle, G. (2009). Amine scrubbing for CO2 capture. *Science, 325*(5948), 1652-1654.

- Rogelj, J., Den Elzen, M., Höhne, N., Fransen, T., Fekete, H., Winkler, H., et al. (2016). Paris Agreement climate proposals need a boost to keep warming well below 2 C. *Nature, 534*(7609), 631-639.
- Rostami, V., Shao, Y., & Boyd, A. (2012). Carbonation curing versus steam curing for precast concrete production. *Journal of Materials in Civil Engineering, 24*(9), 1221-1229.
- Rostami, V., Shao, Y., Boyd, A., & He, Z. (2012). Microstructure of cement paste subject to early carbonation curing. *Cement and Concrete Research, 42*(1), 186-193.
- Sahu, R., Patel, R., & Ray, B. (2010). Neutralization of red mud using CO2 sequestration cycle. *Journal of hazardous materials, 179*(1-3), 28-34.
- Shao, Y., Mirza, M., & Wu, X. (2006). CO2 sequestration using calcium-silicate concrete. *Canadian Journal of Civil Engineering, 33*(6), 776-784.
- Sokolov, S., Kondratenko, E., Pohl, M., Barkschat, A., & Rodemerck, U. (2012). Stable low-temperature dry reforming of methane over mesoporous La2O3-ZrO2 supported Ni catalyst. *Applied Catalysis B: Environmental, 113*, 19-30.
- Spigarelli, B. P., & Kawatra, S. K. (2013). Opportunities and challenges in carbon dioxide capture. *Journal of CO2 Utilization, 1*, 69-87.
- Sweatman, R., Crookshan, S., & Edman, S. (2011). Outlook and technologies for offshore CO2 EOR/CCS projects. *Offshore Technology Conference.* Houston, TX: Offshore Technology Conference.

- Tarek, M., Karim, K., Sarkar, S., Deb, A., Ong, H., Abdullah, H., et al. (2019). Hetero-structure CdS-CuFe2O4 as an efficient visible light active photocatalyst for photoelectrochemical reduction of CO2 to methanol. *International Journal of Hydrogen Energy, 44*(48), 26271-26284.
- Uhm, S., & Kim, Y. (2014). Electrochemical conversion of carbon dioxide in a solid oxide electrolysis cell. *Current Applied Physics, 14*(5), 672-679.
- Ulissi, Z., Medford, A., Bligaard, T., & Nørskov, J. (2017). To address surface reaction network complexity using scaling relations machine learning and DFT calculations. *Nature Communications, 8*(1), 1-7.
- Valluri, S., & Kawatra, S. (2019). A Step Change for Carbon Dioxide Capture - Enhancement with Frothing Agents. *SME Annual Conference and EXPO.* Denver, CO.
- Valluri, S., & Kawatra, S. (2019). Electro catalytic reduction of CO2 to oxalic acid. *SME Annual Conference and EXPO 2019.* Denver, CO: SME.
- Valluri, S., & Kawatra, S.K. 2021a, Use of frothers to improve the absorption efficiency of dilute sodium carbonate slurry for post combustion CO2 capture. *Fuel Processing Technology*, Vol. 212, p.106620.
- Valluri, S., Kawatra, SK. 2021b, Reduced reagent regeneration energy for CO2 capture with bipolar membrane electrodialysis. *Fuel Processing Technology,* p. In press.

- Valluri, S., & Kawatra, SK. 2020, Simultaneous capture of NO, SO2 and CO2 using sodium carbonate solution promoted with H2O2/NaOCl. *Journal of Environmental Sciences*, p. In press.
- Vass, C., Noble, A., & Ziemkiewicz, P. (2019). The Occurrence and Concentration of Rare Earth Elements in Acid Mine Drainage and Treatment Byproducts: Part 1 -- Initial Survey of the Northern Appalachian Coal Basin. *Mining, Metallurgy & Exploration, 36*(5), 903-916.
- Wallace, M., Leewen, T., & Kuuskraa, V. (2011). *Improving domestic energy security and lowering CO2 emissions with 'next generation' CO2-enhanced oil recovery.* NETL.
- Wang, H., Zhu, R., Wang, X., & Li, Z. (2017). Utilization of CO2 in metallurgical processes in China. *Mineral Processing and Extractive Metallurgy, 126*(1-2), 47-53.
- Wang, J., Li, G., Li, Z., Tang, C., Feng, Z., An, H., et al. (2017). A highly selective and stable ZnO-ZrO2 solid solution catalyst for CO2 hydrogenation to methanol. *Science Advances, 3*(10), 1-10.
- Wang, L., Sun, N., Tang, H., & Sun, W. (2019). A review on comprehensive utilization of red mud and prospect analysis. *Minerals, 9*(6), 362.
- Wei, N., Li, X., Dahowski, R., Davidson, C., Liu, S., & Zha, Y. (2015). Economic evaluation on CO2-EOR of onshore oil fields in China. *International Journal of Greenhouse Gas Control, 37*, 170-181.

- Weng, W., Jiang, B., Wang, Z., & Xiao, W. (2020). In situ electrochemical conversion of CO_2 in molten salts to advanced energy materials with reduced carbon emissions. *Science Advances, 6*(9), 1-7.
- Whipple, D., Finke, E., & Kenis, P. (2010). Microfluidic reactor for the electrochemical reduction of carbon dioxide: the effect of pH. *Electrochemical and Solid-State Letters, 13*(9), B109-B111.
- Wilcox, J. (2012). *Carbon capture.* New York: Springer.
- Yan, Y., Zeitler, E., Gu, J., Hu, Y., & Bocarsly, A. (2013). Electrochemistry of aqueous pyridinium: exploration of a key aspect of electrocatalytic reduction of CO_2 to methanol. *Journal of the American Chemical Society, 135*(38), 14020-14023.
- Yang, H., Hung, S., Liu, S., Yuan, K., Miao, S., Zhang, L., et al. (2018). Atomically dispersed Ni (I) as the active site for electrochemical CO_2 reduction. *Nature Energy, 135*(38), 140-147.
- Yi, C., Zhu, R., Chen, B., Wang, C., & Ke, J. (2009). Experimental research on reducing the dust of BOF in CO_2 and O_2 mixed blowing steelmaking process. *ISIJ International, 49*(11), 1694-1699.
- Zhang, D., & Shao, Y. (2016). Effect of early carbonation curing on chloride penetration and weathering carbonation in concrete. *Construction and Building Materials, 123*, 516-526.

- Zhang, K., Li, S., & Liu, L. (2020). Optimized foam-assisted CO2 enhanced oil recovery (EOR) with the optimization of CO2 supply. *Fuel, 267*, 117099.
- Zhou, F., Liu, S., Yang, B., Wang, P., Alshammari, A., & Deng, Y. (2014). Highly selective electrocatalytic reduction of carbon dioxide to carbon monoxide on silver electrode with aqueous ionic liquids. *Electrochemistry Communications, 46*, 103-106.

2. Use of frothers to improve the absorption efficiency of dilute sodium carbonate slurry for post combustion CO_2 capture

2.1 Abstract:

With current environmental regulations, CO_2 capture is very crucial for the survival of coal-fired power plants in the near future. In this work, the CO_2 absorption performances of Na_2CO_3, NaOH, Monoethanolamine (MEA) and frother-enhanced Na_2CO_3 were investigated experimentally in a pilot scale gas−liquid countercurrent column. A surfactant was added to the sodium carbonate solution in order to increase the surface area available for CO_2 transport within the packed bed. This increased the CO_2 capture efficiency of dilute sodium carbonate slurry from 55.6% to 99.9%, before reaching saturation. The main intent of this study is to compare the efficiency of frothers and conventional reagents for chemical absorption CO_2 capture. We analyzed the advantages and disadvantages of each of these reagents along with frother-enhanced sodium carbonate slurry.

2.2 Introduction:

Efforts to capture CO_2 at some power plants have been successful, but the cost of installing and operating the required equipment is high. As such, very few power plants have carbon capture and storage (CSS) systems. In order for the sale of captured CO_2 to become a profitable venture, the cost of capturing the CO_2 from a flue gas must be reduced. Several post-combustion CO_2 capture technologies exist, such as chemical absorption, physical adsorption and membrane separation (Zeng et al., 2013; Rochelle, 2009; Toan et al., 2019; Dietrich et al., 2018). Among all of these technologies, chemical absorption CO_2 capture is the most competitive and economically viable for CO_2 capture from fossil fuel fired power plants (Zeng et al., 2013; Wang et al., 2017).

An efficient CCS process should have substantially lower operating costs compared to conventional aqueous absorbents without sacrificing effectiveness. Amines have been dominant in CO_2 capture research (Rochelle, 2009). However, the cost for thermal regeneration of amine reagents is high (Toan et al., 2019; Laribi et al., 2019; Salmón et al., 2018). Amines also present other problems, including: corrosion of equipment, fouling smell from equipment and reagent degradation due to the high volatility of amines. Although aqueous amine technology could easily scale-up to commercial plants, there is a need for alternative solvents to overcome the drawbacks mentioned above. Carbonate-based solvents have recently garnered attention, due to their low cost and non-corrosive nature. CO_2 capture with dilute sodium carbonate solution was first patented by Kawatra et al. (2011). Later there were several improvements made for this process, most recently Barzagli et al. (2017) have tested dilute sodium carbonate solution for CO_2 capture and were able to achieve 80% CO_2 absorption efficiency.

The rate of absorption of CO_2 in carbonate solutions is limited by the rate of physical mass transfer. Thus, increasing the mass transfer kinetics with the help of surfactants can increase the CO_2 absorption efficiency of sodium carbonate. In this paper, we will show that the increased efficiency provided by surfactants allows even dilute sodium carbonate solutions to achieve 99.9% CO_2 capture.

2.2.1 CO_2 Capture through Chemical Absorption:

In the chemical absorption process, flue gas enters the bottom of a column while a scrubbing solution is pumped to the top. The scrubbing solution is an alkaline solution suitable for the absorption of CO_2. The fluids interact in a packed bed, where the CO_2 is transported from the gaseous phase to the liquid phase. The absorbed CO_2 exits the bottom of the column either reacting or complexing with the absorbent (Liu and Okazaki, 2003). After passing through the scrubbing column, the CO_2 loaded scrubbing solution should be regenerated for reuse. Commonly, the regeneration is performed by thermal decomposition. The CO_2 loaded solution is heated so as to reverse the absorption reaction between the absorbent and the CO_2. The resulting off-gas is a nearly pure CO_2 stream while the liquid phase is a solution of the regenerated absorbent. The regenerated scrubbing solution is then returned to the column (Metz et al., 2005; Yang et al., 2008; Olajire, 2010; Pires et al., 2011). The overall CO_2 absorption reactions with sodium carbonate, sodium hydroxide and amines can be seen in equations 1-3 respectively (Peng et al., 2012). The reagent make-up cost is one of the largest operating costs in post-combustion CO_2 capture. Table 1 shows the reagent cost and CO_2 loading capacity of amines, NaOH and sodium carbonate. Reagent costs are to-date (2020) $/ton prices from Alibaba. Sodium carbonate has the lowest cost and least regeneration energy (Table 1) compared to the other two reagents. If sodium carbonate absorption kinetics can be enhanced then CO_2 capture can be achieved at a lower cost. This can be achieved by improving the mass transfer of CO_2 into the aqueous phase with an additive.

$$\mathrm{Na_2CO_{3(s)} + H_2O_{(l)} + CO_{2(g)} \rightarrow 2NaHCO_{3(aq)}} \quad (1)$$

$$\mathrm{NaOH_{(aq)} + CO_{2(g)} \rightarrow NaHCO_{3(aq)}} \quad (2)$$

$$\mathrm{CO_2 + RR'NH + H_2O \leftrightarrow (RR'NH_2^+)(HCO_3^-)} \quad (3)$$

Table 7: Comparison table for cost and CO_2 capture capacity of different reagents.

(Laribi et al., 2019; Spigarelli and Kawatra, 2013; Mahmoudkhani and Keith, 2009; Rao et al., 2006; Nelson et al., 2013; Olutoye and Eterigho, 2008).

Type of Absorbent	**Capacity (kg CO_2/kg absorbent)**	**Regeneration Energy (MJ/Kg CO_2)**	**Reagent Cost ($/ton of reagent)**	**Corrosion**
Amines (MEA, DEA, etc.)	0.40	3.9 - 4.3	1400-1800	Highly corrosive to pipes and equipment
Alkali solution (NaOH, KOH)	0.55	3.5 - 3.9	400-450	Corrosive to pipes and equipment due to high pH

Sodium carbonate (Na_2CO_3)	0.42	3.2 - 3.8	225-240	Non-corrosive

The only drawback of sodium carbonate slurry is the slower absorption rate of CO_2 when compared to amines and NaOH. This will result in tall absorption columns for sodium carbonate system. This slower absorption rate dictates that rate-increasing additives like surfactants are required for Na_2CO_3 slurry to be feasible for CO_2 capture. Previous literature suggests that hypochlorite, formaldehyde, piperazine (PZ), phenols, dextrose, diethanolamine (DEA), and monoethanolamine (MEA) will increase the absorption rate, but these additives will also make the energy required for reagent regeneration higher (Cullinane and Rochelle, 2004; Mahajani and Danckwerts, 1983; Mahajani and Danckwerts, 1963; Hairul et al., 2017). These additives also cause undesirable oxidative degradation and corrosion (Stowe and Hwang, 2017).

We have identified an additive that will increase the absorption rate of Na_2CO_3 slurry but will have no effect on the energy required for reagent regeneration. This additive is a frother, added at 5-20ppm. To the best of the authors' knowledge, this method is novel and has never previously been reported in literature.

2.3 Frother Mechanism:

Frothers are surfactants that adsorb on the liquid-air interface of the bubbles, reducing the surface tension and thereby decreasing the bubble size as shown in Figure 13. The

CO_2 absorption rate of sodium carbonate is low compared to NaOH and MEA due to limited kinetics from the low concentration of CO_2 in aqueous solution. One way to overcome this obstacle is to increase the rate of physical mass transfer, which can be achieved by creating smaller and uniform bubbles. This decrease in size will increase the interfacial interaction area between gas and liquid increasing the mass transfer rate and allowing more gas to be absorbed faster.

Bubble size can be influenced by adding surfactants known as frothers. Frothers prevent bubble coalescence, which stops the bubbles from becoming bigger and thereby producing tiny and uniform bubbles (Cho and Laskowski, 2002; Castro et al., 2013). Frothers have a polar hydrocarbon group and a non-polar group, with the non-polar group will be oriented towards the air and the polar group adsorbed at the air-liquid interface as shown in Figure 13(b).

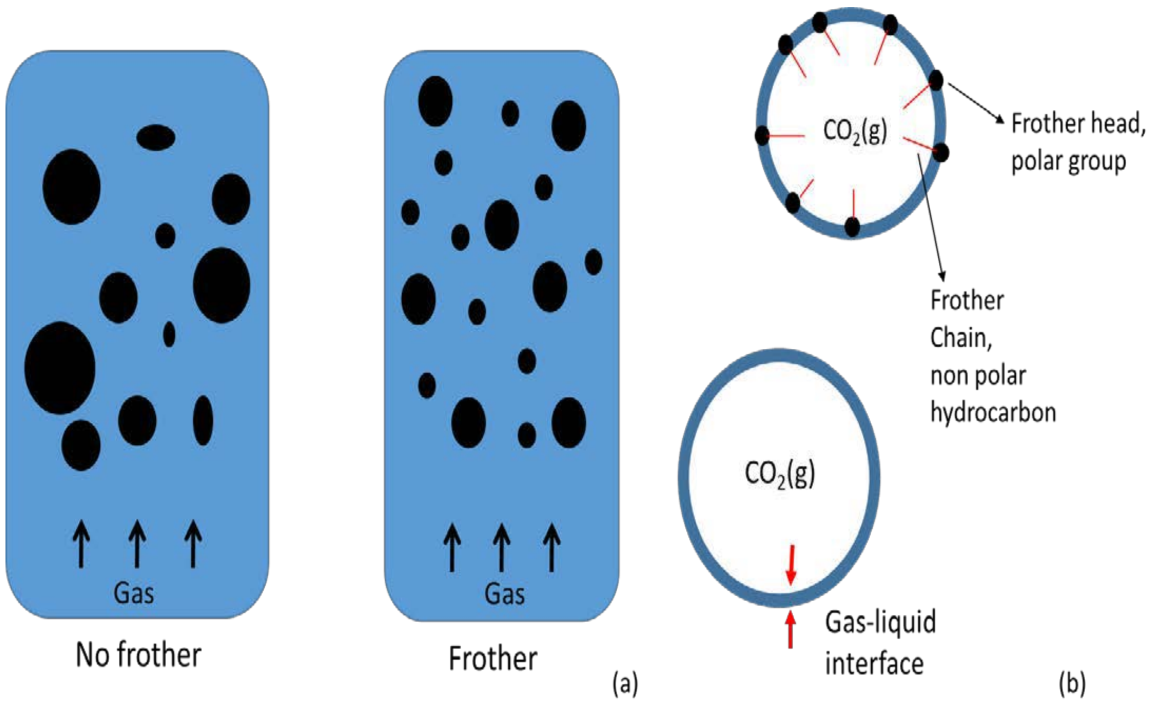

Figure 13: (a) Effect on bubble generation with and without frother (b) Frother attachment to the bubble.

2.3.1 Frother effect on bubble size

Cho and Laskowski (2002) have studied the frother effect on bubble size extensively. They found that frother effect on bubble size is determined by their ability to prevent coalescence of the bubbles. As frother concentration increases, the magnitude of bubble coalescence decreases. Concentration of critical coalescence (CCC) is defined as the concentration beyond which the coalescence of the bubbles is completely hindered.

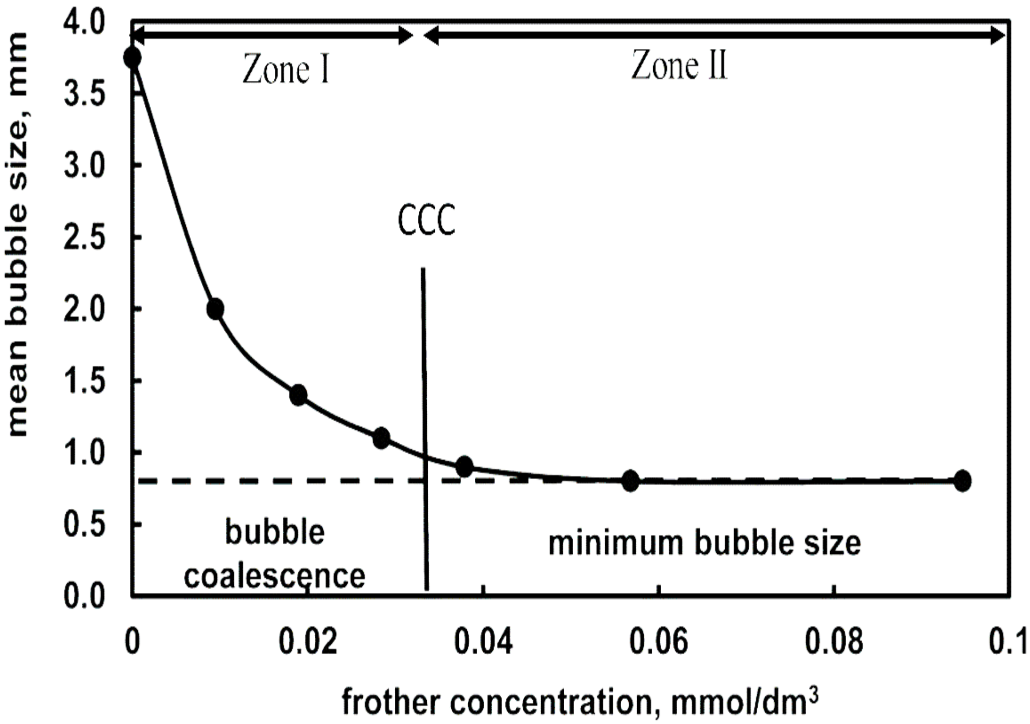

Figure 14: Effect of frother concentration on bubble size

(Kowalczuk, 2013)

After critical coalescence concentration (CCC) is reached as shown in Figure 14, the curve reaches an asymptote to the horizontal. Beyond CCC increasing the frother concentration does not affect the bubble size. In Zone I coalescence determines bubble size, and in Zone II the breakage process in the impeller neighborhood and dynamic conditions control the size of the bubbles. A single value called the mean diameter can represent the diameter of a collection of these bubbles. There are several ways to calculate the mean diameter of a population of bubbles, one of which is Sauter mean diameter (Kowalczuk and drzymala, 2016). The Sauter mean diameter (D_{32}) is widely used to characterize the influence of surfactants on the size of bubbles (Kowalczuk and drzymala, 2017).

Critical coalescence concentration (CCC) characterizes a frother's ability to prevent coalescence of bubbles. At frother concentrations lower than CCC, coalescence is the main factor deciding the bubble size. At frother concentrations exceeding CCC, coalescence no longer determines the bubble size. It will then depend on hydrodynamic conditions, sparger's geometry and speed. Table 8 shows CCC values of different frothers.

Table 8: Summary of CCC and HLB values for different frothers.

(Kowalczuk, 2013; Khoshdast and Sam, 2011; Zhang et al., 2012)

Frother Type	**Frother Name**	**Molecular Weight (g/mol)**	**HLB**	**CCC (ppm)**
Aliphatic Alcohols	1-Propanol	60	7.48	236
	1-Butanol	74	7	63
	1-Pentanol	88	6.53	25
	1-Hexanol	102	6.05	11
	1-Heptanol	116	5.58	8

	1-Octanol	130	5.1	8
	2-Propanol	60	7.48	307
	2-Butanol	74	7	77
	2-Pentanol	88	6.53	30
	2-Hexanol	102	6.05	11
	2-Heptanol	116	5.58	9
	2-Octanol	130	5.1	8
	3-Pentanol	88	6.53	41
	3-Hexanol	102	6.05	13
Polypropylene Glycol Ethers	Propylene Glycol Methyl Ether	90	8.28	44
	Propylene Glycol Propyl Ether	118	7.33	29
	Propylene Glycol Butyl Ether	132	6.85	21
	Di(Propylene Glycol) Methyl Ether	148	8.13	26

	Di(Propylene Glycol) Propyl Ether	176	7.18	16
	Di(Propylene Glycol) Butyl Ether	190	6.7	12
	Tri(Propylene Glycol) Methyl Ether	206	7.98	15
	Tri(Propylene Glycol) Propyl Ether	234	7.03	11
	Tri(Propylene Glycol) Butyl Ether	248	6.55	7

Polypropylene Glycols	Di Propylene Glycol	134	9.25	53
	Tri Propylene Glycol	192	9.125	33
	Tetra Propylene Glycol	250	9	22
	Polypropylene Glycol 425	425	8.625	6
	Polypropylene Glycol 725	725	8	7
	Polypropylene Glycol 1000	1000	7.375	8
Commercial Frothers	DF250	264	7.83	10
	DF1012	420	7.48	6
	F150	425	8.625	6
	F160	217	6.63	8

Castro et al. (2013) have studied the effect of frothers on bubble coalescence and foaming. They concluded that CCC values of MIBC is much higher than DF-250 and other polyglycol type frothers. Also among Polyglycol type frothers, with increasing molecular weight CCC value decreases as shown in Figure 15. This figure shows the bubble size vs. frother concentration curves of frothers DF-250, DF-400, DF-1012 and MIBC demonstrating the phenomenon of bubble coalescence and the critical concentration of coalescence in tap water. The results show that DF-250 frother prevents bubble coalescence more effectively than MIBC frother. This behavior is in accordance with their activity on the surface.

If we consider the surface chemistry point of view, alcohols are weak surface-active agents and thus unable to significantly reduce surface tension (Laskowski, 1998). Polyglycol frothers are highly surface-active agents capable of significantly decreasing surface tension and creating deep froth. In industrial flotation processes, pentanol and MIBC are commonly used alcohol frothers, and when it comes to poly-glycol type frothers Polypropylene Glycols (PPG) and Dowfroths (DF) are frequently used.

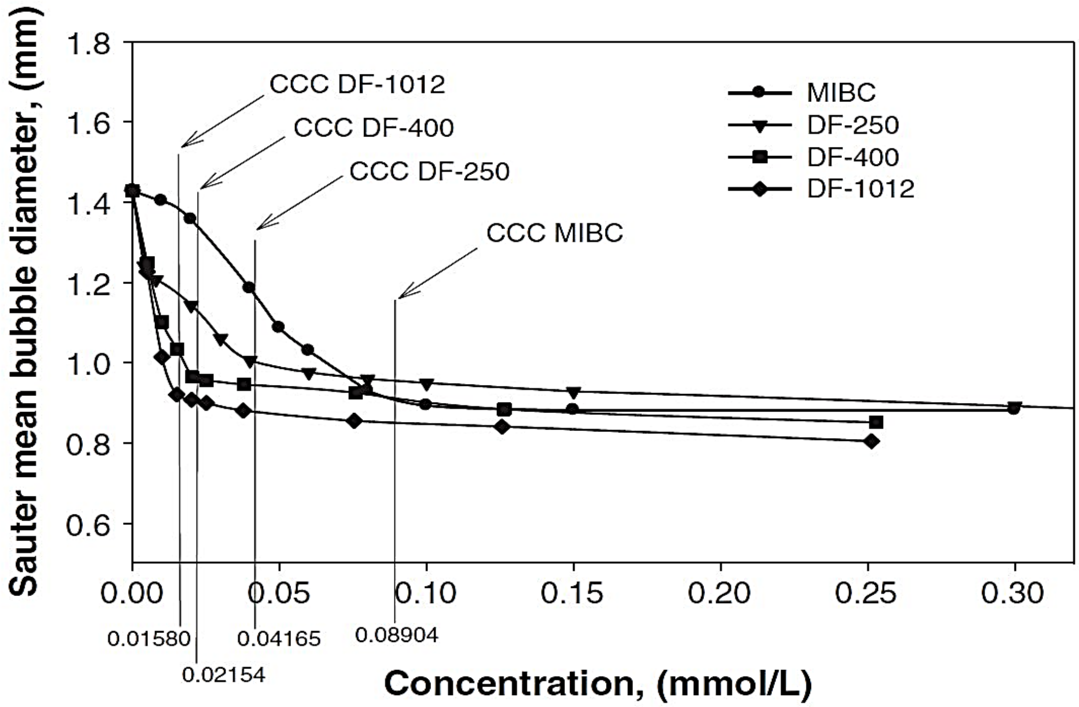

Figure 15: Bubble size distribution vs frother concentration

(Reproduced with permission from Castro et al., 2013 with the kind permission of Elsevier. Copyright 2013).

2.3.2 Influence of frother type on bubble size:

Grau et al. (2005) studied the effect of frother type on bubble size. They observed that the general trend was similar for all the investigated frother types, with increasing frother dosage bubble size decreased and the size of the bubble was levelled off at a particular concentration. This can be seen in Figure 9. Frothers control the size of the bubble by reducing the coalescence of the bubble in the cell and that coalescence is completely prevented in a dynamic system at concentrations exceeding the critical coalescence concentration (CCC) (Cho and Laskowski, 2002).

Figure 9 shows the bubble size distributions measured by Grau and Heiskanen (2005) at different frother dosages. From Figure 16 it is clear that different bubble sizes were observed at concentrations of frother above the CCC values. It can therefore be said that DF-200 was the most effective frother in reducing the size of the bubble and DF-1012 was the least efficient one. These results indicate that the frothers will not only prevent coalescence but also in some ways effect the disintegration of bubbles in turbulent situations, and this effect does not appear to be related directly to the solution's surface tension. These results do not mean that a particular frother is more efficient in flotation than the other, but actually compares them in terms of the distribution of bubble size.

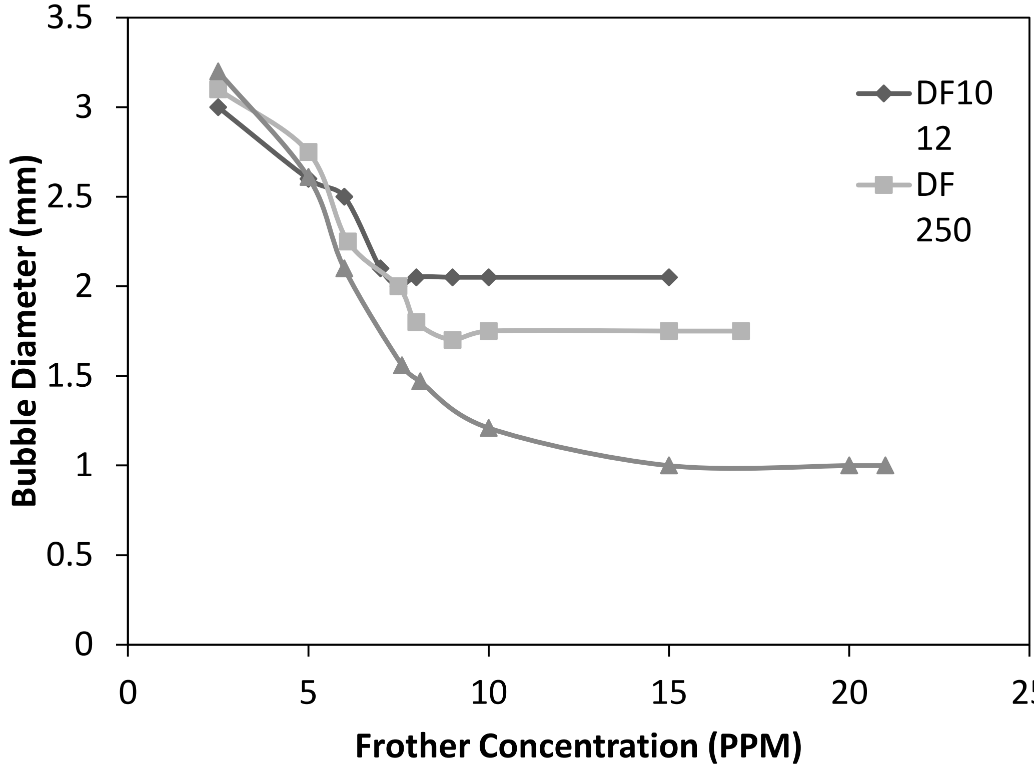

Figure 16: Bubble size distribution vs frother concentration

(Adapted from data published by Grau and Heiskanen 2005).

2.4 Experimental:

2.4.1 Column Properties:

A CO_2 capture system was designed and built as shown in Figure 17. Polypropylene pall rings (1.2cm×1.2cm) are used as packing in the scrubber column. The height of a packed bed scrubbing column (Z) is calculated using the contact tower design equation (Equation 4). Where G_s represents molar flow of solute-free gas per cross-sectional area of the column. a is the interfacial area available for mass transport. K_y accounts for overall gas phase mass transfer coefficient. Y is the fraction of moles of gas phase solute per moles of solute-free gas, and Y^* denotes the gas phase mole fraction in equilibrium with the liquid phase. The denominator of the integral represents the driving force for mass transfer and is integrated over the condition of the gas phase from the top to the bottom of the column (Geankoplis, 1997).

$$Z = \frac{G_S}{K_y * a} \int_{Y_2}^{Y_1} \frac{dY}{Y - Y^*} \qquad (4)$$

Given that the interfacial area a is in the denominator of the design equation, it is advantageous to have a large amount of interfacial area within the scrubbing column (Tan et al., 2016).

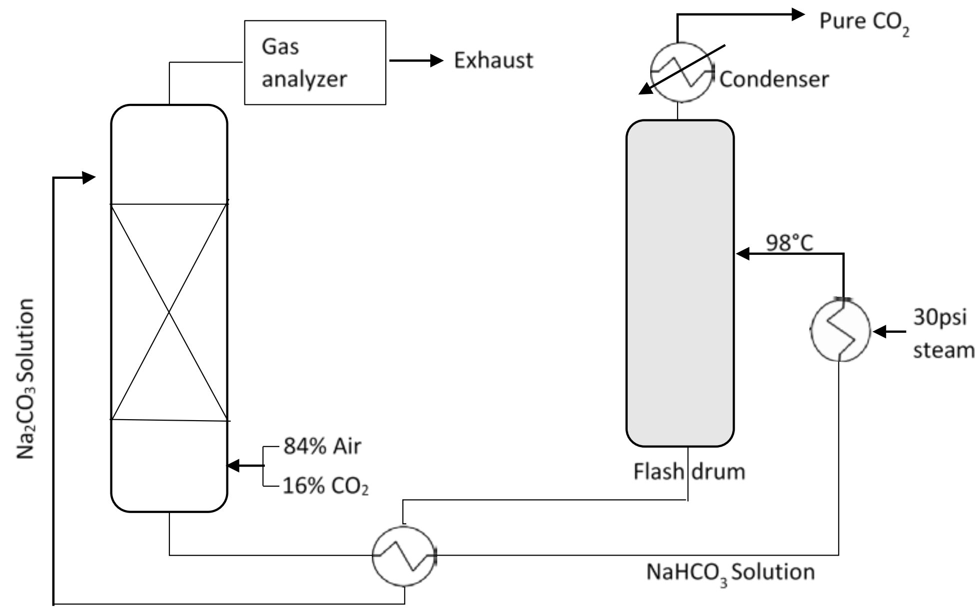

Figure 17: Process flow diagram for CO_2 Scrubber System

As shown in Figure 17, CO_2 mixed with air is fed into the scrubbing column from the bottom. After CO_2 is absorbed with sodium carbonate solution, the resultant sodium bicarbonate solution is preheated by the regenerated sodium carbonate solution from the flash drum, thus cooling down the scrubbing solution before pumping it back into the scrubber.

2.5 Materials and Methods:

2.5.1 CO_2 absorption experiments without frother addition.

The mini-pilot scale setup shown in Figure 17 was used to conduct experiments on % of CO_2 absorbed with sodium carbonate and other reagents. The packed-bed absorption column (Height: 274.3cm, Diameter: 10.16cm; Packing: Polypropylene pall rings

1.2cm×1.2cm; Packed bed height: 121.92cm) shown on the left side in Figure 17 is used as a counter current absorption column. The top portion of the capture column (213.36cm) is made of see through polyacrylic plastic and the bottom portion is made of steel to ensure robustness. For the absorption experiments Na_2CO_3 (99.8% pure) was obtained from Duda Energy while NaOH (99%) and MEA (reagent grade) were obtained from Sigma-Aldrich. The CO_2 gas cylinders (99% pure) were obtained from Grainger. In order to simulate the flue gas, a gaseous mixture containing 16% by volume CO_2 and rest air was continuously fed into the bottom of the scrubbing column with the help of a gas diffuser. Gas flow rate was maintained at 21LPM. Separate flow meters were installed for CO_2 and air to measure the volumetric flow and to control the percentage of CO_2 in the gas stream. CO_2 and air flow rates were measured with gas flow meters (OMEGA) equipped with gas controllers (McMaster-Carr).

The %CO_2 of the simulated flue gas exiting out from the top of the column was measured with Quantek Model 906 infrared gas analyzer calibrated with a 20-vol% CO_2/N_2 reference gas. Several flow rates (3 - 10 Liters per minute) were tested for the aqueous solutions of Na_2CO_3, NaOH and MEA. The data on % of CO_2 absorbed was continuously recorded by the data logger connected to the gas analyzer. After each experiment the data logger was connected to the computer and the graph generated from it was integrated to calculate the total moles of CO_2 absorbed per minute. The accuracy of the data was ensured by repeating these experiments in triplicates. For a 16% CO_2 gas stream (simulating a power plant flue gas) the optimum parameters were found to be: 0.2M sodium carbonate solution at 7.5 Liters per minute flow rate. The effect of temperature on absorption efficiency was also studied by heating the scrubbing solution with immersion tank heater to vary the temperature of the Na_2CO_3 solution from 25°C to 60°C. The CO_2 is regenerated along with the scrubbing solution as shown in Figure 2 and is again recycled through the scrubbing column. Table 2 shows the typical operating conditions for the CO_2 scrubbing and regeneration setup.

Table 9: Typical operating parameters for the scrubbing setup shown in Figure 17.

Experimental Conditions	
Scrubbing solution flowrate	7.5L/min
Gas inlet temperature	31°C
Scrubbing solution inlet temperature	38.5°C
Column Operating pressure	101.325 kPa
Liquid/ gas-ratio (Kg/Kg)	4.3
Gas composition	16%vol CO_2, rest air
Desorption temperature	98°C

2.5.2 CO_2 absorption experiments with frother addition.

Frothers were added in traces to the Na_2CO_3 solution to create small and uniform bubbles when air is introduced into the liquid solution. We tested several frothers (Table 10) at varying concentrations from 5ppm to 20ppm at 5ppm increments. Absorption efficiency of frother modified sodium carbonate solution was recorded at regular intervals of time. These frothers were obtained from Cytec Solvay group. Although prices of most of these frothers are considered a trade secret, our average estimate from internal sources is around 1.2 -1.4$/Kg.

Table 10: Type of the frother used and their properties.

Frother Name	**Manufacturer**	**Frother Type**	**Molecular Formula**	**Molecular Weight (MW)**
DF200	DOW Chemicals	Polyglycol	$CH_3(C_3H_6O)_3OH$	206.29
DF250	DOW Chemicals	Polyglycol	$CH_3(C_3H_6O)_4OH$	264.37
DF400	DOW Chemicals	Poly glycol	$H(C_3H_6O)_{6.5}OH$	395.61

AF68	Solvay	Polyglycol (Mixture)	-	-
AF70	Solvay	Alcohol	$(CH_3)_2CHCH_2CHOHCH_3$	102.17

2.5.3 Reagent regeneration and heat duty:

The reagent regeneration setup (CO_2 stripper) consists of a series of heat exchangers accompanied by a 19 Liter flash drum and a condenser. The overall heat recycle loop is provided in Figure 18. The waste heat is reused with the help of heat exchangers for the thermal regeneration setup. Looking at the regeneration system energetically, the heat required to heat the inlet is already present in the outlet, so the heat that needs to be added should be no more than required to make up the heat lost due to entropy. This should allow us to significantly reduce the energy cost from 90kWhr/m^3 to something closer to 3 to 7kWhr/m^3. The total regeneration energy is calculated based on energy provided and also enthalpy change (ΔH) of the reagent used.

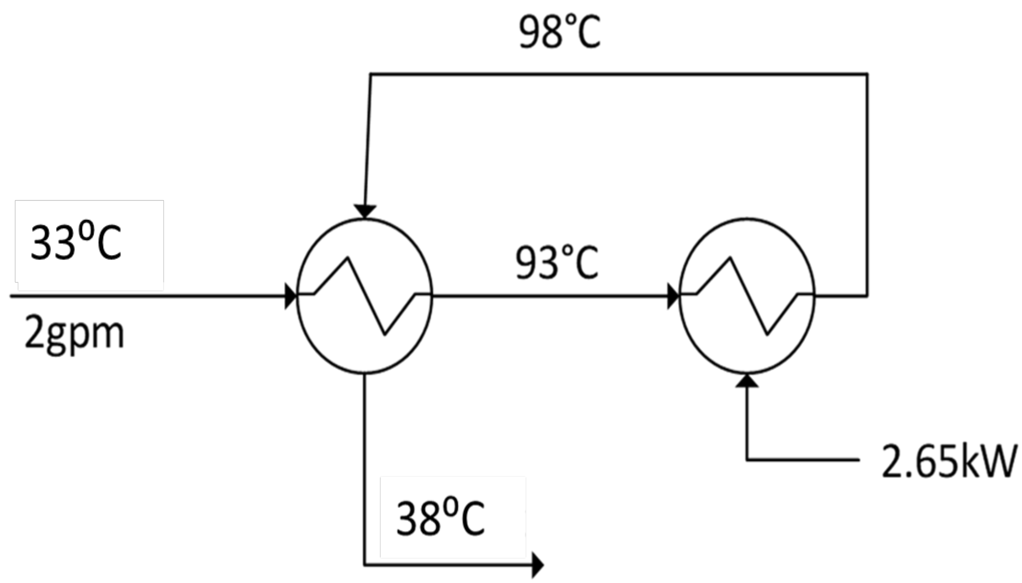

Figure 18: Heat recycle loop. Input heat is provided by steam (30psi), and the regeneration process is omitted from this view (but would take place in-line with the 98°C stream).

2.6 Experimental Procedure:

The setup shown in Figure 17 was used to conduct continuous CO_2 capture and regeneration experiments. The experiment was started by turning the gas on with 16% vol CO_2 and rest air in order to simulate flue gas. Once the gas analyzer starts recording the CO_2 data, sodium carbonate solution from a reserve tank (100 Liter) was pumped to the top of the scrubbing column at 7.5 Liters per minute flow rate and CO_2 absorption data was continuously recorded by data logger on the gas analyzer. After 5 minutes from start, the CO_2 absorption reaches steady state, and then the bicarbonate solution coming out of the scrubbing column deposited in the bicarbonate reserve tank is sent through the desorption setup and the desorbed solution is pumped back into the sodium carbonate reserve tank. The entire CO_2 absorption and desorption setup was then continuously run for 2 hours to ensure no discrepancy. The CO_2 absorption data was continuously recorded by the gas analyzer for 2 hours and no decrease in absorption rate was observed for the entire experiment. Each experiment was repeated three times to ensure reproducibility.

2.7 Results and Discussion:

The gas analyzer continuously measures the percentage concentration of the CO_2 going in and leaving out from the top of the scrubbing column. The absorption efficiency of CO_2 (as % of CO_2 absorbed) is calculated by the following equation:

$$\text{Absorption efficiency (or) \% of } CO_2 \text{ absorbed} = \frac{X_{in}-X_{out}}{X_{in}} \times 100 \qquad (5)$$

Where X_{in} is number of moles of the gas going into the scrubbing column and X_{out} is number of moles of the gas coming out of the scrubbing column.

Initial experiments were conducted on Na_2CO_3 solution, without the addition of frother to compare the CO_2 absorption efficiency of Na_2CO_3 with that of MEA and NaOH. Later, frothers were added to Na_2CO_3 solution at 5ppm incremental concentrations. Adding frothers improved the absorption efficiency of Na_2CO_3 solution from 55.6% to 99.9%. The 99.9% removal is based on 0.05 to 0.1% instrument error of the gas analyzer. Based on the work of Mai and Babb (1955) on vapor-liquid equilibria for carbonate-bicarbonate-water-CO_2 system at 101kPa and 38°C, we have stayed on the lower end of the sodium carbonate concentrations (0.1 - 0.3 mol/L) for conducting CO_2 absorption experiments. Depending on the molar ratio of CO_2 converted and sodium carbonate (0.2 mol/L) used, the fraction of sodium carbonate converted to bicarbonate is only 0.46 without the surfactant, due to slower absorption kinetics. After the addition of surfactant, the conversion increased to 0.81. Which corresponds to 43.2% increase.

The experimental uncertainty is calculated and the error bars are plotted within the 95% confidence interval for all the experiments. These results are discussed in detail in further sections.

2.7.1 Absorption results without the addition of frothers:

Based on equation (5), the % of CO_2 absorbed was calculated from start of the experiment until it reaches steady state and a maximum absorbance as shown in figure 19. We have conducted initial experiments with NaOH, monoethanolamine (MEA) and Na_2CO_3 on our scrubbing column to compare the reagents for CO_2 capture efficiency. Experimental results suggest that the absorption efficiency of amines and NaOH is almost the same, while the absorption efficiency of Na_2CO_3 is much less compared to the other two. The absorption efficiency of these reagents was noted at a concentration of 0.1M, 0.2M and 0.3M in water, with 2-3% uncertainty.

The % of CO_2 absorbed at 0.1M concentration for NaOH and MEA is almost the same and is 95%, but for Na_2CO_3 it is between 30-40%. Curves in Figure 19 show the %CO_2 absorbance of all the three reagents at 0.2M concentration. With the increase in concentration from 0.1M to 0.2M, the % of CO_2 absorbed for NaOH and MEA increased from 95 to 97% and for Na_2CO_3 it increased from 40% to 55.6%. We have also tested 0.3M concentration in solution for all three reagents, but no further increase in absorption was observed.

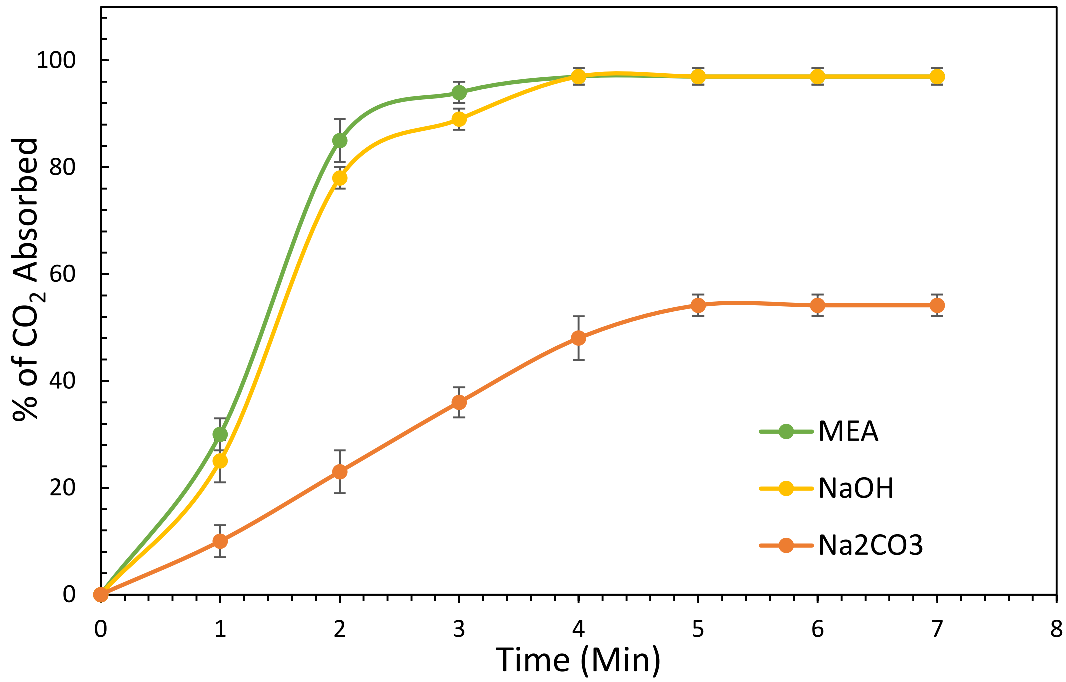

Figure 19: Effect of reagents on CO_2 capture (% of CO_2 absorbed vs. time) at 0.2M Na_2CO_3/NaOH/MEA concentration at 38.5^oC, with the error bars representing standard error.

As shown in Figure 19, in the first three minutes from the start of experiment the % of CO_2 absorbed in case of MEA and NaOH rises to 80-85% very fast and then finally reaching a maximum value of 97% after 5 minutes. For Na_2CO_3 the % of CO_2 absorbed gradually increases to 36% in the first 3 minutes and reaches an asymptote at 55.6% after 5 minutes.

2.7.2 Effect of Temperature on Absorption Efficiency:

Previous studies suggest that a temperature range of 30°-40°C is optimum for CO_2 absorption with sodium carbonate slurry (Spigarelli and Kawatra, 2013). Studies conducted at MTU indicate that with increased temperature, the absorption rate of CO_2 decreases. As the temperature is increased from 25°C to 60°C the rate of absorption of CO_2 decreased by 55%. The reason for decrease in absorption efficiency at higher temperatures is because of decrease in gas solubility at elevated temperatures. Van't Hoff's equation; Equation 6 (Butler, 2019) explains the effect of temperature on the solubility of gas.

$$k_H = k_H^{\circ} \exp\left[\frac{-\Delta H_{solution}}{R}\left(\frac{1}{T} - \frac{1}{T^{\circ}}\right)\right] \qquad (6)$$

$$C = k_H \times (P) \qquad (7)$$

k_H° - Henry's coefficient units - mol/L atm

$\Delta H_{solution}$ - Enthalpy of the solution units - Joules/mol

T - Slurry temperature units – K

R - Universal gas constant units - Joules/mol K

T°- 298 K

C - CO_2 Concentration in the solution units - mol/L

P - Partial pressure of CO_2 in gas phase units - atm

k_H - Henry's Law constant units - mol/L atm

With increase in temperature, from Equation 6, k_H should decrease. Hence, according to Henry's Law (Eq.7), the dissolved CO_2 in solution will decrease. Therefore, the rate of CO_2 absorption decreases at higher temperatures. The optimum temperature was observed to be around 30°C to 39°C.

2.7.3 Addition of Frothers for Improving Rate of Absorption of Na_2CO_3 Slurry:

Adding frothers modifies the bubble surface of the absorbent solution when gas is introduced. Frothers generate smaller and more uniform bubble sizes. This increases the surface area of contact between the gas and liquid improving mass transfer. This improves the absorption efficiency of the scrubbing solution significantly.

The rate at which CO_2 is absorbed into carbonate solutions can be described as follows (Danckwerts, 1951):

$$R_{C02} = -\frac{d[CO_2]}{dt} = k_L a(c^* - c) = k\ [CO_2] \tag{8}$$

Where k_L is mass transfer coefficient and k is the rate constant assuming first order kinetics. Rate of absorption of CO_2 is proportional to gas-liquid interfacial area a, as shown in Equation 8. Increasing the interfacial area available for mass transport is advantageous for a scrubbing solution with slower absorption kinetics. The addition of a frothing agent to the scrubbing solution allows a stable bed of small bubbles to form within the column, increasing the area of gas-liquid interface within the column. This effectively makes up for the low CO_2 absorption rate of sodium carbonate slurry.

Figure 20 clearly shows that enhancing the sodium carbonate solution with a frother greatly increases CO_2 absorption efficiency. The % of CO_2 absorbed is recorded from start of the experiment and is continued to be recorded after reaching steady state as well. Initially it takes time for the bubbles to develop, but after reaching steady state the process is continuous. The frother-enhanced sodium carbonate solution was able to increase the CO_2 absorption efficiency of sodium carbonate solution from 55.6% to 99.9%, which is greater than the absorption performance given by NaOH and MEA. From Figure 20 we can see that the % of CO_2 absorbed reaches 99.9% with DF200, DF250, and AF68. DF400 and AF70 were only able to increase the % of CO_2 absorbed from 55.6% to 62.8%. This can be attributed to the fact that AF70 (MIBC) is a weak frother (Dey et al., 2014), and that DF400 produces larger bubbles compared to the other polyglycols. The effect of bubble size on CO_2 absorbance is discussed in section 3.3.1.

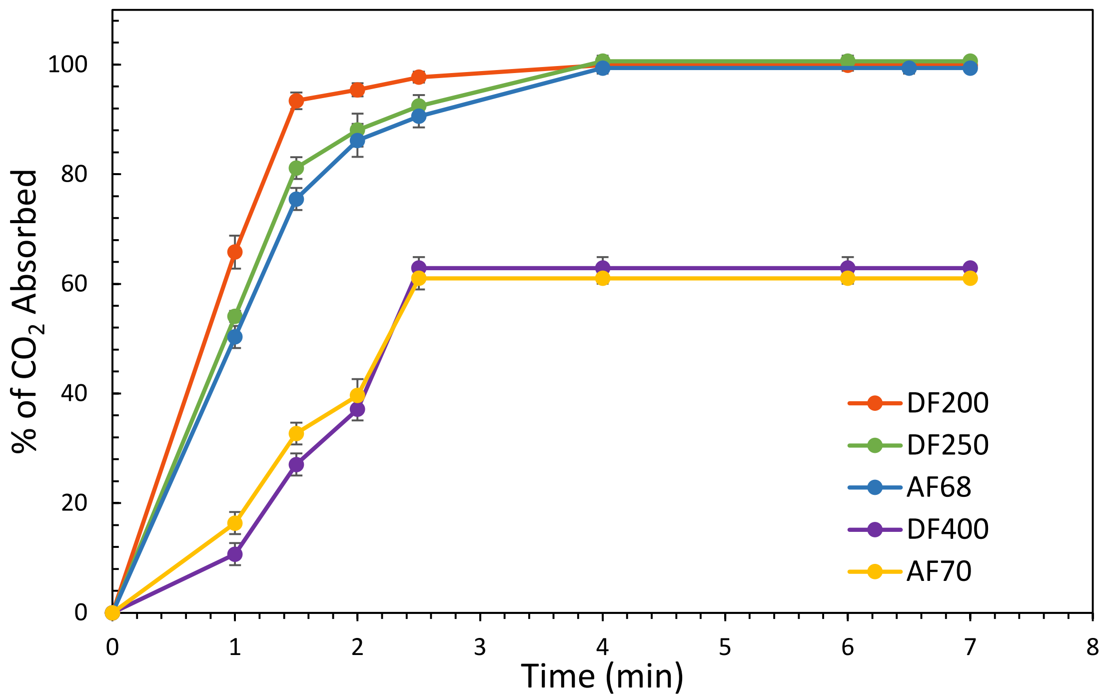

Figure 20: Efficiency of frother enhanced 0.2M Na_2CO_3 solution for capturing CO_2 at 10ppm frother concentration at 38.5^oC, with the error bars representing standard error.

As shown in Figure 20, in the first two minutes the % of CO_2 absorbed reaches 93% in case of DF200 frother, reaching a maximum value of 99.9% after 5 minutes. DF200 gave the best performance. AF70 and DF400 were only able achieve a maximum absorbance of 62.8%.

2.7.4 Bubble size analysis:

Pictures of the bubbles in the column were captured using a digital video camera (Sony Alpha A7 ll). The column was illuminated to avoid unnecessary shadows. High shutter speeds were used to avoid blurring. These pictures were processed by edge detection in MATLAB to determine the bubble size distribution. The effect of frothers on bubble size is shown at 10ppm concentration in Figure 21. Figure 21 reports the estimated bubble size distribution for each individual frother.

From Figure 21a it can be noted that for polyglycol type frothers, bubble size increases with increasing molecular weight or chain length of the frother. Grau et al. (2005) studied the effect of frother type on bubble size and observed a similar trend. At the same frother concentration MIBC generates larger bubbles than polyglycols, shown in Figure 21. DF200 gave a narrow size distribution with smaller bubble size, making it ideal for this process. Although DF250 and AF68 have the same size range AF68 has a wider size distribution which makes its initial CO_2 absorption efficiency slightly less than DF250, which is also observed in Figure 20. DF400 and AF70 gave similar size distributions but with larger bubble size, making the effective mass transfer area less.

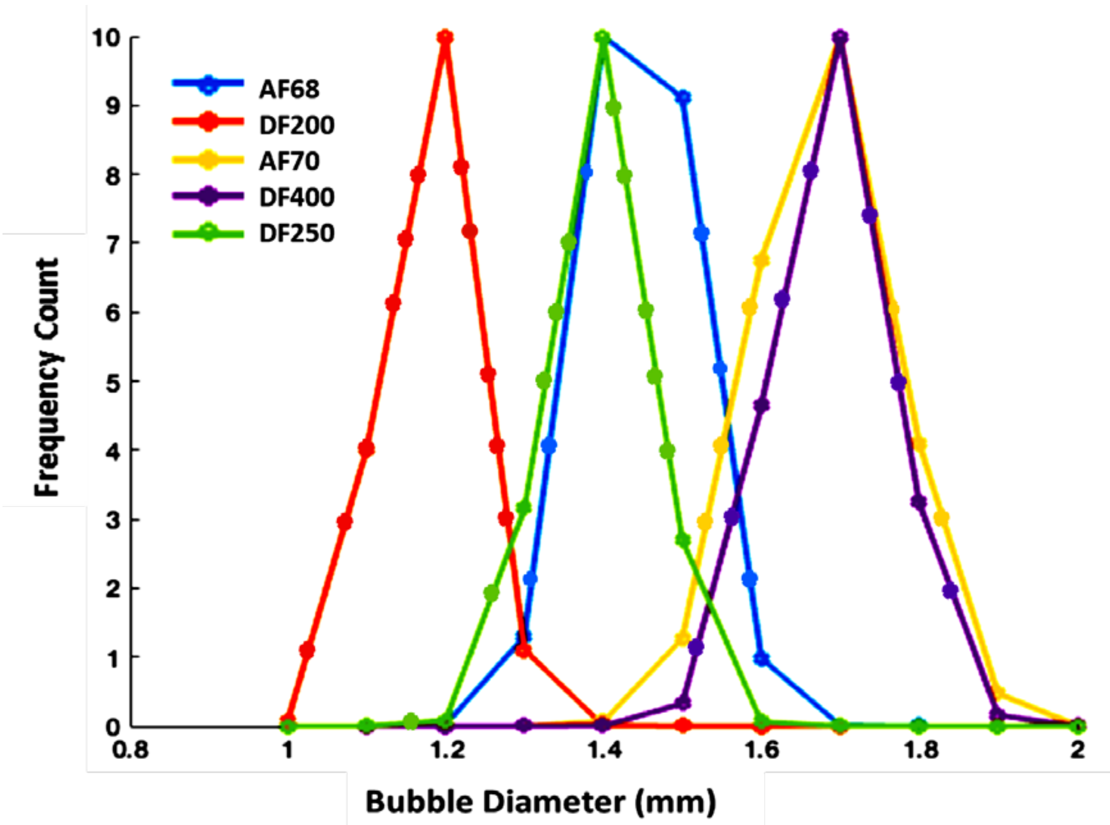

Figure 21a: Bubble size distribution of CO_2 in sodium carbonate solution with different frothers.

The graph shows bubble diameter (x-axis) vs number of bubbles/frequency count (y-axis). DF200 gave the smallest and more uniform bubble size distribution compared to other frothers. DF250 and AF68 gave similar size distributions. AF70 and DF400 gave the largest bubble sizes. Figure 21 (b) shows the detected bubbles in the column using Edge detection program in MATLAB.

Figure 21 (b): The Image on the left shows scrubber column with bubbles after the addition of surfactant. The image on the right shows the cross-section of scrubber column with detected bubbles (red circles) with the help of MATLAB program.

2.7.5 Effect of Frother Concentration on CO2 Absorption:

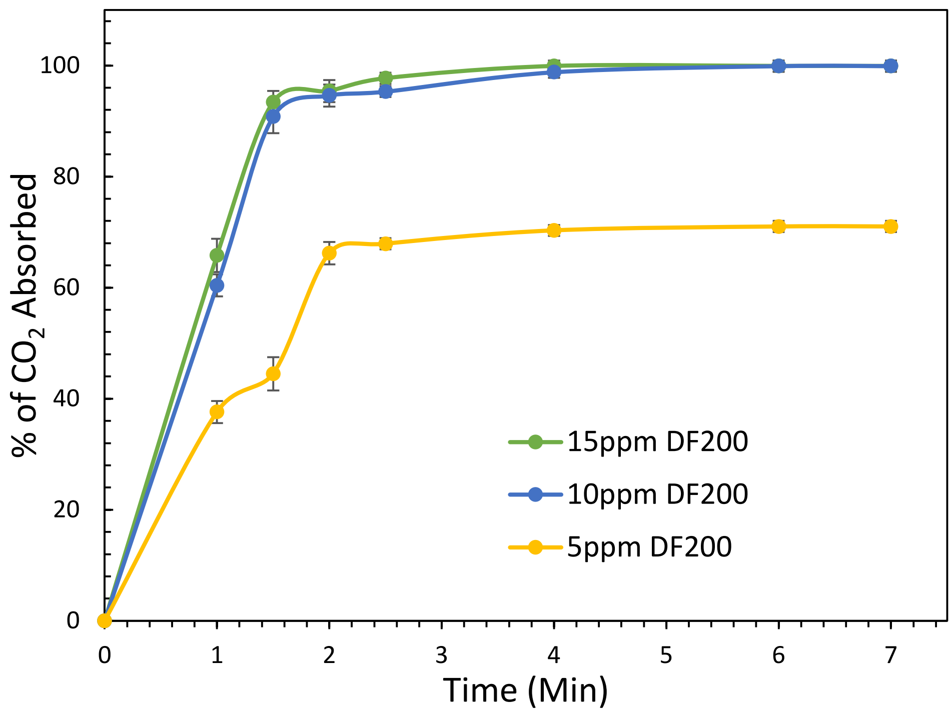

Figure 22: % of CO_2 absorbed with different concentrations of DF200 in 0.2M sodium carbonate solution at 38.5°C, with the error bars representing standard error.

We tested various concentrations of DF200, DF250 and AF68 to study the effect of frother concentration on absorption performance. Frother concentrations of 10ppm and 15ppm showed similar absorption performance, reaching a maximum value of 99.9%. 5ppm could only achieve a 70.3% maximum absorbance.

Since DF200 gave the best performance, we show three different concentrations (5ppm, 10ppm and 15ppm) of DF200 in Figure 22. We concluded that 10ppm is the optimum dosage. This data suggests that a solution enhanced with less frothing agent requires slightly more time for the amount of CO_2 in the exhaust stream to reach its minimum.

This is due to the amount of time required for stable bubble formation. The froth forms very readily when larger concentrations of frothers are used in the scrubbing solution. For very short batch processes, using a higher concentration of frother is advantageous, as it captures slightly more CO_2 during the early stages of a trial. During longer trials, or continuous process, the difference in the bubble building period becomes negligible. With the addition of 10ppm DF200, the scrubbing efficiency of sodium carbonate slurry reached 99.9% after reaching steady state, and any further addition of frothers would result in only very minimal improvements.

Foaming is usually observed when higher concentrations (more than 15ppm) of surfactants are used. This is the reason these tests were restricted to a range of 5-20ppm frother. With lower concentrations, the frothers are aimed towards generating uniform bubble characteristics rather than stable froth/foam formation. Using too much frother may cause adverse effects such as foaming, where the gas gets completely trapped in the bubble swarm. Table 11 compares the CO_2 capture efficiency of different reagents with frother enhanced sodium carbonate solution.

Table 11: Effect of solvent type on CO_2 capture efficiency.

Absorbent	CO_2 capture efficiency (%)
0.2M Na_2CO_3	55.60
0.2M NaOH	97.01
0.2M MEA	97.12
0.2M Na_2CO_3 + 10ppm DF200	99.90

2.7.6 Absorption kinetics:

The rate of the absorption reaction was estimated by calculating the slope between the number of moles of CO_2 absorbed vs time. The number of moles absorbed was calculated by performing trapezoidal integration on the graph generated by the data logger on the gas analyzer. The rate constant was estimated from Equation 8, assuming first order kinetics based on the work of Sharma and Danckwerts (1963). The rate constant is directly correlated to the rate of absorption. From Figure 23 it is evident that rate of absorption is highest with DF200, closely followed by DF250 and AF68. Compared to the baseline, these three frothers increased the absorption rate of Na_2CO_3 solution significantly. Though sodium carbonate solution by itself has a lower absorption efficiency than NaOH or MEA, the addition of frothers increases it to above either. Additionally, the frother is expected to have no impact on the energy cost of regeneration.

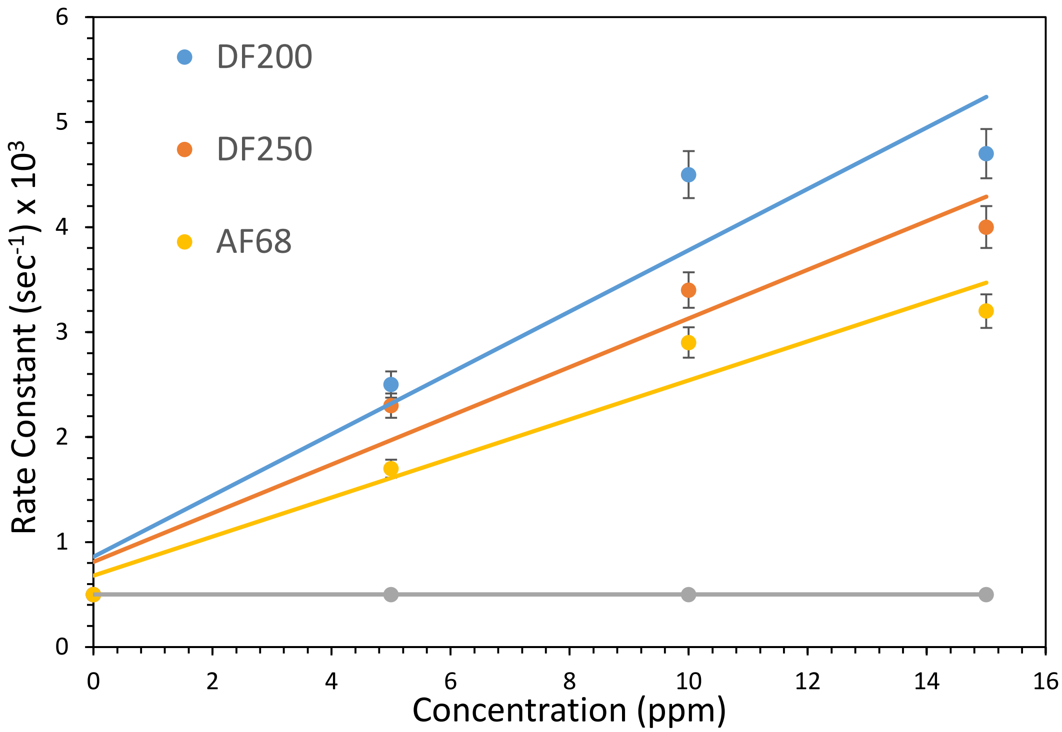

Figure 23: Rate of absorption of CO_2 with 0.2M Na_2CO_3 and various frothers at different concentrations, with the error bars representing standard error.

2.8 Reagent Regeneration:

Reagent regeneration energy was estimated from the heat duty (2.65kwh) from heat recycle loop shown in Figure 18. With 1.13 moles per minute of CO_2 absorbed, heat requirement for the frother-enhanced Na_2CO_3 is around 3.18 MJ/Kg_{CO2}. The frothers had no impact on the energy of the reagent regeneration, perhaps because of their very low concentrations. The typical regeneration energies for MEA-based CO_2 capture from previous literature is around 3.9-4.3MJ/Kg_{CO2} (Laribi et al., 2019; Nagasawa at al., 2009). The energy consumption in this study is much lower than the MEA based system.

Using frother-enhanced dilute sodium carbonate solution will reduce the reagent cost and also other operating costs for post-combustion CO_2 capture. 10ppm DF200 gave the best results among other frothers. Originally, increasing frother concentrations increased the absorption rate as seen in Figures 22 and 23, but over longer trials and after reaching steady state, this gap is negligible. Owing to the very low concentration of the frothers used, the solvent regeneration energy remained the same as sodium carbonate solution. The frothers do degrade at various points throughout the system after 3-4 cycles. As a result, a fresh batch of frothers was added after every 3 cycles. These surfactants do not enter the CO_2 rich stream, because of their high decomposition temperature (200-250°C) compared to desorption temperature of our system (98°C). Before the process water is discharged, these organic compounds can be easily removed with activated carbon, because of their hydrophobicity. A complete guide on low cost flotation frothers treatment methods was reviewed by Li et al. (2019). Considering the recyclability and based on costs from Table 1, the reagent cost for CO_2 capture could be reduced by 78% by switching to this frother-enhanced sodium carbonate system. For future work, we suggest a sensitivity analysis on CAPEX and OPEX and building a continuous onsite pilot scale scrubbing unit.

2.9 Conclusion:

Although amines and NaOH have a very high CO_2 capture efficiency there are some drawbacks associated with both the reagents including equipment corrosion, solvent degradation, high cost, and so on. We have used several frothing agents to enhance the absorption performance of low-cost sodium carbonate solution, and concluded that 10ppm DF200 gave the best performance. The absorption efficiency increased from 55.6% to 99.9%, which is greater than NaOH and amines. Frother-enhanced Na_2CO_3 has a low-cost advantage and is environmentally friendly.

2.10 References:

- Barzagli, F., Giorgi, C., Mani, F. and Peruzzini, M., 2017. CO2 capture by aqueous Na2CO3 integrated with high-quality CaCO3 formation and pure CO2 release at room conditions. *Journal of CO2 Utilization*, *22*, pp.346-354.
- Butler, J.N., 2019. *Carbon dioxide equilibria and their applications*. Routledge.
- Castro, S., Miranda, C., Toledo, P. and Laskowski, J.S., 2013. Effect of frothers on bubble coalescence and foaming in electrolyte solutions and seawater. *International Journal of Mineral Processing*, *124*, pp.8-14.
- Cho, Y.S. and Laskowski, J.S., 2002. Effect of flotation frothers on bubble size and foam stability. *International Journal of Mineral Processing*, *64*(2-3), pp.69-80.
- Cullinane, J.T. and Rochelle, G.T., 2004. Carbon dioxide absorption with aqueous potassium carbonate promoted by piperazine. *Chemical Engineering Science*, *59*(17), pp.3619-3630.
- Danckwerts, P.V., 1951. Significance of liquid-film coefficients in gas absorption. *Industrial & Engineering Chemistry*, *43*(6), pp.1460-1467.

- Dey, S., Pani, S. and Singh, R., 2014. Study of interactions of frother blends and its effect on coal flotation. *Powder technology*, *260*, pp.78-83.
- Dietrich, F., Schöny, G., Fuchs, J. and Hofbauer, H., 2018. Experimental study of the adsorber performance in a multi-stage fluidized bed system for continuous CO2 capture by means of temperature swing adsorption. *Fuel Processing Technology*, *173*, pp.103-111.
- Geankoplis, C.J., 1997. Transport Processes and Unit Operations 3rd ed. Prentice-Hall Inc, pp615-631.
- Grau, R.A., Laskowski, J.S. and Heiskanen, K., 2005. Effect of frothers on bubble size. *International Journal of Mineral Processing*, *76*(4), pp.225-233.
- Hairul, N.A.H., Shariff, A.M. and Bustam, M.A., 2017. Process behaviour in a packed absorption column for high pressure CO2 absorption from natural gas using PZ+ AMP blended solution. *Fuel Processing Technology*, *157*, pp.20-28.
- Kawatra, S.K., Eisele, T.C. and Simmons, J.J., Michigan Technological University, 2011. *Capture and sequestration of carbon dioxide in flue gases*. U.S. Patent 7,919,064.
- Kowalczuk, P.B., 2013. Determination of critical coalescence concentration and bubble size for surfactants used as flotation frothers. Industrial & Engineering Chemistry Research, 52(33), pp.11752-11757.

- Kowalczuk, P.B. and Drzymala, J., 2016. Physical meaning of the Sauter mean diameter of spherical particulate matter. *Particulate Science and Technology*, *34*(6), pp.645-647.
- Kowalczuk, P.B. and Drzymala, J., 2017. Selectivity and power of frothers in copper ore flotation. Physicochem. Probl. Miner. Process, 53(1), pp.515-523.
- Khoshdast, H. and Sam, A., 2011. Flotation frothers: review of their classifications, properties and preparation. *The Open Mineral Processing Journal*, *4*(1), pp.25-44.
- Laribi, S., Dubois, L., De Weireld, G. and Thomas, D., 2019. Study of the post-combustion CO2 capture process by absorption-regeneration using amine solvents applied to cement plant flue gases with high CO2 contents. *International Journal of Greenhouse Gas Control*, *90*, p.102799.
- Laskowski, J.S., 1998. *Frothers and frothing* (pp. 1-49). Gordon and Breach, Australia.
- Li, Y., Xie, S., Zhao, Y., Xia, L., Li, H. and Song, S., 2019. The Life Cycle of Water Used in Flotation: a Review. *Mining, Metallurgy & Exploration*, *36*(2), pp.385-397.
- Liu, H. and Okazaki, K., 2003. Simultaneous easy CO2 recovery and drastic reduction of SOx and NOx in O2/CO2 coal combustion with heat recirculation. *Fuel*, *82*(11), pp.1427-1436.

- Mahajani, V.V. and Danckwerts, P.V., 1983. The stripping of CO2 from amine-promoted potash solutions at 100 C. *Chemical Engineering Science*, *38*(2), pp.321-327.
- Mahmoudkhani, M. and Keith, D.W., 2009. Low-energy sodium hydroxide recovery for CO2 capture from atmospheric air—Thermodynamic analysis. *International Journal of Greenhouse Gas Control*, *3*(4), pp.376-384.
- Mai, K.L. and Babb, A.L., 1955. Vapor-Liquid Equilibria by Radioactive Tracer Techniques-System Carbon Dioxide-Hydrogen Sulfide-Sodium Carbonate-Sodium Bicarbonate-Sodium Sulfide-Water. *Industrial & Engineering Chemistry*, *47*(9), pp.1749-1757.
- Metz, B., Davidson, O., De Coninck, H., Loos, M. and Meyer, L., 2005. Carbon dioxide capture and storage: Intergovernmental panel on climate change. In *Chapter 5: underground geological storage*. IPCC, Cambridge University Press UK.
- Nagasawa, H., Yamasaki, A., Iizuka, A., Kumagai, K. and Yanagisawa, Y., 2009. A new recovery process of carbon dioxide from alkaline carbonate solution via electrodialysis. *AIChE journal*, *55*(12), pp.3286-3293.
- Nelson, T.O., Coleman, L.J., Gupta, R.P., Jozewicz, W., Singer, C. and Hutson, N., 2013. Dry Carbonate Sorbent Technology for CO2 Removal from Flue Gas of Existing Coal-fired Power Plants.

- Olajire, A.A., 2010. CO2 capture and separation technologies for end-of-pipe applications–a review. *Energy*, *35*(6), pp.2610-2628.
- Olutoye, M.A. and Eterigho, E.J., 2008. Modelling of a gas absorption column for CO2-NaOH system under unsteady-state regime. *Leonardo Electronic Journal of Practices and Technologies*, *12*, pp.105-114.
- Peng, Y., Zhao, B. and Li, L., 2012. Advance in post-combustion CO2 capture with alkaline solution: a brief review. *Energy Procedia*, *14*, pp.1515-1522.
- Pires, J.C.M., Martins, F.G., Alvim-Ferraz, M.C.M. and Simões, M., 2011. Recent developments on carbon capture and storage: an overview. *Chemical engineering research and design*, *89*(9), pp.1446-1460.
- Rao, A.B., Rubin, E.S., Keith, D.W. and Morgan, M.G., 2006. Evaluation of potential cost reductions from improved amine-based CO2 capture systems. *Energy Policy*, *34*(18), pp.3765-3772.
- Rochelle, G.T., 2009. Amine scrubbing for CO2 capture. *Science*, *325*(5948), pp.1652-1654.
- Salmón, I.R., Cambier, N. and Luis, P., 2018. CO2 Capture by Alkaline Solution for Carbonate Production: A Comparison between a Packed Column and a Membrane Contactor. *Applied Sciences*, *8*(6), p.996.
- Sharma, M.M. and Danckwerts, P.V., 1963. Fast reactions of CO2 in alkaline solutions—(a) Carbonate buffers with arsenite, formaldehyde and

hypochlorite as catalysts (b) Aqueous monoisopropanolamine (1-amino-2-propanol) solutions. *Chemical Engineering Science*, *18*(12), pp.729-735.

- Sharma, M.M. and Danckwerts, P.V., 1963. Fast reactions of CO_2 in alkaline solutions—(a) Carbonate buffers with arsenite, formaldehyde and hypochlorite as catalysts (b) Aqueous monoisopropanolamine (1-amino-2-propanol) solutions. *Chemical Engineering Science*, *18*(12), pp.729-735.
- Spigarelli, B.P. and Kawatra, S.K., 2013. Opportunities and challenges in carbon dioxide capture. *Journal of CO2 Utilization*, *1*, pp.69-87.
- Stowe, H.M. and Hwang, G.S., 2017. Fundamental understanding of CO_2 capture and regeneration in aqueous amines from first-principles studies: recent progress and remaining challenges. *Industrial & Engineering Chemistry Research*, *56*(24), pp.6887-6899.
- Tan, Y., Nookuea, W., Li, H., Thorin, E. and Yan, J., 2016. Property impacts on Carbon Capture and Storage (CCS) processes: A review. Energy Conversion and Management, 118, pp.204-222.
- Toan, S., O'Dell, W., Russell, C.K., Zhao, S., Lai, Q., Song, H., Zhao, Y. and Fan, M., 2019. Thermodynamics of $NaHCO_3$ decomposition during Na_2CO_3-based CO_2 capture. *Journal of Environmental Sciences*, *78*, pp.74-80.
- Wang, Y., Zhao, L., Otto, A., Robinius, M. and Stolten, D., 2017. A review of post-combustion CO_2 capture technologies from coal-fired power plants. *Energy Procedia*, *114*, pp.650-665.

- Yang, H., Xu, Z., Fan, M., Gupta, R., Slimane, R.B., Bland, A.E. and Wright, I., 2008. Progress in carbon dioxide separation and capture: A review. *Journal of environmental sciences*, *20*(1), pp.14-27.
- Zeng, Q., Guo, Y., Niu, Z. and Lin, W., 2013. The absorption rate of CO2 by aqueous ammonia in a packed column. *Fuel processing technology*, *108*, pp.76-81.
- Zhang, W., Nesset, J.E., Rao, R. and Finch, J.A., 2012. Characterizing frothers through critical coalescence concentration (CCC) 95-hydrophile-lipophile balance (HLB) relationship. *Minerals*, *2*(3), pp.208-227.

3. Simultaneous removal of CO_2, NOx and SOx using single stage absorption column

3.1 Abstract:

Capturing flue gases often require multiple stages of scrubbing, increasing the capital and operating costs. So far, no attempt has been made to study the absorption characteristics of all the three gases (NO, SO_2 and CO_2) in a single stage absorption unit at alkaline pH conditions. We have attempted to capture all the three gases with a single wet scrubbing column. The absorption of all three gases with sodium carbonate solution promoted with oxidizers was investigated in a tall absorption column. The absorbance was found to be 100% for CO_2, 30% for NO and 95% for SO_2 respectively. The capture efficiency of sodium carbonate solution was increased by 40% for CO_2 loading, with the addition of oxidizer. Absorption kinetics and reaction pathways of all the three gases were discussed individually in detail.

3.2 Introduction:

Capturing CO_2, NOx and SOx together has never been done before, but capturing them separately incurs a huge plant capital and operational costs. Capturing flue gases from power plants is a multi-step process. This is usually done in three stages: 1.) Selective catalytic reduction (SCR) for the removal of NOx 2.) Flue gas desulfurization (FGD) for the capture of SO_2 and 3.) CO_2 capture (Astarita et al., 1981; Kawatra et al., 2011; Barzagli et al., 2017; Kawatra, 2020; Xie et al., 2015; Deshwal et al., 2008; Yang et al., 2008). Capturing CO_2 separately from other gases requires an additional 20% footprint for each capture unit operation (Berghout et al., 2015), making it difficult for power plants with space constraints and also increasing the capital and operational costs for each individual unit operation. If these processes could be combined into single capture column, the problems mentioned above could be resolved. In a recent study conducted by Li et al. (2016) at 650-MW coal fired power plant, concluded that total cost of flue gas removal could be reduced by 13.1% by just integrating FGD and CO_2 capture into single stage. If all the three processes can be combined into one step with the help of non-toxic reagents like sodium carbonate, further cost savings could be achieved, making flue gas removal more economical and environment friendly.

To date, no or minimal attempts have been made to combine all three processes into a single step. In the current paper, we have investigated sodium carbonate solution enhanced with rate promoters for the absorption of the three gases CO_2, NO and SO_2 in a single scrubbing column. This will eliminate the need for additional capital and operating costs, especially the high temperature SCR process.

The use of low-cost reagents like sodium carbonate is of great importance for reducing the cost of post combustion CO_2 capture. The carbonate solution also has other advantages such as low toxicity compared to amines, less solvent loss and no thermal degradation (Barzagli et al., 2017). The absorption of carbon dioxide by carbonate solutions is limited at ambient temperature and is governed solely by the rate of physical mass transfer (Astarita et al., 1981; Barzagli et al., 2017). Even at temperatures above 378 K, the reactions are not fast enough to make the absorption instantaneous (Hu et al., 2016). Therefore, the use of rate-enhancing agents such as piperazine (PZ), monoethanolamine (MEA), boric acid, carbonic anhydrase (CA), hydrogen peroxide and sodium hypochlorite is of great importance (Ramazani et al., 2016). But some of these rate-enhancing agents have disadvantages, for example PZ and MEA are volatile and would make heat stable salts in presence of SO_2. Enzymatic catalysts like carbonic anhydrase are very sensitive to presence of NOx and SOx (Sahoo et al., 2018), hence not recommended in a combined capture system. Carbonic anhydrase also loses catalytic activity at temperatures greater than 314K (Floyd et al., 2013).

The composition of NOx in flue gas is mostly 90% inactive NO and the remainder is NO_2 (Deshwal et al., 2008). NO is problematic because it is very inactive in the absorbent solution and has very low water solubility. NO_2 dissolves readily in water, but NO must be oxidized to NO_2 in order to implement the wet scrubbing process (Baveja et al., 1979). In the past, oxidative absorbents such as chlorine dioxide, boric acid, $KMnO_4$, hydrogen peroxide and several others have been tested in aqueous solutions (Deshwal et al., 2008; Baveja et al., 1979; Deshwal and Kundu, 2015; Wei et al., 2009; Phan et al., 2014; Ghosh et al., 2009; Guo et al., 2010; Chu et al., 2001; Chang and Rochelle, 1981; Myers Jr and Overcamp, 2002), to study the absorption kinetics of NO in water. Reagents such as sodium hypochlorite have good oxidizing properties at lower pH, which are converted to good absorbing properties at higher pH, due to high nucleophilic reactivities achieved under alkaline conditions. The majority of recent research has attempted to use these oxidizers alone at acidic pH in aqueous solutions where the reaction rate is higher at acidic pH and the rate progressively decreases at higher pH levels (Deshwal et al., 2008; Baveja et al., 1979; Deshwal and Kundu, 2015).

In this study we have examined the absorption efficiency of sodium carbonate solution promoted with hydrogen peroxide (H_2O_2) and sodium hypochlorite (NaOCl) on NO, CO_2 and SO_2 under alkaline conditions, at pH ranging from 11 to 12. This process with respect to NO is similar to selective non-catalytic reduction (SNCR) at ambient temperature. While sodium carbonate displays slower absorption kinetics for CO_2 absorption compared to traditional amines, adding these rate promoters can enhance the absorption kinetics greatly making its absorption performance surpass that of amines. SO_2 is instantaneously absorbed into aqueous sodium carbonate solutions. The uniqueness of our work is that we have examined the absorption of all three gases with a single stage of sodium carbonate absorption supported with H_2O_2/NaOCl. We also analyzed the absorption kinetics of both H_2O_2 and NaOCl with all three gasses individually. The primary focus of our paper is to explore the absorption characteristics of combined gas system and how the absorption kinetics of each individual gas is affected by the rate promoter.

3.2.1 Theory:

Low cost reagents like sodium carbonate are gaining attention in post combustion CO_2 capture. The reason for adding rate promoters is because the sodium carbonate has slower kinetics compared to amines and other alkali absorbents like NaOH. There are several rate promoters that will increase the kinetics as well as aid in using low concentrations of the reagents by achieving high mass transfer ratio in less time.

<u>CO_2 absorption in aqueous solution:</u>

When CO_2 is introduced in aqueous solution, the first step is hydration where gas phase CO_2 is transferred to liquid phase CO_2 then it forms carbonic acid, which reacts with sodium carbonate to form sodium bicarbonate. The reaction between sodium carbonate and CO_2 are shown in Equations 1-4 below:

$$\mathrm{Na_2CO_{3(s)} + H_2O_{(l)} + CO_{2(g)} \rightarrow 2NaHCO_{3(aq)}} \qquad (1)$$

Equation (1) represents the overall reaction between aqueous sodium carbonate and CO_2 forming sodium bicarbonate, with the following reaction Intermediates.

$$CO_{2\,(g)} \;=\; CO_{2\,(l)} \qquad (2)$$

$$CO_{2\,(l)} + H_2O \;=\; H^+ + HCO_3^- \qquad (3)$$

$$HCO_3^- \;=\; H^+ + CO_3^{2-} \qquad (4)$$

Step (3) is the slowest and rate determining step, so adding a rate promoter would enhance the reaction kinetics and improve the absorption efficiency of carbonate solution. All previous research was unquestionably in agreement that the rate of reaction of CO_2 in alkaline solutions follow first order kinetics (Astarita et al., 1981; Xie et al., 2015; Hu et al., 2016). Enhancing the reaction kinetics for CO_2 absorption in carbonate solution can be done with the help of several rate promoters like vanadate, hypochlorite, piperazine etc. Boric acid, arsenous acid and MEA are among other homogeneous rate enhancing reagents explored previously (Hu et al., 2016; Phan et al., 2014; Ghosh et al., 2009). Arsenous acid gave very good performance for increasing absorption kinetics of CO_2 hydration, but due to toxic and carcinogenic effects of arsenite it is no longer explored as a rate promoter for CO_2 capture. Other reagents like piperazine and boric acid does not have oxidative properties like hypochlorite to enhance NO absorption.

<u>NO absorption in aqueous solution:</u>

NO has very low solubility in water (0.0056gm/100ml at 293K). While NO_2 hydrolyses readily in water, if NO can be oxidized to NO_2 then it can be easily absorbed into aqueous solutions. There are several oxidizing agents like H_2O_2, NaClO, $NaClO_2$, $KMnO_4$ etc. Other previously studied absorbents include Na_2SO_3, $FeSO_4$, EDTA and urea. In most of these studies the reaction was found to follow first order kinetics. Many of these reagents have disadvantages pertaining to mixed gas system. For example, the use of potassium permanganate was known to produce brown precipitates, due to the formation of manganese dioxide (Chu et al., 2001). These precipitates clog the packing material in the scrubbing column, and also causes problems in the pumping system. Urea is certainly out of question because of its dormant activity for CO_2 and SO_2.

NO absorption in aqueous solutions after being oxidized to NO_2 is shown below:

The overall reaction of NO and H_2O_2 in the aqueous phase is as follows

$$NO + H_2O_2 \rightarrow NO_2 + H_2O \qquad (5)$$

$$2NO_2 + H_2O \rightarrow HNO_3 + HNO_2 \qquad (6)$$

Reactions scheme with NaOCl is as follows:

$$NO + NaOCl \rightarrow NO_2 + NaCl \qquad (7)$$

$$3NO_2 + H_2O \rightarrow 2HNO_3 + NO \qquad (8)$$

$$2NO_2 + H_2O \rightarrow HNO_3 + HNO_2 \qquad (9)$$

<u>SO_2 absorption in aqueous solution:</u>

Although different methods have been proposed over the years, wet scrubbing process is the commonly used process for removing SO_2 from flue gas. The following reaction pathways should be considered when sulfur dioxide is introduced into aqueous solutions of $NaHCO_3/Na_2CO_3$:

$$SO_2 + H_2O \;=\; H^+ + HSO_3^- \qquad (10)$$

$$HSO_3^- \;=\; H^+ + SO_3^{2-} \qquad (11)$$

$$H_2O \;=\; H^+ + OH^- \qquad (12)$$

$$HCO_3^- = H^+ + CO_3^{2-} \quad (13)$$

Reaction (10) has very fast kinetics, with a forward rate constant of 3.40×10^6 sec^{-1} (Chang and Rochelle, 1981). Reactions (11) and (12) can be regarded as almost instantaneous, since they are based on simple transfer of H^+. The mass transfer coefficient of SO_2 in aqueous solutions is correlated to temperature and with increase in temperature it increases, at the operating temperature of around 318K the mass transfer coefficient of SO_2 in aqueous solution is two times higher than at 293K (Chang and Rochelle, 1981). Owing to high mass transfer coefficient and instantaneous reactions, SO_2 can be absorbed readily into sodium carbonate solution with or without the presence of rate enhancing reagents.

3.2.2 Kinetic Measurements:

Dankwerts surface renewal model is the widely accepted kinetic model for the absorption of gases in liquid solutions (Danckwerts and Lannus, 1970). Based on the Danckwerts film renewal model the rate of absorption of NO is given by:

$$N_{N0} = \frac{k_g}{RT}\left(p_{NO} - p_{NO_i}\right) \quad (14)$$

Where *R* is universal gas constant, k_g is gas phase mass transfer coefficient (Units: m/s), T is the temperature and p_{NO} is partial pressure of NO. p_{NO_i} is the interfacial pressure of NO in the aqueous solution that can be obtained by Henry's law:

$$p_{NO_i} = H_{NO} c_{NO} \quad (15)$$

H_{NO} is Henry's law constant (Units: Pa m^3/mol). c_{NO} is the concentration of NO at the interface (Units: mol/m^3), and is directly associated with the solution's ionic strength. This relationship is shown in the following expression (Onda et al., 1970):

$$log\left(\frac{c_{N0}}{c_{NOw}}\right) = -(k_{NaClO}I_{NaClO} + k_{0H^-}I_{0H^-}) \quad (16)$$

k_{NaClO} and k_{0H^-} are the salting-out parameters of NaClO and OH^- respectively. I is the ionic strength of the solution (Units: mol/L). The salting out parameters of an electrolyte solution can be obtained by adding their anion, cation and gas contribution numbers respectively, as shown in the equation below.

$$k = x_a + x_c + x_g \quad (17)$$

x_a is contribution by anions, x_c is contribution by cations and x_g by gas, respectively in mol/L

The individual x values can be identified from previous literature (Sada et al., 1978; Sada et al., 1986; Onda et al., 1970). But, x_{ClO-} is not mentioned in the literature so it is presumed that the role of hypochlorite ion is the same as that of chlorite i.e. $x_{ClO-} = 0.3497$ (Chang and Rochelle, 1981).

The rate at which CO_2 is absorbed into carbonate solutions can be described as follows:

$$R_{CO_2} = \frac{dc}{dt} = k_L a(c^* - c) = k\,[CO_2] \quad (18)$$

k_L – mass transfer coefficient. a – gas-liquid interfacial area. c^* - CO_2 concentration at saturation i.e. the solubility of CO_2. c – bulk concentration of CO_2 dissolved. k is the rate constant assuming first order kinetics (Danckwerts and Lannus, 1970).

The percentage concentration of gases going in and out of the scrubbing column is continuously monitored by the gas analyzer. The absorption efficiency for each gas (CO_2, NO and SO_2) is calculated individually by the following equation:

$$\text{Absorption efficiency (or) \% absorbance} = \frac{Y_{in} - Y_{out}}{Y_{in}} \times 100 \qquad (19)$$

Where Y_{in} is number of moles of the gas going into the scrubbing column and Y_{out} is number of moles of the gas coming out of the scrubbing column.

3.3 Experimental:

3.3.1 Column Properties

A CO_2 capture column has been designed and built as shown in Figure 24. The packing material used to fill the scrubber column is polypropylene pall rings 0.5”x0.5”. The height of a packed bed scrubbing column (Z) is calculated using the contact tower design equation (equation 20). G_s represents molar flow of solute-free gas per cross-sectional area of the column. ‘a’ is the interfacial area available for mass transport. K_y accounts for overall gas phase mass transfer coefficient. Y is the fraction of moles of gas phase solute per moles of solute-free gas, and Y* denotes the gas phase mole fraction in equilibrium with the liquid phase. The denominator of the integral represents the driving force for mass transfer and is integrated over the condition of the gas phase from the top to the bottom of the column (Geankoplis, 1997).

$$Z = \frac{G_S}{K_y * a} \int_{Y_2}^{Y_1} \frac{dY}{Y - Y^*} \qquad (20)$$

Given that the interfacial area ‘a’ is in the denominator of the design equation, it is advantageous to have a large amount of interfacial area within the scrubbing column. This is the reason most scrubbing columns are filled with packing.

3.3.2 Materials and Methods

The pilot scale scrubbing column shown in Figure 24 was used to conduct experiments on absorbance of CO_2, NO and SO_2 with sodium carbonate solution in the presence of oxidizer. The top portion of the capture column (7ft) is made of transparent poly acrylic plastic, and the bottom portion is made of steel to ensure robustness. The packed-bed absorption column (Packing: Polypropylene pall rings 0.5”x0.5”) in Figure 24 is used as a counter-current absorption column, where flue gas enters from the bottom of the column, then the gas flows up through the packed bed where it contacts the scrubbing liquid. The scrubbing liquid removes the contaminant and exits out the bottom. Clean gas then exits out from top of the column. In order to simulate the flue gas, a gaseous mixture containing 16vol% CO_2, 600ppm NO, 600ppm SO_2 and remainder nitrogen was continuously fed into the bottom of the scrubbing column with the help of a gas diffuser.

For the absorption experiments, Na_2CO_3 (99.8% pure) was obtained from Genesis Alkali, H_2O_2 and NaOCl (reagent grade) were obtained from Sigma-Aldrich. All gas cylinders were obtained from Air-products. Gas flow rate was maintained at 21LPM. Gas flow rates were measured with gas flow meters (OMEGA) equipped with gas controllers (McMaster-Carr). Separate flow meters were installed for the mixed gases to measure the volumetric flow and to control the percentage of CO_2 in the gas stream.

The composition of gases exiting out from the top of the column is measured with a Nova Multi-Gas Analyzer fitted with nondispersive infrared (NDIR) and electrochemical sensors, calibrated with CO_2/NO/SO_2/N_2 reference gases. A range of concentrations for the oxidizer (H_2O_2/NaOCl) starting from 500ppm to 1500ppm were tested. The pH measurements were taken at regular intervals with Oakton hand held pH meter. The %absorbance data was continuously recorded by the data logger connected to the gas analyzer. After each experiment the data logger was connected to the computer and the graph generated from it was integrated to calculate the total moles of CO_2 absorbed per minute for measuring the kinetic data. The accuracy of the data was ensured by repeating these experiments in triplicates.

Table 12: Typical operating parameters for the column presented in Figure 24.

Experimental Conditions	
Liquid/ gas-ratio (Kg/Kg)	4.3
Scrubbing solution flowrate	2 gallons/min
Gas inlet temperature	313K
Scrubbing solution inlet temperature	318K
Gas composition	CO_2 (16%), NO (600ppm), SO_2 (600ppm), rest N_2

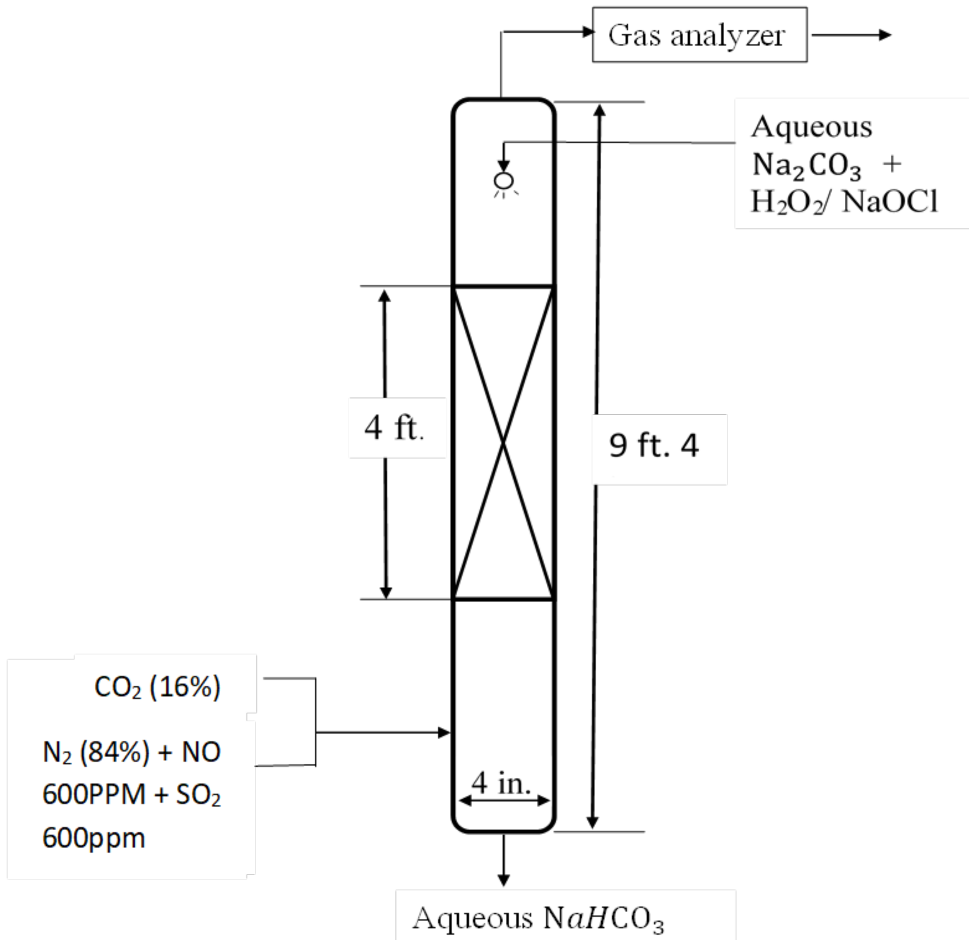

Figure 24: Dimensions of pilot scale CO2 capture column at MTU

3.4 Results and Discussion:

Along with replacing three stage flue gas capture with single stage, we also aim at reducing the reagent costs by switching from amines to dilute sodium carbonate solution enhanced with rate promoters. CO_2 capture with dilute sodium carbonate solution was first patented by Kawatra et al. (2011). Later there were several improvements made for this process, most recently Barzagli et al. (2017) have tested dilute sodium carbonate solution for CO_2 capture and were able to achieve 80% CO_2 absorption efficiency. We have tested various concentrations of sodium carbonate solution ranging from 0.1M to 0.4M with the addition of H_2O_2/NaOCl ranging from 500ppm to 1000ppm. Starting with a 50-gallon solution, the scrubbing solution was recycled through the scrubber for a total duration of 87 minutes before it is completely loaded with bicarbonate. After performing several experiments, the optimum concentration was noted to be 0.2M Na_2CO_3 solution + 750ppm H_2O_2, achieving 99.7% absorbance for CO_2, 31% for NO and 97% for SO_2 respectively. The experimental uncertainty is calculated and the error bars are plotted within the 95% confidence interval. These results, along with reaction kinetics are discussed in detail in further sections.

3.4.1 CO_2 Absorption:

Curves in Figure 25 shows the absorbance of CO_2 in 0.2M Na_2CO_3 solution enhanced with H_2O_2/NaOCl. The absorbance with Na_2CO_3 solution alone is only 61%, but after the addition of oxidizer the absorbance increased to 100%. The rate of absorption increased with increasing H_2O_2 and NaOCl concentrations. Initially with increase in concentration of the oxidizer from 500ppm to 1000ppm showed increased kinetics of CO_2 absorption, but after reaching steady state in 5 minutes, 750ppm and 1000ppm oxidizer gave almost similar absorption efficiency, with 1000ppm concentration showing 0.2% higher absorption than 750ppm. While performing the experiment we have observed effervescence in the liquid solution, though barely visible. In addition to potential chemical kinetic effects, the effervescence is believed to have led to additional bubble formation, increasing the mass transfer area of contact between the gas and the liquid. In equation (18) increasing the interfacial area ‘a’ will increase the absorption rate.

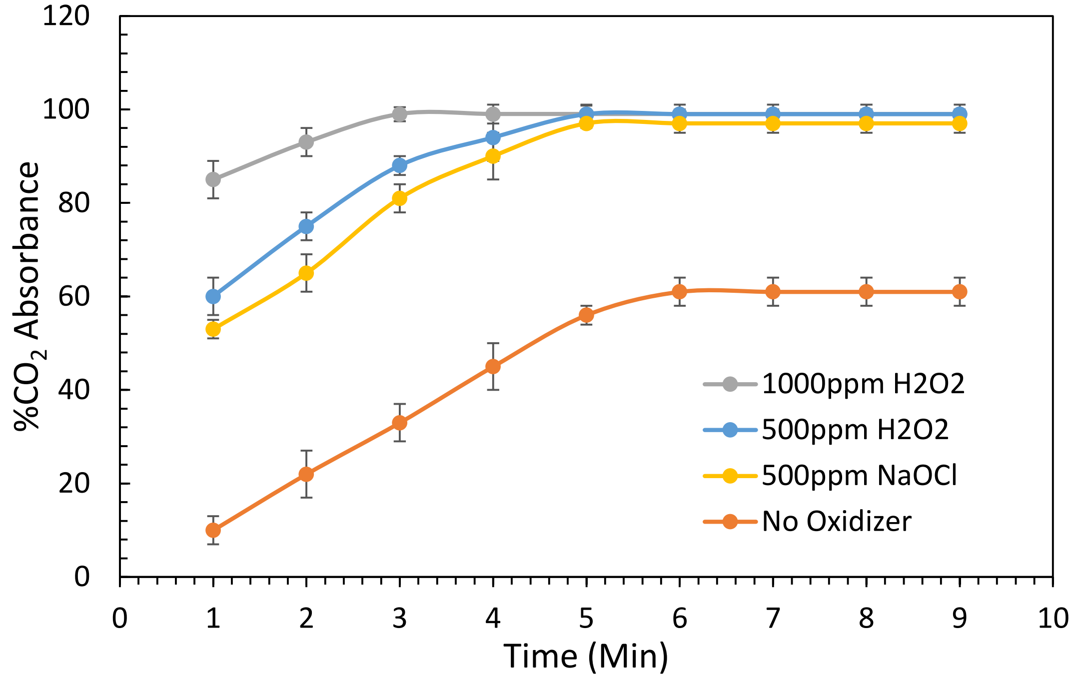

Figure 25: Absorbance of CO2 vs time in 0.2M Na2CO3 solution + varying H2O2/NaOCl at 318K with the error bars representing standard error (n=3).

The %absorbance reached 80% in the first 1 minute with the addition of H_2O_2/NaOCl and finally reaching 99.7% in 5 minutes after reaching steady state.

<u>CO_2 Absorption Kinetics:</u>

The reaction intermediates for CO_2 absorption into sodium carbonate solution are given below (21-22). Step 22 is the rate determining step, since the rest of the reactions are almost instantaneous.

$CO_{2(g)} = CO_{2(aq)}$ (21)

$$CO_2 + H_2O = H^+ + HCO_3^- \quad (22)$$

$$HCO_3^- = H^+ + CO_3^{2-} \quad (23)$$

Adding a small amount of rate promoters can enhance the CO_2 absorption capacity of carbonate solutions significantly at lower temperatures (Chu et al., 2001; Wise and Houghton, 1968; Edwards and Pearson, 1962; Dennard and Williams, 1966; Jencks and Carriuolo, 1960). Since CO_2 is a Lewis acid, Lewis bases with O^- or OH groups can act as rate promoters. The enhanced CO_2 absorption rate in Figure 25 can be attributed to the rate enhancing activity of H_2O_2/NaOCl on the equilibrium rate determining reaction (22). The time required to establish equilibrium was reduced after the addition of H_2O_2/NaOCl. Whether its organic or inorganic additive, both follow a mechanism suggested by Astarita et al. (1981) as shown below:

$$CO_2 + Promoter \rightarrow Intermediate \quad (24)$$

$$Intermediate + OH^- \rightarrow HCO_3{}^- + Promoter \quad (25)$$

For the homogeneous activity with H_2O_2 and NaOCl, carbonyl carbon acts as the substrate. This reaction scheme can be seen below. In case of homogeneous catalysis in the presence of H_2O_2/NaOCl, step (25) follows step (24) immediately. In a broader view these additives do not undergo any major chemical transformation, but rather increase the overall mass transfer phenomenon. Reaction mechanisms can be seen in scheme 1 and scheme 2 based on the alpha effect theory proposed by Edwards and Pearson (1962).

Scheme 1: Proposed theoretical mechanism with H_2O_2

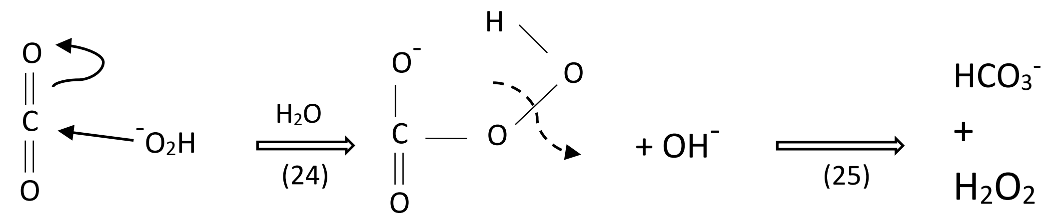

Scheme 2: Proposed theoretical mechanisms with NaOCl

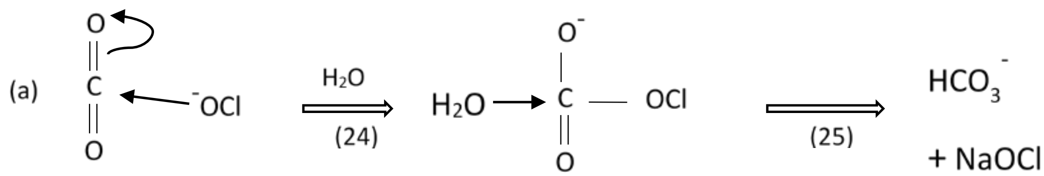

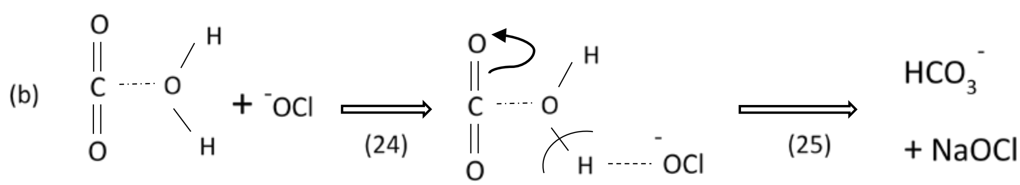

Table 13: Rate constants for nucleophilic activity.

(Edwards and Pearson, 1962; Jencks and Carriuolo, 1960)

REACTANT	**RATE CONSTANT ($MOLE^{-1}$ MIN^{-1})**

H_2O_2	2×10^5
NAOCL	1.6×10^3

Rate of reaction was estimated by calculating the slope of number of moles of CO_2 absorbed vs time. Number of moles absorbed was calculated by performing trapezoidal integration on the graph generated by the data logger on the gas analyzer. The rate constant shown in Figure 26 was estimated from the rate of reaction in equation (18) assuming first order kinetics. In alkaline pH conditions certain nucleophiles like peroxide and hypochlorite react very rapidly. This nucleophilic substitution is described as “Alpha Effect” by Edwards and Pearson (1962). In this scenario, carbonyl carbon acts as the substrate, so under these conditions the rate constants shown in Table 13 clearly indicate that peroxide has higher absorption kinetics compared to hypochlorite. We have observed a similar trend in case of CO_2 absorption kinetics with H_2O_2 and NaOCl as shown in Figure 26, which supports the theory. Few researchers have previously tested ClO_2 and ClO_3 as well (Wei et al., 2009; Guo et al., 2010). From our point of view, the reason that ClO functions as a stronger nucleophile compared to ClO_2 and ClO_3 is because the exchange of electrons on the oxygen atom in ClO_n occurs at a faster rate with a lower n value and thus Cl having a lower oxidation state. Overall H_2O_2 gave slightly better kinetics compared to NaOCl as shown in Figure 26.

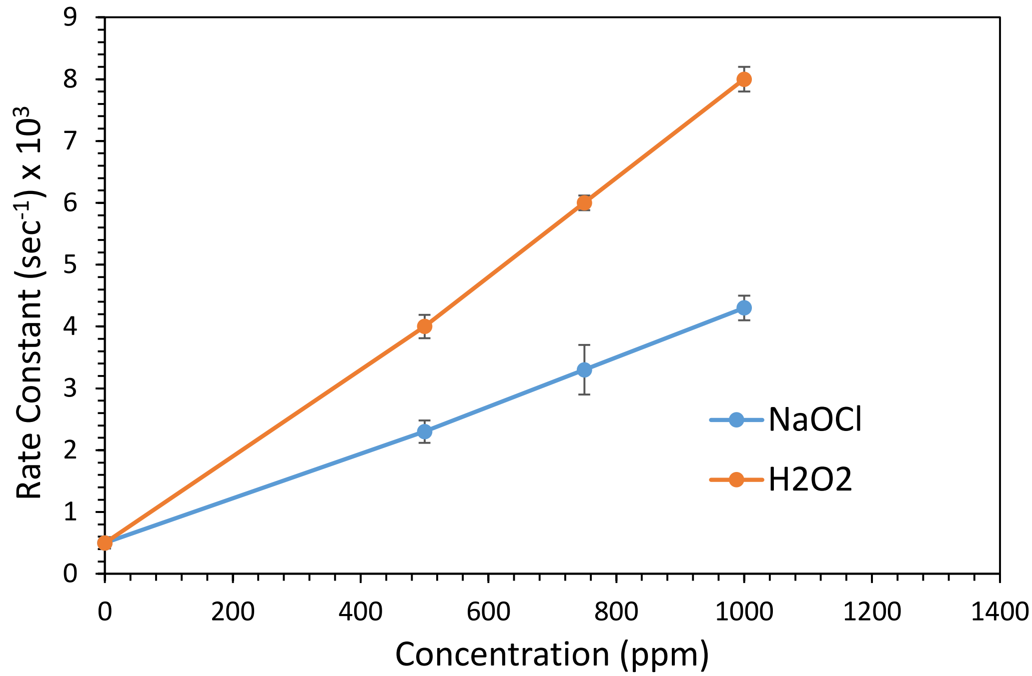

Figure 26: Rate constant vs concentration for CO_2 absorption in 0.2M Na_2CO_3 + H_2O_2/NaOCl solution with the error bars representing standard error (n=3). The observed rate constant represents that H_2O_2 is a better homogeneous catalyst than NaOCl.

3.4.2 NO Absorption:

Figure 27 and Figure 28 shows the percentage absorbance of NO in 0.2M Na_2CO_3 solution enhanced with 500ppm to 1500ppm H_2O_2 and NaOCl respectively. The NO absorption efficiency increased with increase in oxidizer concentration from 500ppm to 750ppm. The absorbance increased only slightly thereafter and reached an asymptotic maximum at 1000ppm concentration. It can be noted that H_2O_2 gave better absorption kinetics than NaOCl, which is discussed in detail in section 3.1.1. The absorption performance of both rate promoters is limited at ambient conditions in the absence of a heterogeneous catalyst. We were able to achieve 30.2% absorbance with 0.2M Na_2CO_3 solution + 1000ppm H_2O_2 at pH 11.45 and 318K temperature.

Since the NO oxidation reaction is limited after a certain value at 318K, increasing temperature might increase the absorption performance, but due to other mixed gases and physical limitations of our system, we cannot increase the temperature of the absorbent solution. One other possibility is adding a heterogeneous catalyst like platinum to reduce the activation energy and promote the reaction rate at 318 K.

Also, pH plays a crucial role in limiting the NO absorption efficiency of the solution. At pH of $\sim$ 11.5 reaction tend to limit itself after certain interfacial concentration is reached (Guo at al., 2010; Chu et al., 2001; Chang and Rochelle, 1981; Myers and Overcamp, 2002). So, the absorbance stopped at 30.2%. In retrospect NO oxidation continues to increase with increased oxidizer at lower pH values of around 5 (Deshwal and Kundu, 2015).

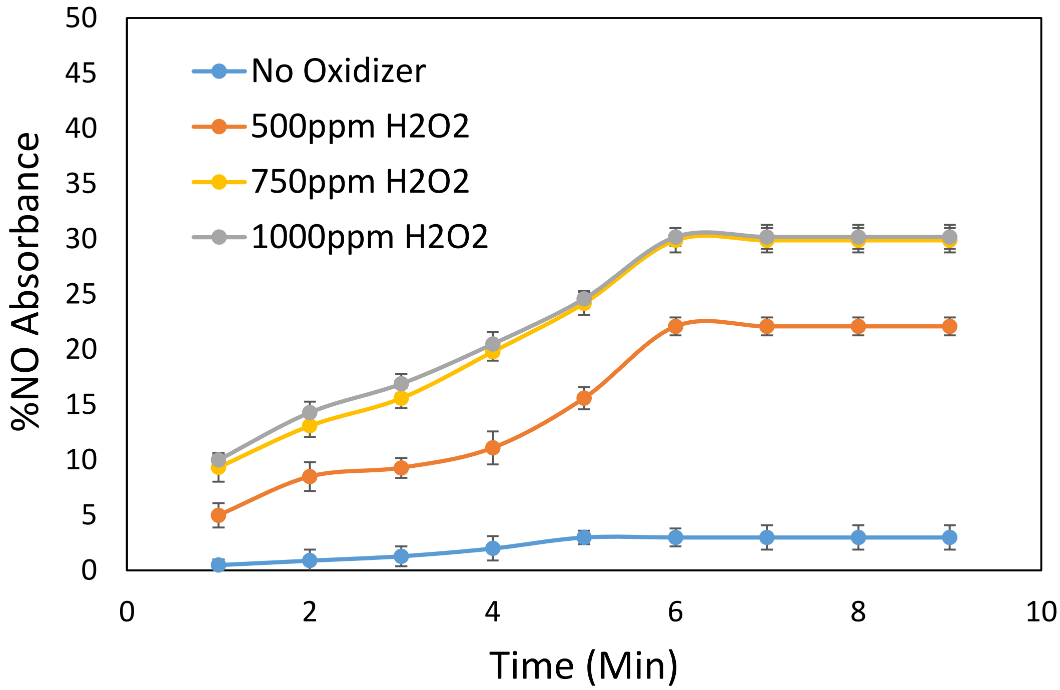

Figure 27: Absorbance of NO vs time in 0.2M Na_2CO_3 solution + H_2O_2 at 318K with the error bars representing standard error (n=3). The %absorbance reached 10% in the first 1 minute with the addition of H_2O_2 and finally reaching 31% in 5 minutes.

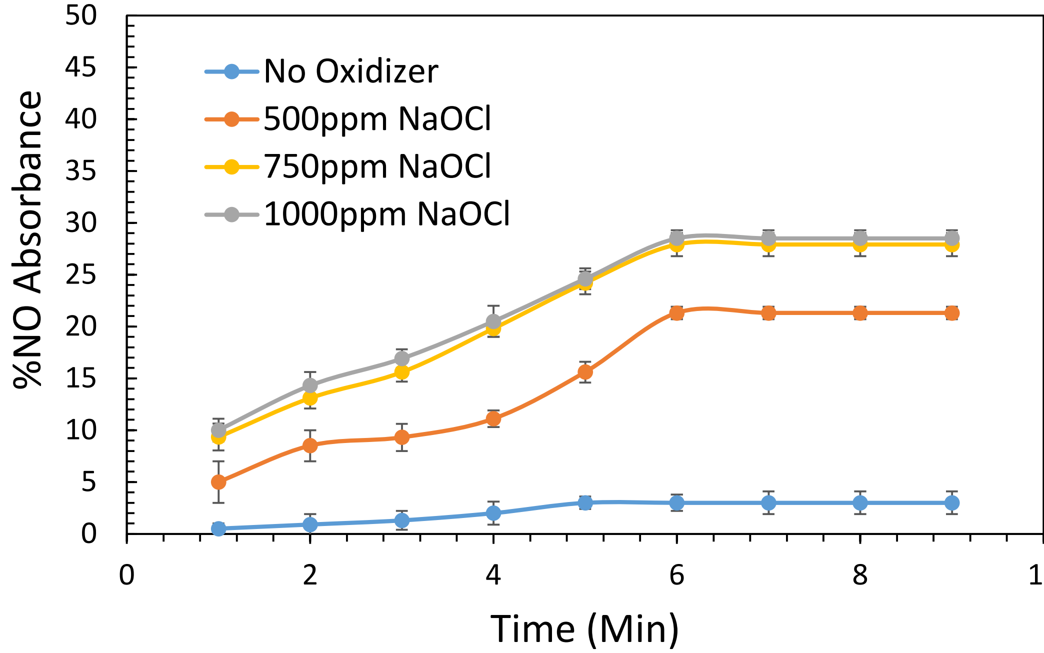

Figure 28: Absorbance of NO vs time in 0.2M Na_2CO_3 solution + NaOCl at 318K with the error bars representing standard error (n=3). The %absorbance reached 9% in the first 1 minute with the addition of NaOCl and finally reaching 29% in 5 minutes.

NO Absorption Kinetics:

The absorption rate of NO can be expressed by equation (26), based on the gas-liquid mass transport theory proposed by Dackwerts and Lannus (1970).

$$R_{NO} = \sqrt{\frac{2}{m+1} \times k_{m,n} \times D_{NO} \times C_{NO}^{m+1} \times C_{NaOCl}^{n}} \qquad (26)$$

Where R_{NO} is the rate of absorption of NO, $k_{m,n}$ is the rate constant and D_{NO} is the diffusion coefficient of NO in water, which can be considered as 2.076×10^{-9} m^2/s at 318K (Wise and Houghton, 1968). C_{NO} is the interfacial concentration of NO, which can be obtained from equation (16). Baveja et al. (1979) studied the absorption kinetics of nitric oxide in hydrogen peroxide solution and concluded that first-order kinetics followed. The reaction was found to follow first-order kinetics with NaOCl as well (Chu et al., 2001). So, the values of *m, n* are considered to be *m*=1 and *n*=1. The rate constant was estimated from Arrhenius equation, where the activation energy and frequency factor are E_a: 57.3 kJ/mol, A:6.52×10^9 $m^3/(mol\ s)$ and E_a:28.15 kJ/mol, A:7.96×10^8 $m^3/(mol\ s)$ for H_2O_2 and NaOCl respectively (Baveja et al., 1979; Deshwal and Kundu, 2015).

The effect of oxidizer concentration on the rate of absorption of NO at 318K and 0.2M Na_2CO_3 concentration can be seen in Figure 29. The rate of absorption of NO initially increases with increasing oxidizer concentration and attains a steady state after 1000ppm for both NaOCl and H_2O_2. This can be attributed to the fact that rate constant reaches a limiting value at higher pH levels beyond certain concentration of the rate promoter (Deshwal and Kundu, 2015). At pH > 10 the absorption efficiency decreases due to decrease in oxidizing potential of the catalyst. We have observed a slowdown of absorption of NO because of the decrease in oxidizing ability of NaOCl at higher pH values. The potential for the half cell reaction of NaOCl in alkaline pH conditions can be seen below:

$$ClO^- + 2H^+ + 2e^- = Cl^- + H_2O \qquad E^o = 1.48V$$

According to Nernst equation higher H^+ concentration implies higher potential (E) and hence higher oxidizing ability. So, at higher pH values the oxidizing power reduces rapidly. Concentration of Na_2CO_3 also has a direct effect on NO absorption efficiency. With increase in Na_2CO_3 concentration from 0.2 to 0.3M the rate of reaction of NO drastically reduced. Wei et al. (Wei et al., 2009) have also observed reduced NO absorption rate with increase in sodium carbonate concentration from 0.01M to 0.05M with $NaClO_2$ as the rate promoter. The same applies for other alkali absorbent solutions as well. In case of NaOH as the absorbent solution Sada et al. (1978) have observed an exponential decrease in rate of reaction.

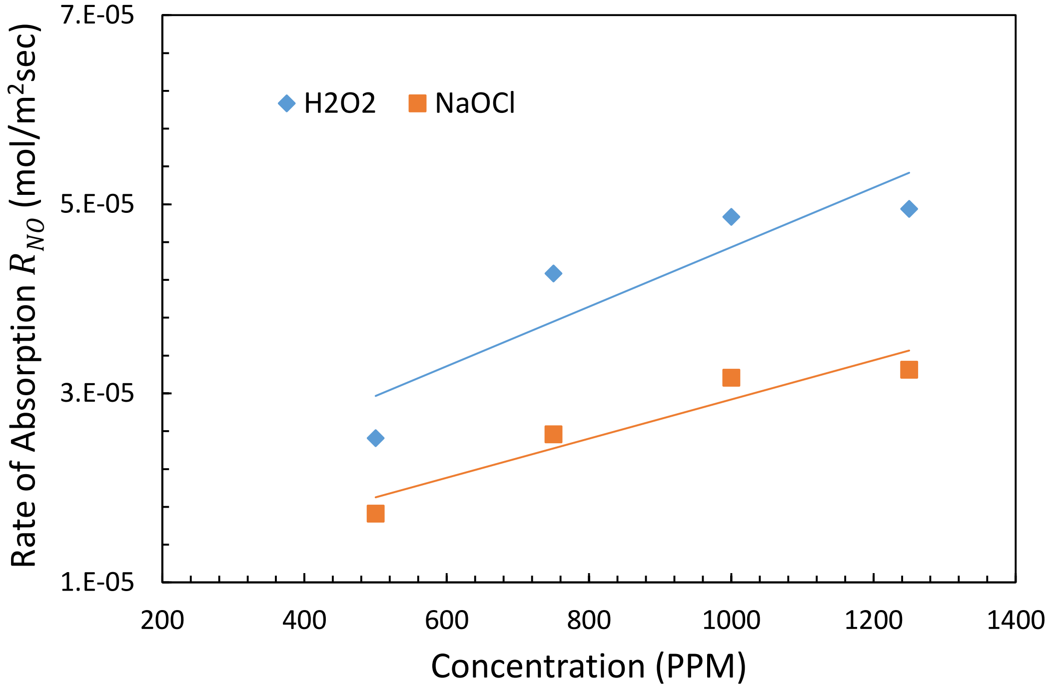

Figure 29: Effect of oxidizer concentration on the absorption rate of NO at 318K. The rate of absorption of NO increased with increasing concentration of the oxidizer until it flat lines after 1000ppm concentration.

3.4.3 SO_2 Absorption:

Since the reactions (10) - (13) are almost instantaneous, the rate of absorption of SO_2 is very high compared to CO_2 and NO in aqueous medium. Figure 30 shows the absorbance of SO_2 in 0.2M Na_2CO_3 solution enhanced with H_2O_2/NaOCl. Absorbance reached 95% very fast, hitting a maximum value of 96.2%. The rate promoters show almost negligible/minimal effect on absorption performance of SO_2 in aqueous Na_2CO_3 solution. These rate promoters do increase the absorbance of SO_2 but since it is already readily absorbed, this difference is minute. Presence of NO_2 from NO oxidation have not shown any significant effect on the absorption performance of SO_2.

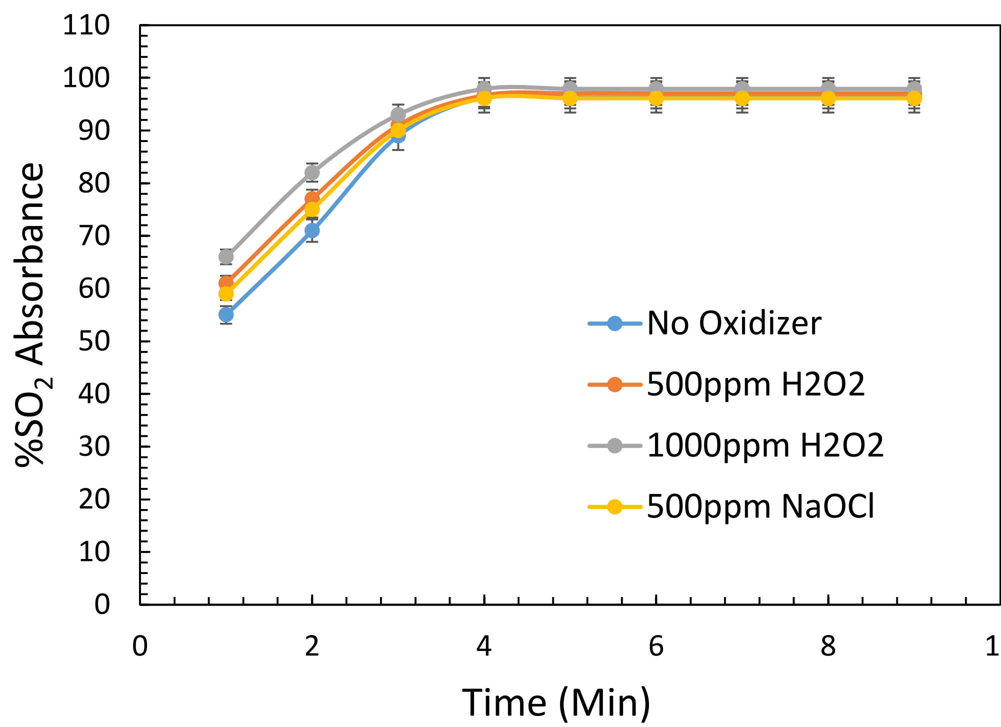

Figure 30: Absorbance of SO_2 vs time in 0.2M Na_2CO_3 solution + H_2O_2/NaOCl with the error bars representing standard error (n=3).

The %absorbance reached 65% in the first 1 minute and finally reaching 97% in 5 minutes after reaching steady state. The oxidizer did not show any major effect.

3.4.4 Effect of Solution pH on Absorption Efficiencies of CO_2, NO and SO_2

Initial pH of the absorbent solution plays a crucial role in determining the mass transfer rate of gases into liquids. The pH of the solution was varied from 10.62 to 11.73 by changing the Na_2CO_3 concentration. Figure 31 shows the effect of pH on the absorbance of all the three gases at 750ppm H_2O_2 concentration after 5 minutes of reaching steady state. The absorbance of SO_2 remained mostly unaffected, while that of CO_2 reduces rapidly at lower pH values due to low H^+ buffering capacity of the solution. The absorption efficiency for NO increases slightly at lower pH values. As evidenced by previous literature, where they studied NO absorption in acidic pH and observed that with increase in pH, absorption lowered.

Few researchers have previously studied the NO absorption characteristics in acidic pH conditions and observed a decrease in NO oxidation rate with increased pH (Deshwal et al., 2008; Baveja et al., 1979; Myers and Overcamp, 2002; Krzyzynska and Hutson, 2012). We have observed quite a similar trend in our study in the pH range of 10 to 12, where the rate of absorption of NO decreased with increased pH, because of the weak ability of H_2O_2/NaOCl to act as an oxidizer in alkaline conditions. Since the primary goal of this unit is to capture CO_2, operating at a pH of 11.6 or higher is ideal.

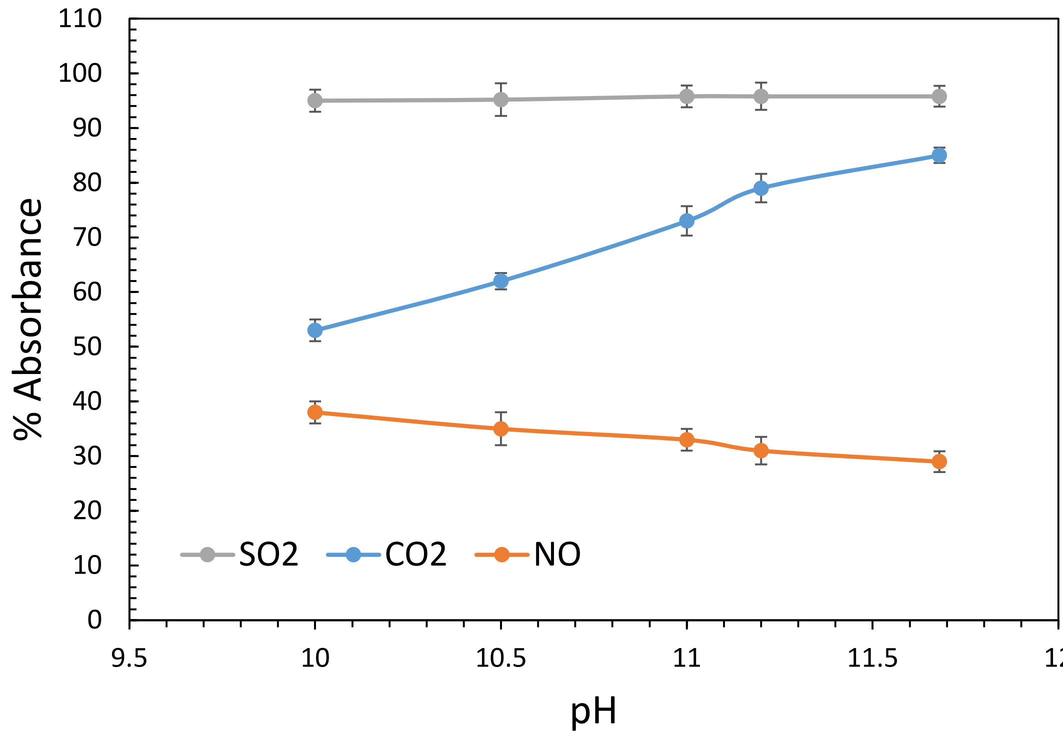

Figure 31: Absorbance vs pH with 750ppm H_2O_2 concentration at 318K at 5min interval with the error bars representing standard error (n=3). The pH did not have any major effect on SO_2 absorption, while the absorption of NO increases with decreasing pH.

Further investigation is needed into studying the overall feasibility of the process on a full plant scale unit. Next steps would be to build a full pilot scale continuous capture unit at a power plant to capture flue gas from a single boiler and test the feasibility of the overall process and also doing cost and sensitivity analysis for commercial applicability of this technology, which is beyond the scope and funding of this paper.

3.5 Conclusion:

The present investigation suggests that it is possible to capture CO_2, NO and SO_2 with a single scrubbing column. The efficacy of our system is clearly higher with a CO_2 absorption efficiency of 99.7%, compared to previous studies on CO_2 capture using low cost dilute sodium carbonate solution. Absorbance of CO_2 in a sodium carbonate scrubber column increased from 61% to 99.7% after the addition of H_2O_2 or NaOCl. NO was also absorbed, but was limited by the alkaline pH to less than 31% absorbance. Lowering the pH decreased CO_2 absorption while increasing NO absorption. Excessive supply of oxidizer did not improve the absorption efficiency of NO. SO_2 absorption reached 95% almost instantaneously, with or without the addition of oxidizer. H_2O_2 acted as better rate enhancing agent than NaOCl. Enhancing the dilute sodium carbonate solution with H_2O_2 increases its CO_2 absorption performance reducing the need for additional alkaline reagent.

3.6 References

- Astarita, G., Savage, D.W. and Longo, J.M., 1981. Promotion of CO2 mass transfer in carbonate solutions. *Chemical Engineering Science*, *36*(3), pp.581-588.
- Barzagli, F., Giorgi, C., Mani, F. and Peruzzini, M., 2017. CO2 capture by aqueous Na2CO3 integrated with high-quality CaCO3 formation and pure CO2 release at room conditions. *Journal of CO2 Utilization*, *22*, pp.346-354.

- Baveja, K.K., Rao, D.S. and Sarkar, M.K., 1979. Kinetics of absorption of nitric oxide in hydrogen peroxide solutions. *Journal of Chemical Engineering of Japan*, *12*(4), pp.322-325.
- Berghout, N., Kuramochi, T., van den Broek, M. and Faaij, A., 2015. Techno-economic performance and spatial footprint of infrastructure configurations for large scale CO2 capture in industrial zones: A case study for the Rotterdam Botlek area (part A). *International Journal of Greenhouse Gas Control*, *39*, pp.256-284.
- Chang, C.S. and Rochelle, G.T., 1981. SO2 absorption into aqueous solutions. *AIChE Journal*, *27*(2), pp.292-298.
- Chu, H., Chien, T.W. and Li, S.Y., 2001. Simultaneous absorption of SO2 and NO from flue gas with KMnO4/NaOH solutions. *Science of the total environment*, *275*(1-3), pp.127-135.
- Danckwerts, P.V. and Lannus, A., 1970. Gas-liquid reactions. *Journal of The Electrochemical Society*, *117*(10), p.369C.
- Dennard, A.E. and Williams, R.J.P., 1966. The catalysis of the reaction between carbon dioxide and water. *Journal of the Chemical Society A: Inorganic, Physical, Theoretical*, pp.812-816.
- Deshwal, B.R. and Kundu, N., 2015. Reaction kinetics of oxidative absorption of nitric oxide into sodium hypochlorite solution. *Int. J. Adv. Res. Sci. Technol*, *4*, pp.313-318.

- Deshwal, B.R., Jin, D.S., Lee, S.H., Moon, S.H., Jung, J.H. and Lee, H.K., 2008. Removal of NO from flue gas by aqueous chlorine-dioxide scrubbing solution in a lab-scale bubbling reactor. *Journal of Hazardous Materials*, *150*(3), pp.649-655.
- Deshwal, B.R., Lee, S.H., Jung, J.H., Shon, B.H. and Lee, H.K., 2008. Study on the removal of NOx from simulated flue gas using acidic NaClO2 solution. *Journal of Environmental Sciences*, *20*(1), pp.33-38.
- Edwards, J.O. and Pearson, R.G., 1962. The factors determining nucleophilic reactivities. *Journal of the American Chemical Society*, *84*(1), pp.16-24.
- Floyd III, W.C., Baker, S.E., Valdez, C.A., Stolaroff, J.K., Bearinger, J.P., Satcher Jr, J.H. and Aines, R.D., 2013. Evaluation of a carbonic anhydrase mimic for industrial carbon capture. *Environmental science & technology*, *47*(17), pp.10049-10055.
- Ghosh, U.K., Kentish, S.E. and Stevens, G.W., 2009. Absorption of carbon dioxide into aqueous potassium carbonate promoted by boric acid. *Energy Procedia*, *1*(1), pp.1075-1081.
- Guo, R.T., Gao, X., Pan, W.G., Ren, J.X., Wu, J. and Zhang, X.B., 2010. Absorption of NO into NaClO3/NaOH solutions in a stirred tank reactor. *Fuel*, *89*(11), pp.3431-3435.
- Hu, G., Nicholas, N.J., Smith, K.H., Mumford, K.A., Kentish, S.E. and Stevens, G.W., 2016. Carbon dioxide absorption into promoted potassium carbonate

solutions: A review. *International Journal of Greenhouse Gas Control*, *53*, pp.28-40.

- Jencks, W.P. and Carriuolo, J., 1960. Reactivity of nucleophilic reagents toward esters. *Journal of the American Chemical Society*, *82*(7), pp.1778-1786.
- Kawatra, S.K., 2020. *Advanced Coal Preparation and Beyond: CO2 Capture and Utilization*. CRC Press.
- Kawatra, S.K., Eisele, T.C. and Simmons, J.J., Michigan Technological University, 2011. *Capture and sequestration of carbon dioxide in flue gases*. U.S. Patent 7,919,064.
- Krzyzynska, R. and Hutson, N.D., 2012. Effect of solution pH on SO2, NOx, and Hg removal from simulated coal combustion flue gas in an oxidant-enhanced wet scrubber. *Journal of the Air & Waste Management Association*, *62*(2), pp.212-220.
- Li, K., Yu, H., Yan, S., Feron, P., Wardhaugh, L. and Tade, M., 2016. Technoeconomic assessment of an advanced aqueous ammonia-based postcombustion capture process integrated with a 650-MW coal-fired power station. *Environmental science & technology*, *50*(19), pp.10746-10755.
- Myers Jr, E.B. and Overcamp, T.J., 2002. Hydrogen peroxide scrubber for the control of nitrogen oxides. *Environmental engineering science*, *19*(5), pp.321-327.

- ONDA, K., SADA, E., KOBAYASHI, T., KITO, S. and ITO, K., 1970. Salting-out parameters of gas solubility in aqueous salt solutions. *Journal of Chemical Engineering of Japan*, *3*(1), pp.18-24.
- ONDA, K., SADA, E., KOBAYASHI, T., KITO, S. and ITO, K., 1970. Solubility of gases in aqueous solutions of mixed salts. *Journal of Chemical Engineering of Japan*, *3*(2), pp.137-142.
- Phan, D.T., Maeder, M., Burns, R.C. and Puxty, G., 2014. Catalysis of CO2 absorption in aqueous solution by inorganic oxoanions and their application to post combustion capture. *Environmental science & technology*, *48*(8), pp.4623-4629.
- Ramazani, R., Mazinani, S., Jahanmiri, A. and Van der Bruggen, B., 2016. Experimental investigation of the effect of addition of different activators to aqueous solution of potassium carbonate: absorption rate and solubility. *International Journal of Greenhouse Gas Control*, *45*, pp.27-33.
- Sada, E., Kumazawa, H. and Hikosaka, H., 1986. A kinetic study of absorption of nitrogen oxide (NO) into aqueous solutions of sodium sulfite with added iron (II)-EDTA chelate. *Industrial & engineering chemistry fundamentals*, *25*(3), pp.386-390.
- Sada, E., Kumazawa, H., Kudo, I. and Kondo, T., 1978. Absorption of NO in aqueous mixed solutions of NaClO2 and NaOH. *Chemical Engineering Science*, *33*(3), pp.315-318.

- Sahoo, P.C., Kumar, M., Puri, S.K. and Ramakumar, S.S.V., 2018. Enzyme inspired complexes for industrial CO2 capture: opportunities and challenges. *Journal of CO2 Utilization*, *24*, pp.419-429.
- Wei, J.C., Yu, P., Cai, B., Luo, Y.B. and Tan, H.Z., 2009. Absorption of NO in aqueous NaClO2/Na2CO3 solutions. *Chemical Engineering & Technology: Industrial Chemistry-Plant Equipment-Process Engineering-Biotechnology*, *32*(1), pp.114-119.
- Wise, D.L. and Houghton, G., 1968. Diffusion coefficients of neon, krypton, xenon, carbon monoxide and nitric oxide in water at 10–60 C. *Chemical Engineering Science*, *23*(10), pp.1211-1216.
- Xie, H., Wang, P., He, N., Yang, X. and Chen, J., 2015. Toward rational design of amines for CO2 capture: Substituent effect on kinetic process for the reaction of monoethanolamine with CO2. *Journal of Environmental Sciences*, *37*, pp.75-82.
- Yang, H., Xu, Z., Fan, M., Gupta, R., Slimane, R.B., Bland, A.E. and Wright, I., 2008. Progress in carbon dioxide separation and capture: A review. *Journal of environmental sciences*, *20*(1), pp.14-27.

4. Reduced reagent regeneration energy for CO_2 capture with bipolar membrane electrodialysis.

4.1 Abstract

Post combustion CO_2 capture with reagents such as amines, sodium carbonate and sodium hydroxide is the most mature CO_2 capture technology. One of the major challenges facing post combustion CO_2 capture is the high energy requirement for reagent regeneration. Thermal regeneration energy is in the range of 3-4MJ/Kg CO_2 captured. We were able to achieve reagent regeneration energy as low as 1.18MJ/Kg CO_2 with the help of electrodialysis with bipolar membrane separation (EDBM). This value is significantly lower compared to thermal regeneration. Also, switching from toxic reagents like amines to alkali absorbents like sodium carbonate and sodium hydroxide will save reagent costs. This technology will be particularly attractive in the future as membrane prices go down. These traits not only make this technology economically feasible, but also environmentally benign.

4.2 Introduction:

CO_2 capture technologies are deemed essential to reduce emissions and prevent extinction of fossil fuel fired power plants (Dietrich et al., 2018; Kawatra, 2020; Valluri and Kawatra, 2021a). Out of all the CO_2 capture technologies, post combustion chemical absorption capture is the most mature technology (Bazhenov et al., 2015; Barzagli et al., 2017; Hwang et al., 2019; Huang et al., 2006; Huang and Xu, 2006; Kroupa et al., 2015; Nagasawa et al., 2009; Knuutila et al., 2009; Spigarelli and Kawatra, 2013; Salmón et al., 2018; Toan et al., 2019; Valluri and Kawatra, 2021b; Wang et al., 2017). The only drawback associated with post combustion capture is the high energy requirement for CO_2 capture reagent regeneration. Reagent regeneration energy accounts for 70% of the CO_2 capture costs (Knuutila et al., 2009). Previously reported thermal regeneration energy with amine solvents is in the range of 3-4MJ/Kg of CO_2 captured (Knuutila et al., 2009; Wang et al., 2017). This makes thermal regeneration highly energy intensive, increasing the overall CO_2 capture costs to around 55-60$/ton of CO_2 captured. In order to reduce this cost and make CO_2 capture affordable, alternate reagent regeneration routes have to be explored. Our paper presents a novel concept for reducing reagent regeneration energy. We were able to achieve energy as low as 1.18MJ/Kg of CO_2 captured.

Our process included capturing CO_2 in a scrubbing column with NaOH solution and then regenerating pure CO_2 by reacting $NaHCO_3$ solution with H_2SO_4. The resultant Na_2SO_4 solution is subjected to electrodialysis with bipolar membrane (EDBM) for regenerating the NaOH solution. Previously, people have examined CO_2 capture with NaOH and direct electrodialysis of resulting $NaHCO_3$ solution for regenerating NaOH and CO_2 in the EDBM cell, which has a lot of process inefficiencies that are discussed in detail in section 1.3. The uniqueness of our process is that with acid regeneration, we recover 100% CO_2 and then use the EDBM method to essentially separate the salt solution into acid and base, thus achieving the lowest reagent regeneration energy reported so far in the literature. This will eliminate all the disadvantages of direct electrodialysis of $NaHCO_3$, such as low current efficiency, low CO_2 recovery (40-60%) and high cell resistance etc. We have done a detailed techno-economic analysis of our process in further sections.

CO_2 capture with alkali absorbent solution:

Amines, ammonia and alkaline solutions have been thoroughly studied by several researchers as absorbents to capture CO_2 from post-combustion flue gases. Extensive research has been performed on the aspects of absorption process, reagent efficiency, mass transfer coefficient etc. (Salmón et al., 2018). The chemical reactions for CO_2 capture with alkali absorbent solutions of NaOH and Na_2CO_3 are shown below.

$$\mathrm{CO_2\ (aq) + H_2O\ (l) \rightarrow H_2CO_3\ (aq)} \qquad (1)$$

$$\mathrm{H_2CO_3\ (aq) + Na_2CO_3\ (aq) \rightarrow NaHCO_3\ (aq)} \qquad (2)$$

$$\mathrm{NaOH(aq) + H_2CO_3(aq) \leftrightarrow NaHCO_3(aq) + H_2O(l)} \qquad (3)$$

When CO_2 is dissolved in water it forms carbonic acid, which reacts with alkali absorbent (Na_2CO_3 and NaOH) to form sodium bicarbonate as shown in equations 1-3 (Barzagli et al., 2017). We have previously investigated the effectiveness of Na_2CO_3 solution and NaOH solution individually for chemical absorption CO_2 capture from flue gas. We have achieved approximately 65% CO_2 capture efficiency with pure sodium carbonate solution, 99% capture efficiency with frother enhanced sodium carbonate solution (Valluri and Kawatra, 2021b), and 97% capture efficiency with pure NaOH solution.

Thermal regeneration:

We have previously investigated a continuous setup which regenerates the sodium carbonate solution from the CO_2 loaded sodium bicarbonate solution (Valluri and Kawatra, 2021b). By heating the sodium bicarbonate solution to 80-98°C, the bicarbonate decomposes to release CO_2 and regenerate the carbonate solution, as shown in Equation 4 (Toan et al., 2019). Figure 32 shows the CO_2 capture and thermal regeneration loop.

$$2NaHCO_3\ (aq) \rightarrow Na_2CO_3\ (aq) + H_2O\ (l) + CO_2\ (g) \quad (4)$$

Reagent regeneration is the most energy intensive step in post combustion CO_2 capture process. Thermal regeneration costs a massive amount of energy. With our alkali CO_2 capture and thermal regeneration system, the reagent regeneration energies were around 3.18MJ/kg of CO_2 captured (Valluri and Kawatra, 2021b). This value is slightly lower compared to amine solvents, but still significantly high to reduce the reagent regeneration costs drastically. A solution for this is proposed in the next section.

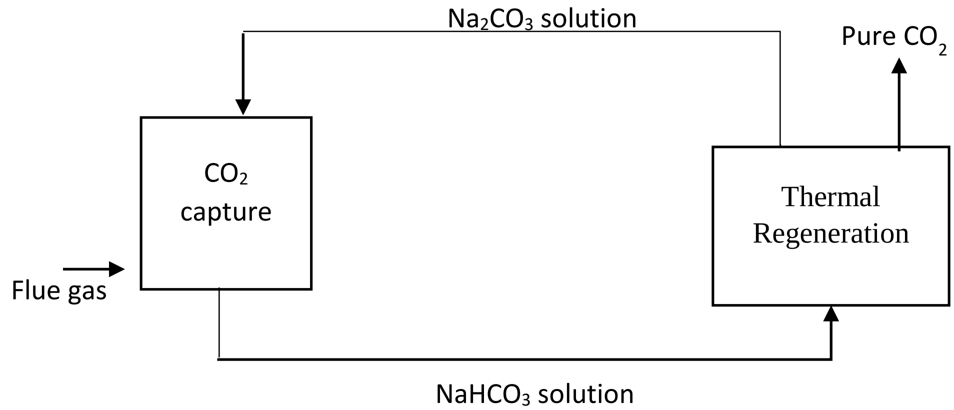

Figure 32: Block diagram of continuous CO_2 capture and thermal regeneration

<u>Alternative to thermal regeneration:</u>

One of the alternatives for thermal regeneration is through electrodialysis with bipolar membrane (EDBM) separation. EDBM process would consume very less energy compared to thermal regeneration, and solar energy can be used for energizing EDBM cell. EDBM is a common technique used for desalination and water treatment (Huang and Xu, 2006). This method, generally used for salt separation can be extended to CO_2 capture for regenerating the scrubbing solution. An alternative to thermal regeneration would be by exposing the bicarbonate to a strongly acidic solution as shown in Figure 33. For example, the following reaction has been found to effectively liberate CO_2 from bicarbonate:

$$H_2SO_4 + 2NaHCO_3 \rightarrow Na_2SO_4 + 2H_2O + 2CO_2 \quad (5)$$

The Na_2SO_4 salt solution from reaction (5) can be separated back into acid (H_2SO_4) and base (NaOH) with the help of EDBM process. The resultant base solution can be recirculated back for the absorption of CO_2. We have achieved 100% CO_2 recovery from this regeneration method, with significantly less energy consumption. This process is novel and also economically feasible.

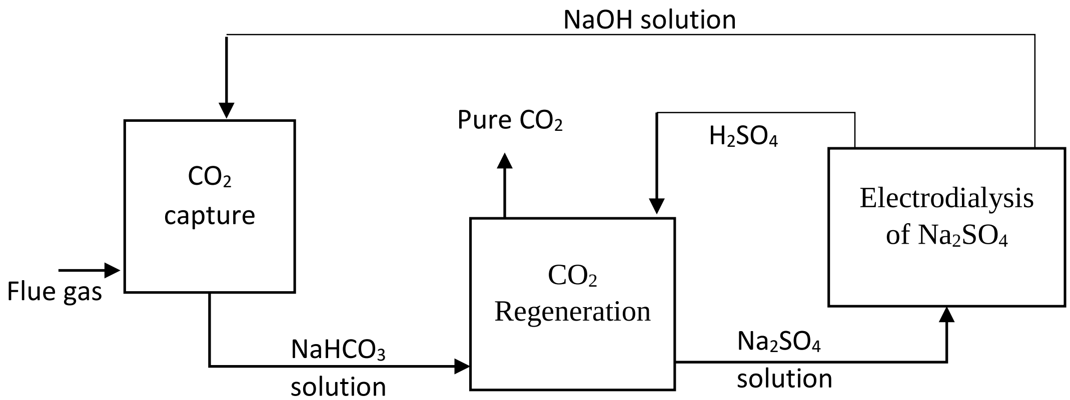

Figure 33: Block diagram of continuous CO_2 capture and regeneration with EDBM system.

CO_2 is captured with NaOH solution and then regenerated by reacting with H_2SO_4, the resultant Na_2SO_4 solution is subjected to Electrodialysis with bipolar membrane to separate acid and base. The base (NaOH) is circulated back to capture additional CO_2.

Very few authors (Bazhenov et al., 2015; Iizuka et al., 2012; Nagasawa et al., 2009) have previously studied a different approach to thermal regeneration, where they capture CO_2 with alkali absorbent solution and then directly regenerate the CO_2 by electrodialysis of $NaHCO_3$ solution. There are many drawbacks associated with direct electrodialysis of $NaHCO_3$ solution. Part of the energy is spent for catalyzing the reaction between H^+ and HCO_3^- for producing CO_2. Another drawback is that the presence of CO_2 gas bubbles in the electrodialysis cell increases electrical resistance across the cell, reducing electrical conductivity and resulting in low current efficiency and high energy consumption. Also, the CO_2 recoveries reported by this method were only 40-60%, and the lowest energy reported was 2.1MJ/Kg CO_2 (Nagasawa et al., 2009).

Iizuka et al. (2012) have observed that CO_2 recovery with direct electrodialysis is only 50%, even at high current density, due to low current efficiency of 60-70%. Bazhenov et al. (2015) did the electrodialysis of CO_2 loaded MEA solution and observed membrane degradation due to heat stable salt anions. During direct electrodialysis, as the current density of the EDBM cell increases, the CO_2 recovery often increases, but the tremendous increase in energy consumption does not make the high CO_2 recovery a very good trade off at higher current densities (Eisaman et al., 2011). Due to the presence of gas bubbles in the EDBM cell, elevated pressures as high as 10atm has to be applied to keep the CO_2 in the solution phase until the pressure is released downstream, which drastically increases pumping and other variable costs (Eisaman et al., 2011; Iizuka et al., 2012).

<u>EDBM theory:</u>

Electrodialysis with bipolar membrane (EDBM) process uses a bipolar membrane to specifically catalyze water dissociation to form free protons and hydroxide anions as shown in equation (6). Then, using a series of cation exchange and bipolar membranes,

Na^+ is allowed to diffuse into the cathode side of the cell, where it meets the hydroxide anion to form sodium hydroxide in the base compartment; while SO_4^{2-} reacts with H^+ generated from bipolar junction to form H_2SO_4 in the acid compartment. This mechanism is shown in Figure 33. In contrast to EDBM, using conventional electrolysis for water splitting reaction generates H_2 and O_2 gases, which consumes almost half the energy provided to the cell.

$$H_2O \rightarrow H^+ + OH^- \qquad (6)$$

<u>Ion exchange membranes:</u>

The function of an ion exchange membrane is to act like a thin selective barrier. Such membranes enable the electrically-driven selective transfer of ions between the two solutions which they separate. Ion exchange membranes are composed of a polymer matrix on which are fixed ionized functional groups. These fixed charges are neutralized by mobile ions of opposite charge, called counter ions. Due to the Donnan effect, in an electrolyte solution, such membrane tends to reject ions with the same charge as the ionized groups, called co-ions (Huang and Xu, 2006). Cation exchange membranes (CEM) exchange only cations between cathode and anode compartments, while anion exchange membranes (AEM) exchange only anions between the electrode compartments in an electrolysis cell.

<u>Bipolar membranes:</u>

A bipolar membrane is composed of one cation-exchange layer and one anion-exchange layer joined together. This membrane is used for water splitting. In contrast to cationic and anionic membranes, bipolar membranes have a required orientation between the electrodes: the anion-exchange layer should be oriented towards the cathode, and cation-exchange layer should be oriented towards the anode. If bipolar membranes are placed with the wrong orientation, ions accumulate between the two layers resulting in blistering of the membranes. Unlike the conventional electrolysis, gas generation is minimized in the EDBM process due to membranes restricting the H^+ and OH^- ions from reaching the electrode. Hence, theoretically the energy requirement is reduced to about 40% of what is required for water electrolysis (Jaroszek and Dydo, 2016) With increase in number of unit cells or membrane stacks in the EDBM compartment, total energy consumption decreases, due to decrease in energy consumption in electrode compartment with minimized gas generation (Nagasawa, 2009).

4.3 Experimental

Continuous CO_2 capture and regeneration experiments were conducted on our mini pilot scale setup. The block diagram of this setup is shown in Figure 34.

4.3.1 Materials and Methods:

CO_2 absorption with NaOH:

The scrubber column shown on the left side in Figure 34 is used as a counter current packed-bed absorption column. Column dimensions: Height: 275cm; Diameter:

10.16cm; Packing: Polypropylene pall rings 1.2cm×1.2cm; Packed bed height: 122cm. In order to simulate the flue gas, a gaseous mixture containing 16% vol CO_2 and rest air was continuously fed into the bottom of the scrubbing column with the help of a gas diffuser. Gas flow rate was maintained at 25LPM. Separate flow meters were installed for CO_2 and air to measure the volumetric flow and to control the percentage of CO_2 in the gas stream. CO_2 and air flow rates were measured with gas flow meters (OMEGA) equipped with gas controllers (McMaster-Carr).

The %CO_2 of the simulated flue gas exiting out from the top of the column was measured with Quantek Model 906 infrared gas analyzer calibrated with a 20-vol% CO_2/N_2 reference gas. CO_2 capture efficiency of NaOH solution was measured by continuously recording %CO_2 absorption data by the data logger connected to the gas analyzer. After each experiment the data logger was connected to the computer and the graph generated from it was integrated to calculate the total moles of CO_2 absorbed per minute. The accuracy of the data was ensured by repeating these experiments in triplicates. For a 16% CO_2 gas stream (simulating a power plant flue gas), the optimum parameters were found to be: 0.3 mol/L NaOH solution at 6.4 Liters per minute flow rate.

NaOH Regeneration with EDBM:

NaOH is regenerated through EDBM as shown in Figure 34. The electrodialysis setup shown in Figure 34 consists of a DC power supply (XHR 40-25, AMETEK; 0-40V, 0-25A) to maintain constant current field. The electrodialysis cell components and membrane stack were obtained from Ameridia - The Eurodia Group (properties given in Table 14). Membranes are separated by 0.8 mm thick spacers. To maintain the same pressure between acid, salt, and base compartments, pressure gauges (15psi max) were installed. Volumetric flow is measured with flow meters (OMEGA). The EDBM unit was equipped with instruments to measure conductivity, voltage, current and temperature.

In this setup, after CO_2 is absorbed in the scrubber column, the absorbent solution ($NaHCO_3$) is reacted with H_2SO_4 solution and the resultant Na_2SO_4 solution is fed into electrodialysis cell. The salt solution (0.2M Na_2SO_4) was prepared by mixing Na_2SO_4 in water. Na_2SO_4 >99% reagent grade was obtained from Sigma-Aldrich. To ensure an initial conductivity greater than 20mS/cm, acid and base tanks were mixed with H_2SO_4 and NaOH respectively. NaOH >98% reagent grade was obtained from Sigma-Aldrich. 98%w/w H_2SO_4 was obtained from Fisher Scientific. NaOH concentration from the base compartment was measured by titration with 0.01 mol/L HCl standard solution. Acid concentration was estimated by measuring the pH constantly with Oakton 150 hand held pH meter. The solution in the acid-base reaction tank was continuously stirred with an immersion drum mixer. Table 14 shows the experimental conditions used for the setup shown in Figure 34. For the idling procedure, each compartment was filled with deionized water. If the idle time lasts more than a day, each compartment was filled with salt solution at 30g/L (50mS/cm conductivity).

Table 14: Operating parameters for the experimental setup shown in Figure 34.

Experimental conditions	
Scrubbing liquid to gas ratio (L/G: Kg/Kg)	4.3
Gas composition	16%vol CO_2, rest air
Gas inlet temperature (^oC)	31
EDBM cell volume (m^3)	0.012
EDBM cell Voltage (V)	10 - 20
Current (A)	1 - 16
Temperature (^oC)	30
Pressure (kPa)	101.32
Na_2SO_4 concentration (mol/L)	0.2
Initial conductivity of acid/salt and base compartment (mS/cm)	20
Maximum conductivity (mS/cm)	220
Single membrane area (m^2)	0.04

Note: For the efficient functioning of the EDBM cell a minimum current of 1A should be maintained. The EDBM unit must be stopped when the system reaches less than 1A for a max voltage of 20V.

Table 15: Properties of membranes used in EDBM stack.

Membrane	Thickness (mm)	Area resistance ($\Omega \cdot cm^2$)	Burst strength (kPa)	Selectivity (%)	Efficiency (%)
CMB cation-exchange membrane	0.21	4.5	≧ 400	> 98	--
Neosepta® bipolar membrane	0.22	--	≧ 400	--	> 98

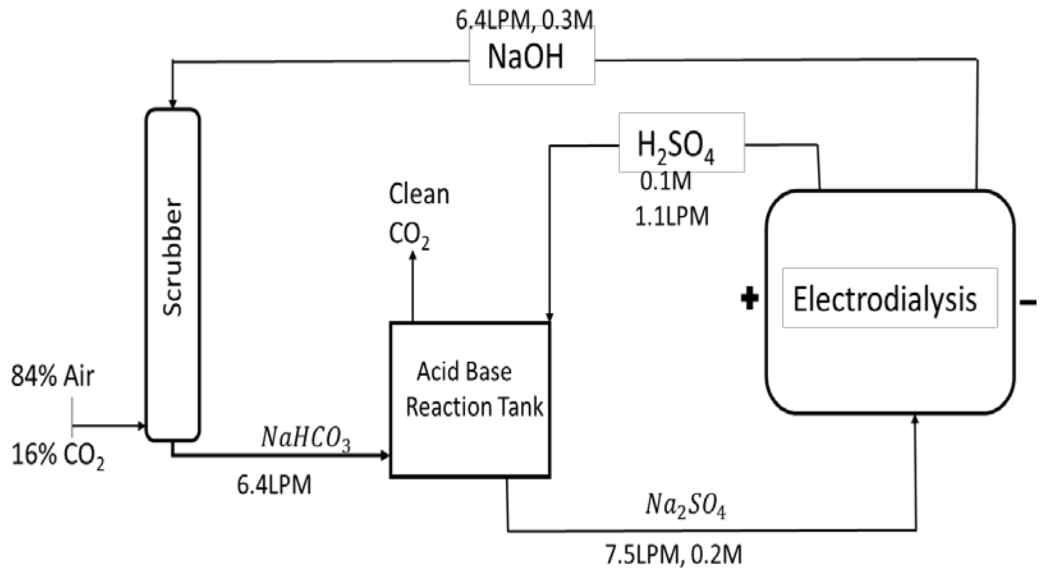

Figure 34: Flow diagram of CO_2 capture and regeneration with acid followed by EDBM separation. The acid (H_2SO_4), base (NaOH) and salt (Na_2SO_4) solutions have 100-liter individual reserve tanks before pumping them through the scrubber and EDBM system.

LPM-Liters per min.

4.4 Experimental procedure:

CO_2 capture and regeneration experiments were conducted with the setup shown in Figure 34. Before running this setup in continuous mode, CO_2 capture experiments were conducted in the scrubber with different concentrations of NaOH. Concentrations of 0.1-0.4mol/L were tested and a maximum CO_2 capture efficiency of 97% was observed at concentrations of 0.3 mol/L and higher. After finding that 0.3 mol/L was the optimum concentration for achieving maximum absorption efficiency, the EDBM setup was run for 30 minutes to achieve desired NaOH concentration.

Before running and regeneration setup in continuous mode with the capture column, EDBM cell was run for 30 minutes until the desired acid and base concentrations were reached, starting with 0.2 mol/L Na_2SO_4, 0.1 mol/L NaOH and 0.02 mol/L H_2SO_4 concentrations. Acid and base concentrations are started at 0.024 mol/L and 0.1mol/L respectively to ensure the initial conductivity of the cell is greater than 20mS/cm, for proper functioning of EDBM. Several voltage ranges were tested for the EDBM cell, and for each constant voltage, current density was recorded every minute until it reaches a maximum value. Then the setup shown in figure 34 was run in continuous mode for 3 hours to ensure no discrepancy in CO_2 capture and regeneration. CO_2 absorption data was continuously recorded by the gas analyzer for the entire duration of the experiment. CO_2 absorption was continuous at 97% absorption efficiency throughout the duration of 3 hours. Each experiment was repeated three times to ensure reproducibility.

4.5 Results and discussion:

4.5.1 CO_2 absorption with NaOH:

Figure 35 shows the CO_2 absorption efficiency of NaOH solution at different concentrations. Initial absorption experiments were conducted with NaOH concentration ranging from 0.1 mol/L to 0.4 mol/L. As shown in Figure 35, the absorption efficiency of the solution slowly increased with increasing NaOH concentration, finally reaching an asymptote after 0.3 mol/L at 97% capture efficiency.

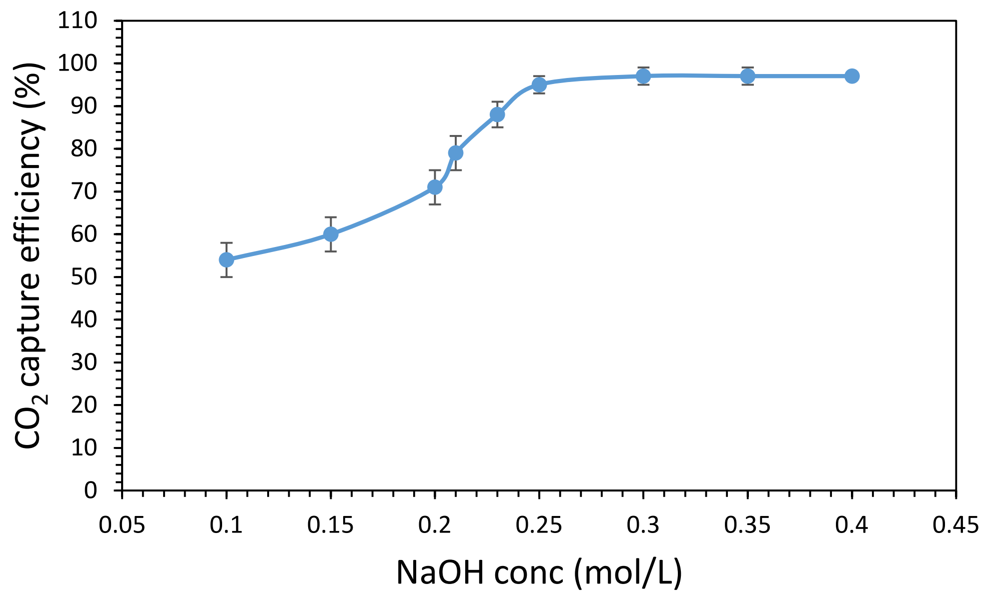

Figure 35: CO_2 capture efficiency of NaOH at various concentrations at 38^oC. The error bars represent standard error (n=3).

4.5.2 NaOH regeneration with EDBM:

Initial batch tests were conducted on EDBM cell for 30 minutes until the desired acid and base concentrations were reached. Figure 5 shows that maximum acid and base concentrations were reached in 30 Minutes. Figure 36(a) shows an increase in acid and base concentration with time, until they reach asymptote after about 30 minutes, then the continuous CO_2 capture and regeneration experiments were run for 3 hours with constant current intensity. As shown in Figure 36(b), at constant voltage the current density increases with an increase in time, acid and base concentration due to an increase in conductivity. Once maximum conductivity is reached, the cell operates at a constant current intensity for a given voltage. All the experiments were repeated through three independent measurements. The experimental uncertainty was calculated and the results were plotted within 95% confidence interval.

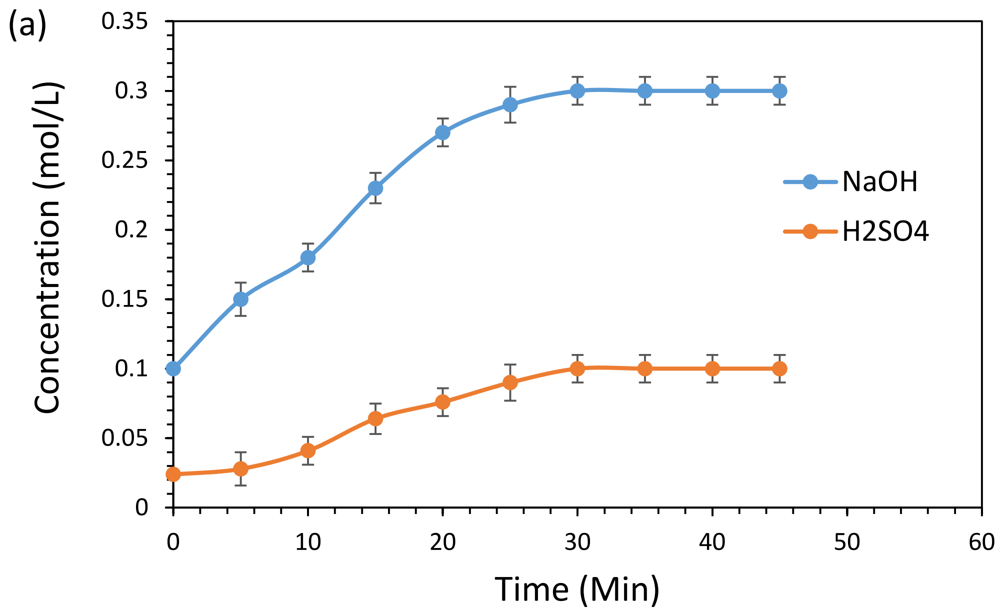

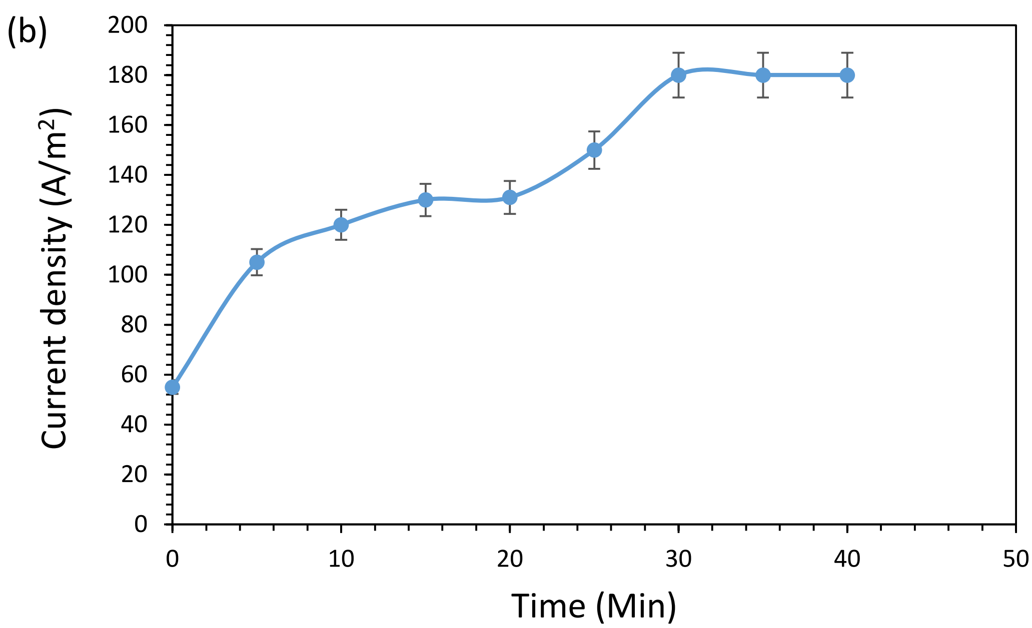

Figure 36: (a) Change in acid and base concentration with time at temperature T= 30^{o}C, voltage V = 18V (b) Current density vs time until the current reaches a maximum value. Error bars represent standard error from three independent measurements.

Comparing two compartment configuration with three compartment configuration:

Figure 37 shows two compartment EDBM configuration used in our system. The two compartment configuration has BPM and CEM as the repeating unit cell. The number of repeating unit cells in this case is n=7. In three compartment configurations, the repeating unit cell has AEM, CEM and BPM in respective order. Three compartment configurations are generally used for creating higher concentration of both acid and base. Three compartment configurations tend to create concentrations of more than twice that of two compartment cells (Kroupa et al., 2015). In our case, we require dilute concentrations of acid and base so having a two compartment configuration is advantageous in achieving high current efficiency at low voltage ranges. Kroupa et al. (2015) have previously observed that a two compartment EDBM configuration reaches desired maximum acid and base concentrations in less time (within first 60 minutes) compared to three compartment configurations (few hours). In our case the maximum acid and base concentrations were reached in 30 minutes as shown in Figure 36(a). Although, this time is only significant during the batch testing, in continuous mode two compartment configuration consumes less energy due to lower acid and base concentrations required for our system.

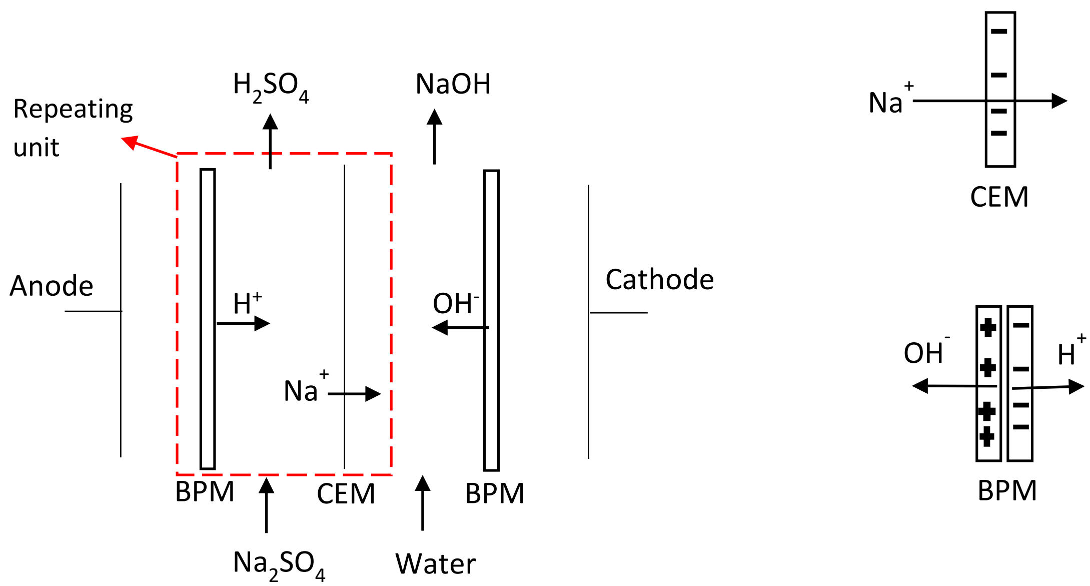

Figure 37: Two-compartment configuration of electro dialysis with bipolar membrane (EDBM) separation. CEM – Cation exchange membrane, BPM- Bipolar membrane.

4.5.3 Effect of current density on energy consumption, current efficiency and NaOH concentration:

Since the energy consumption is our primary focus, the effect of current density on energy consumption is studied. Current density and energy consumption also have a direct influence on NaOH concentration, which in turn has an effect on CO_2 capture efficiency. With increase in the concentration of electrolyte solution (0.2M Na_2SO_4), the current efficiency decreases. Also, higher concentration leads to high osmotic pressures and reduction in water dissociation at the bipolar membrane (Huang et al., 2006).

Current efficiency:

Current efficiency defines how effectively the ions are transported across the membranes. Current efficiency decreases as the electrolyte and base concentrations increase. A low current efficiency may also result from the imperfect orientation of the membranes that allow the transfer of some co-ions, particularly when the concentrations are higher. Current efficiency is calculated from equation (7) (Huang et al., 2006).

$$\eta = \frac{z \cdot F \cdot V\ (C_t - C_0)}{n \cdot I \cdot t} \qquad (7)$$

where n is the number of cells (repeating membrane units; n = 7 in our case). V (L) is the circulated volume of the solution. F is Faraday's constant (96,500 coulombs/mol). C_0 and C_t are the concentrations (mol/L) of NaOH at time 0 and time t. z = 1 in this case because of OH^- carrying unit negative charge. I (A) is the current across the cell.

Energy consumption:

Total energy consumption in kWh Kg^{-1} of CO_2 captured is calculated from equation (8) (Tongwen and Weihua, 2002). This energy is converted to MJ Kg^{-1} by multiplying with a conversion factor of 3.6.

$$\text{Energy consumption} = \int \frac{U \cdot I \cdot dt}{V_t \cdot C_t \cdot M} \qquad (8)$$

Where U (V) is voltage across EDBM cell. I (A) is the current across the cell. C_t is the concentration of CO_2 at time t. V_t (L) is the volume of the solution circulating through the setup. M is the molecular weight of CO_2 (44.01 g/mol).

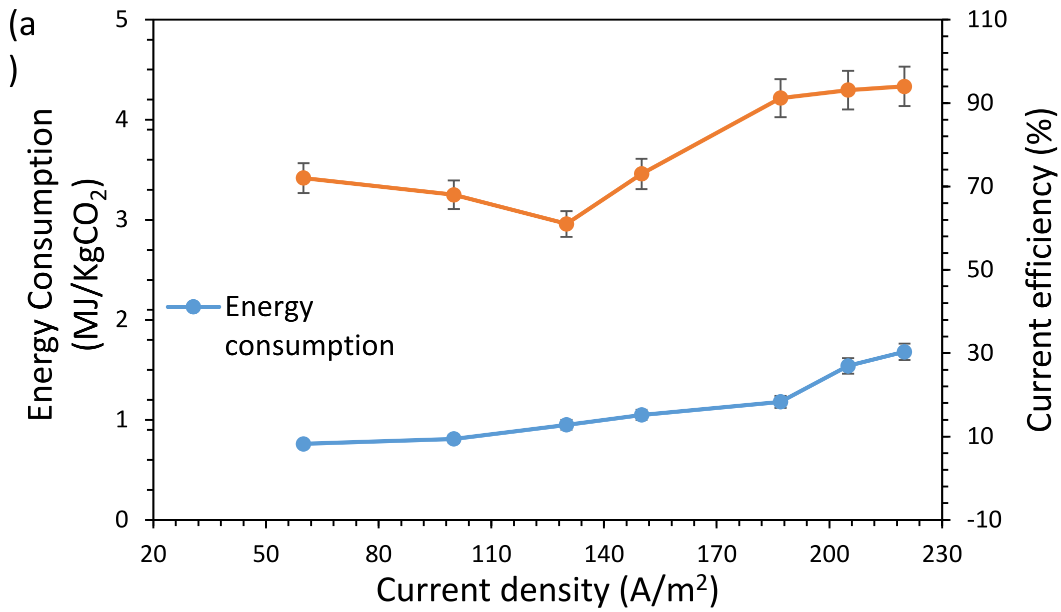

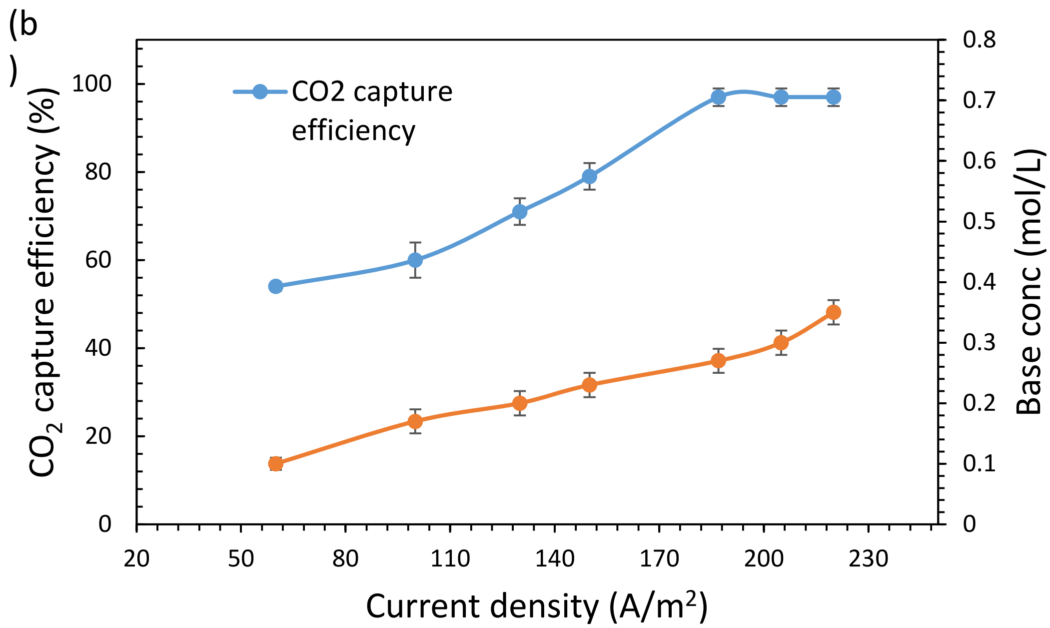

Figure 38: (a) Effect of current density on energy consumption per Kg of CO_2 captured and current efficiency. (b) Effect of current density on NaOH concentration and CO_2 capture efficiency, with the error bars representing the standard error (n=3).

Figure 38(a) shows the effect of current density on energy consumption and current efficiency. Current efficiency initially decreases with increase in current density because of low ion selectivity of membranes at lower ranges of current density, but current efficiency starts to increase once the current density is over 140 A/m^2 due to higher ion transport in the base compartment because of higher conductivity. Increase in current density from 150A/m^2 to 180A/m^2 only increases the energy slightly from 1.03 to 1.18MJ, but this increase is more pronounced from 190 to 200A/m^2 due to increase in base concentration at peak current (I) from equation 8. Increasing the base concentration by more than 0.3 mol/L increased the current efficiency but it also increased the overall energy consumption. Considering the total energy consumption as the criteria for the overall process, it would be desirable to stay below the current density of 180A/m^2.

Decrease in current efficiency was observed at lower current density and base concentrations. In the two-compartment configuration the hydron (H^+) which migrate through the cation exchange membrane recombines with hydroxide ion (OH^-), slightly reducing the current utilization. The energy consumption is less in case of two compartment configurations because of dilute base concentration, while that of acid concentration effect on energy consumption follows the opposite trend as previously observed by Kroupa et al. (2015) when conducting studies on recovery of H_2SO_4 from Na_2SO_4 salt solution.

Figure 38(b) indicates that as the current density increases, the base concentration keeps increasing, but the CO_2 capture efficiency reaches a plateau at 97% capture efficiency. Increasing the base concentration further will leave unreacted NaOH in the captured solution. Further increasing the base concentration will increase the energy consumption of EDBM cell at higher current densities as shown in Figure 38(a). So, the optimum values for the current density and base concentration are: 181.7A/m^2 and 0.3 mol/L respectively, keeping the energy consumption minimum and achieving 97% CO_2 capture efficiency. Therefore, the optimum operating conditions of the cell are: 18V, 7.5A.

4.5.4 Performance evaluation:

The regeneration energy of 1.18MJ/KgCO_2 when compared to 3-4MJ/KgCO_2 in case of thermal regeneration with amines and other absorbent solutions is a huge breakthrough in terms of energy savings. In the case of thermal regeneration, evidence suggests that an increase in stripper energy from 3MJ/KgCO_2 to 4MJ/KgCO_2 will reduce the power plant output by at least 20% (Knuutila et al., 2009; Karimi et al., 2011). The important advantage of using EDBM process is that renewable sources like photovoltaics can be used to energize the EDBM cell. Some researchers who worked on direct electrodialysis of $NaHCO_3$ solution were able to achieve low energy values (2-3MJ/KgCO_2) compared to thermal regeneration, but the direct electrodialysis process has its own fair share of process complications as mentioned earlier in section 1.3, and more importantly very low CO_2 recoveries (40-60%) (Eisaman et al., 2011; Iizuka et al., 2012).

As opposed to direct electrodialysis, the most important trait in our process is the 100% recovery rate of CO_2. Since all the CO_2 is recovered before the EDBM step, it eliminates the presence of gas bubbles in the cell, avoiding unnecessary resistance across the cell. Hence, a very high current efficiency of 91% was observed, due to relatively lower concentration of acid and base generated. The limitation in current efficiency could be due to the leakage of protons through the cation exchange membrane. In a commercial scale EDBM unit, the number of unit cells could be much larger as opposed to our lab scale unit, in which case voltage drop across the EDBM stack would be much less at lower current densities. Thus, the energy requirement could be further lowered in a commercial scale unit.

A process advantage for our regeneration method is that it can be performed at room temperature and atmospheric pressure conditions, as opposed to high pressures required for direct electrodialysis of $NaHCO_3$ as mentioned earlier. This ensures high process safety and also easier start-up and shutdown. Also, particulate filtration step is recommended before the scrubber to ensure no particulates enter the EDBM cell. The usual norm in industrial flue gas capture is to remove/filter suspended particulates before sending the gas for Flue gas desulfurization (FGD) and subsequently CO_2 capture. So, we suggest adding a particulate filter step before the scrubber in order to avoid suspended solids going into the EDBM cell and fouling membranes.

4.6 Cost estimation:

Economic analysis was carried out by considering a hypothetical case of 400MW coal-fired power plant, which corresponds to 300 tons/hour of CO_2 emissions and a continuous operation of CO_2 capture and regeneration for 350 days a year at 24 hours per day (Iizuka et al., 2012). With 97% CO_2 capture efficiency of NaOH from our experimental results, this accounts to 2.4 Mton/year of CO_2 captured. All assumptions for cost estimation are shown in Table 16. Considering the above-mentioned base case scenario for capital cost, the operating cost is estimated by calculating the direct energy cost.

<u>Cost of CO_2 absorption:</u>

Cost of CO_2 capture with thermal regeneration from previous literature was estimated to be around 45-60$/ton of CO_2 captured (Wang et al., 2017; Karimi et al., 2011) , and Knuutila et al. (2009) estimated that 30% of this cost corresponds to CO_2 absorption equipment, which includes absorption column and pumping system. Considering the same base case scenario, the CO_2 absorption cost is estimated to be 13.5$/ton of CO_2 captured.

<u>Cost of CO_2 regeneration:</u>

Cost of CO_2 regeneration or reagent regeneration was estimated based on our results from laboratory EDBM experiments. Our cell in the lab has a cell volume of 0.012 m^3 and handles 7.5 L/min of solution. At the L/G ratio of 4.3 and gas flow of 5 tons/min the total liquid to be handled by EDBM cells is 21500LPM. Therefore, the number of cells required are 2867. Cost of each EDBM stack was estimated as 1.5 times the cost of membranes, based on the work of Strathmann and Koops (2000). Table 17 shows total equipment cost and operating costs.

Table 16: Operating parameters and assumptions made for cost estimation of CO2 capture with EDBM regeneration.

Parameter		**Life span**	**Reference**
Number of EDBM cells	2867	15 years	-
Bi-polar membrane price ($/cm^2)	0.43	5 years	Iizuka et al., 2012
Cation exchange membrane price ($/cm^2)	0.24	5 years	Yee et al., 2012
Electricity cost ($/kWh)	0.06	-	Keith et al., 2018
Cost of each EDBM stack ($/cm^2)	1.005	-	Strathmann and Koops, 2000

Table 17: Total equipment costs (TEC) and operating costs.

Capital Costs	**(Million $)**
Cost of EDBM cells (including membrane cost)	26.62
Other equipment*	28.5

TEC	55.12
Operating costs	**($/ton of CO_2 captured)**
Energy cost	19.62
Labor and Maintenance (13% of Investment Cost (Karimi et al., 2011))	0.52
Other variable costs**	0.39

Note: *Other equipment includes spacers, pipelines, pumps, CO_2 compression etc. Cost of other equipment was estimated from the work of Sabatino et al. (2020), who considered the same volume of CO_2 processed per hour. **Other variable costs include pumping costs and other miscellaneous expenses.

Total capital cost including equipment cost, construction, valves, piping, etc. is calculated based on NETL guidelines as follows (Sabatino et al., 2020; Spallina et al., 2016):

Total installation cost [TIC] = 80% TEC

Total direct plant cost [TDPC] = TEC + TIC

Indirect costs [IC] = 13% TDPC

Engineering, procurement, and construction [EPC] =	TDPC + IC
Total contingencies and owner's cost [C&OC] =	30% EPC
Total capital [TC] =	EPC + C&OC

The total capital investment is 145.73M$ for 15 years of operation and 36Mtons of total CO_2 processed. So, for 1ton of CO_2 captured the total capital investment turns out to be 4.04$/ton of CO_2 captured. If we combine both capital expenditure and variable operating costs, the total cost of CO_2 capture and regeneration would be 38.07$/ton of CO_2 captured. Although the operating costs are very low, the capital cost increases the total cost due to high EDBM unit prices and membrane prices. Membrane prices are expected to go down further in the future, in such a case the total cost can be less than 38.07$/ton of CO_2.

Depending on the project timeline, EDBM will be advantageous if the project period is extended over 15 years. It can also be made profitable over a shorter period of time if the membrane prices are lowered. Further decreases in electricity costs may also be anticipated by 2050, with developments in renewable energy technologies.

An additional benefit of the EDBM method is that you can regulate the base concentration as required by adjusting the voltage and current across the cell. If the CO_2 concentration from the flue gas is fluctuating due to load variation from the power plant, this tuning might help reduce the cost on daily basis. Considering 15 years of project timeline, the average cost per ton of CO_2 captured is roughly 38$. We also believe that the reagent regeneration energy of 1.18MJ / kg could be further reduced with numerous performance improvements and careful design choices, making CO_2 capture economically feasible and environmentally benign.

4.7 Conclusion:

We have developed a new regeneration method for CO_2 capture with alkali absorbent solution, by reacting sodium bicarbonate with sulfuric acid and the resultant sodium sulphate solution is subjected to EDBM process for regenerating NaOH. We were able to achieve reagent regeneration energy as low as 1.18MJ/kg of CO_2 captured at a current efficiency of 91.2% for the EDBM cell. The cost of our process is around 38.07$/ton of CO_2 captured based on 2020 prices. This cost could be even lower if membrane costs were competitive. This approach could be a very promising choice for post-combustion CO_2 capture in the future.

4.8 References:

- Barzagli, F., Giorgi, C., Mani, F. and Peruzzini, M., 2017. CO2 capture by aqueous Na2CO3 integrated with high-quality CaCO3 formation and pure CO2 release at room conditions. *Journal of CO2 Utilization*, *22*, pp.346-354.
- Bazhenov, S., Rieder, A., Schallert, B., Vasilevsky, V., Unterberger, S., Grushevenko, E., Volkov, V. and Volkov, A., 2015. Reclaiming of degraded MEA solutions by electrodialysis: Results of ED pilot campaign at post-combustion

CO_2 capture pilot plant. *International Journal of Greenhouse Gas Control*, *42*, pp.593-601.

- Dietrich, F., Schöny, G., Fuchs, J. and Hofbauer, H., 2018. Experimental study of the adsorber performance in a multi-stage fluidized bed system for continuous CO_2 capture by means of temperature swing adsorption. *Fuel Processing Technology*, *173*, pp.103-111.
- Eisaman, M.D., Alvarado, L., Larner, D., Wang, P., Garg, B. and Littau, K.A., 2011. CO_2 separation using bipolar membrane electrodialysis. Energy & Environmental Science, 4(4), pp.1319-1328.
- Huang, C. and Xu, T., 2006. Electrodialysis with bipolar membranes for sustainable development. *Environmental science & technology*, *40*(17), pp.5233-5243.
- Huang, C., Xu, T. and Jacobs, M.L., 2006. Regenerating flue-gas desulfurizing agents by bipolar membrane electrodialysis. *AIChE journal*, *52*(1), pp.393-401.
- Hwang, J., Kim, J., Lee, H.W., Na, J., Ahn, B.S., Lee, S.D., Kim, H.S., Lee, H. and Lee, U., 2019. An experimental based optimization of a novel water lean amine solvent for post combustion CO_2 capture process. Applied Energy, 248, pp.174-184.
- Iizuka, A., Hashimoto, K., Nagasawa, H., Kumagai, K., Yanagisawa, Y. and Yamasaki, A., 2012. Carbon dioxide recovery from carbonate solutions using

bipolar membrane electrodialysis. *Separation and purification technology*, *101*, pp.49-59.

- Jaroszek, H. and Dydo, P., 2016. Ion-exchange membranes in chemical synthesis–a review. *Open Chemistry*, *14*(1), pp.1-19.
- Karimi, M., Hillestad, M. and Svendsen, H.F., 2011. Capital costs and energy considerations of different alternative stripper configurations for post combustion CO2 capture. *Chemical engineering research and design*, *89*(8), pp.1229-1236.
- Karimi, M., Hillestad, M. and Svendsen, H.F., 2011. Capital costs and energy considerations of different alternative stripper configurations for post combustion CO2 capture. *Chemical engineering research and design*, *89*(8), pp.1229-1236.
- Kawatra, S.K., 2020. *Advanced Coal Preparation and Beyond: CO2 Capture and Utilization*. CRC Press.
- Keith, D.W., Holmes, G., Angelo, D.S. and Heidel, K., 2018. A process for capturing CO2 from the atmosphere. *Joule*, *2*(8), pp.1573-1594.
- Knuutila, H., Svendsen, H.F. and Anttila, M., 2009. CO2 capture from coal-fired power plants based on sodium carbonate slurry; a systems feasibility and sensitivity study. *International journal of greenhouse gas control*, *3*(2), pp.143-151.

- Kroupa, J., Kinčl, J. and Cakl, J., 2015. Recovery of H_2SO_4 and NaOH from Na_2SO_4 by electrodialysis with heterogeneous bipolar membrane. *Desalination and Water Treatment*, *56*(12), pp.3238-3246.
- Nagasawa, H., Yamasaki, A., Iizuka, A., Kumagai, K. and Yanagisawa, Y., 2009. A new recovery process of carbon dioxide from alkaline carbonate solution via electrodialysis. AIChE journal, 55(12), pp.3286-3293.
- Sabatino, F., Mehta, M., Grimm, A., Gazzani, M., Gallucci, F., Kramer, G.J. and van Sint Annaland, M., 2020. Evaluation of a Direct Air Capture Process Combining Wet Scrubbing and Bipolar Membrane Electrodialysis. *Industrial & Engineering Chemistry Research*, *59*(15), pp.7007-7020.
- Salmón, I.R., Cambier, N. and Luis, P., 2018. CO_2 Capture by Alkaline Solution for Carbonate Production: A Comparison between a Packed Column and a Membrane Contactor. *Applied Sciences*, *8*(6), p.996.
- Spallina, V., Pandolfo, D., Battistella, A., Romano, M.C., Annaland, M.V.S. and Gallucci, F., 2016. Techno-economic assessment of membrane assisted fluidized bed reactors for pure H_2 production with CO_2 capture. *Energy conversion and management*, *120*, pp.257-273.
- Spigarelli, B.P. and Kawatra, S.K., 2013. Opportunities and challenges in carbon dioxide capture. *Journal of CO_2 Utilization*, *1*, pp.69-87.
- Strathmann, H. and Koops, G.H., 2000. Process economics of the electrodialytic water dissociation for the production of acid and base. In *Handbook Bipolar*

Membrane Technology-Ed. AJB Kemperman (pp. 191-220). Twente University Press (TUP).

- Toan, S., O'Dell, W., Russell, C.K., Zhao, S., Lai, Q., Song, H., Zhao, Y. and Fan, M., 2019. Thermodynamics of NaHCO3 decomposition during Na2CO3-based CO2 capture. *Journal of Environmental Sciences*, *78*, pp.74-80.
- Tongwen, X.U. and Weihua, Y., 2002. Citric acid production by electrodialysis with bipolar membranes. *Chemical Engineering and Processing: Process Intensification*, *41*(6), pp.519-524.
- Valluri, S. and Kawatra, S.K., 2020. Simultaneous removal of CO_2, NO_X and SO_X using single stage absorption column. *Journal of Environmental Sciences.* In press.
- Valluri, S. and Kawatra, S.K., Use of frothers to improve the absorption efficiency of dilute sodium carbonate slurry for post combustion CO2 capture. *Fuel Processing Technology*, *212*, p.106620.
- Wang, Y., Zhao, L., Otto, A., Robinius, M. and Stolten, D., 2017. A review of post-combustion CO2 capture technologies from coal-fired power plants. *Energy Procedia*, *114*, pp.650-665.
- Yee, R.S.L., Rozendal, R.A., Zhang, K. and Ladewig, B.P., 2012. Cost effective cation exchange membranes: A review. *Chemical Engineering Research and Design*, *90*(7), pp.950-959.

5. Electrochemical approach for converting carbon dioxide to oxalate.

5.1 Abstract

With increased CO_2 emissions into atmosphere, there is great opportunity to capture CO_2 and utilize the captured CO_2 for economic advantage. Developing energy-efficient processes that reductively couple CO_2, an abundant and renewable carbon source, for the production of value-added chemicals (methanol, ethanol, and oxalic acid) using electrochemical processes is a goal of great importance. In many cases, these chemicals can be reused elsewhere in the refining process or sold as valuable byproducts. Electrochemical reduction of CO_2 to Oxalic acid and other chemicals is a complex multistep reaction with adsorbed intermediates. The exact reaction mechanism is not clear from the literature to date and will likely change over a range of conditions like electrode type, electrode potential, Current density, catalyst, etc. We have successfully produced Oxalic acid from CO_2 with the help of electro-catalytic reduction, and the results are discussed in this section.

5.2 Introduction.

The large contribution in total CO_2 emission originates from coal or natural gas power plants, and a considerable amount from steel plants. Capturing the available CO_2 from the steel and coal industries for economic advantage is a win-win situation for the industry. This technology is not only important scientifically but is also vital for a sustainable future. The various ongoing investigations can be categorized as biochemical, thermochemical, photochemical, and electrochemical approaches. Among these, the electrochemical method shows the most promise as an efficient form of CO_2 conversion technology, because of its many advantages like high reactivity under ambient conditions and good extensibility from small- to large-scale processes (Savéant, 2008).

CO_2 is thermodynamically quite stable, as shown by its highly negative heat of formation. Thus, it is expected that the formation of any useful chemical from CO_2 will require the input of at least as much energy as geological sequestration. This lends itself to two extremes: one where the quantity of energy required is low and one where the economic value of the additional energy is low.

It is expected that CO_2 can be reduced via electrolysis to several compounds. Of particular interest are formic acid, oxalic acid, methanol, ethanol, formaldehyde, and carbon monoxide (as a component to syn-gas). These chemicals have been reported as electrolytic products previously in literature and have considerable potential for application.

5.3 Background

Extensive research has been done on the chemistry of transforming carbon dioxide into more useful products. Methods are known to convert carbon dioxide into a wide variety of substances, including methanol, isobutanol, carbohydrates, methane, carbonates, urea, formic acid, oxalic acid, carbon monoxide, epoxides, formaldehyde, and so on. Several of these (carbohydrates, formaldehyde, isobutanol etc.) are primarily results from biological processes. The rest are results of strong reduction reactions or electrolytic reduction. In short, electrolytic reduction can be used to form methane, methanol, formic acid, oxalic acid, carbon monoxide from carbon dioxide (Oloman and Li, 2008).

CO_2 reduces at the cathode in an electrolysis cell. These processes have the general form of generating the carbon dioxide anion radical ($CO_2^{\cdot-}$) and allowing it to react with itself or the electrolyte (Gennaro et al., 1996). Catalysts can be added to influence the formation of the anion radical or to suppress side reactions (Gennaro et al., 1996). The electrolyte, catalyst, voltage, electrode material and CO_2 content are all known to affect the reaction pathway (Abbott and Eardley, 2000; Eggins et al., 1997; Hori et al., 1994; Kushi et al., 1994; Malik et al., 2017; Qiao et al., 2014; Costentin et al., 2013). Table 18 shows the overall reactions and energy requirements for electrochemical conversion of CO_2 to chemicals.

Table 18: Energy cost for Producing Products from Carbon Dioxide.

(Malik et al., 2017; Qiao et al., 2014).

Product	Overall Reaction	EE* (MJ/Kg)
Oxalate	$2CO_2 \rightarrow C_2O_4^{2-}$	2.68
Formic acid	$2CO_2 + 2H_2O \rightarrow 2\mathrm{HCOO}H + O_2$	5.51
Syn-gas	$2CO_2 + H_2O \rightarrow 2CO + O_2 + H_2O$	9.19
Methanol	$CO_2 + 2H_2O \rightarrow 1.5O_2 + CH_3OH$	21.71
Ethanol	$2CO_2 + 3H_2O \rightarrow C_2H_5OH + 3O_2$	28.70
Propanol	$3CO_2 + 4H_2O \rightarrow C_3H_7OH + 4.5O_2$	29.53
Methane	$CO_2 + 2H_2O \rightarrow 2O_2 + CH_4$	51.15

*EE-Electrical Energy

5.4 Experimental

5.4.1 Electrocatalytic Production of Oxalate from CO_2

Initially we used a membrane electrolysis cell to produce oxalate from CO_2. A membrane electrolysis cell is a 2-chamber electrolysis cell where the chambers are separated by a selectively permeable membrane. To produce oxalate, a cation exchange membrane (which selectively exchanges cations) was used. Previous literature suggests that in the cathode chamber an organic electrolyte, such as tetraethylammonium perchlorate or tetraethylammonium bromide (TEA-Br) in dimethylformamide (DMF), are preferred. In the anode chamber, a sodium hydroxide solution water is used. Carbon dioxide is then bubbled into the cathode chamber as a current is applied. The above-described process is shown in Figure 1(a).

<u>Catholyte and anolyte concentrations:</u>

Catholyte: DMF, 0.1M TEA-Br, 0.01M o-tolunitrile. Anolyte: Water, NaOH buffered with sodium bicarbonate to a pH of 9.8. The above-described process is shown in Figure 1.

We have modified the electrolysis cell for improved cathode surface area to adsorb more CO_2 for more conversion. We have wrapped the cathode in a cylindrical fashion around the anode, keeping the total cell volume constant, as shown in Figure 1(b). This way we can eliminate the membrane separated catholyte and anolyte region.

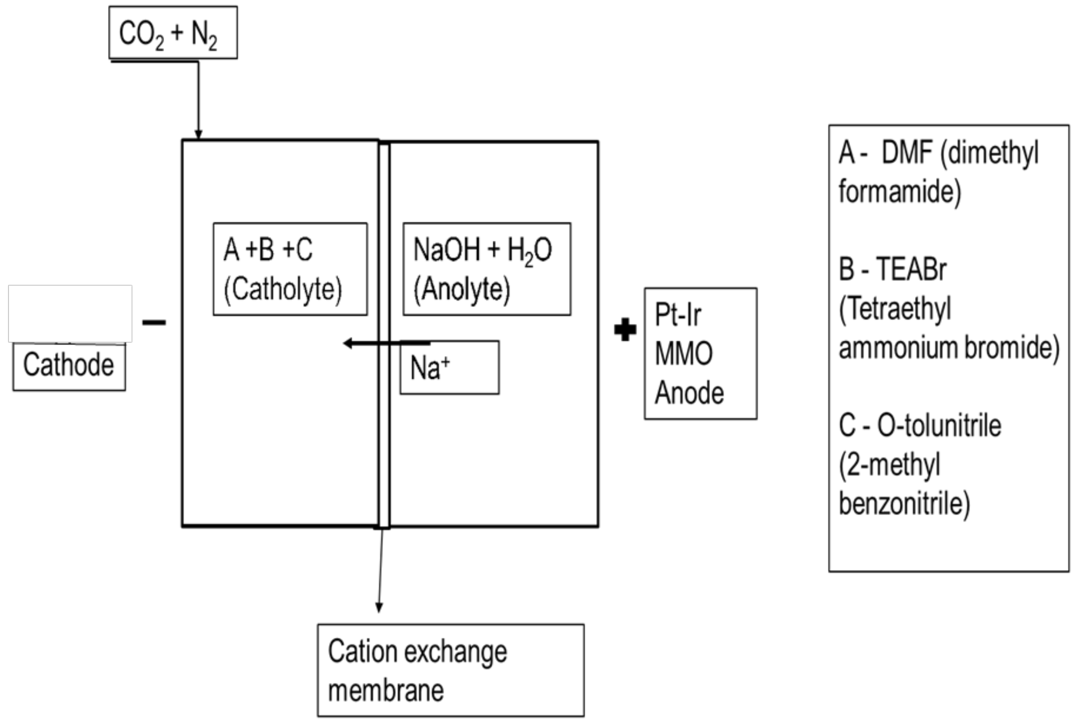

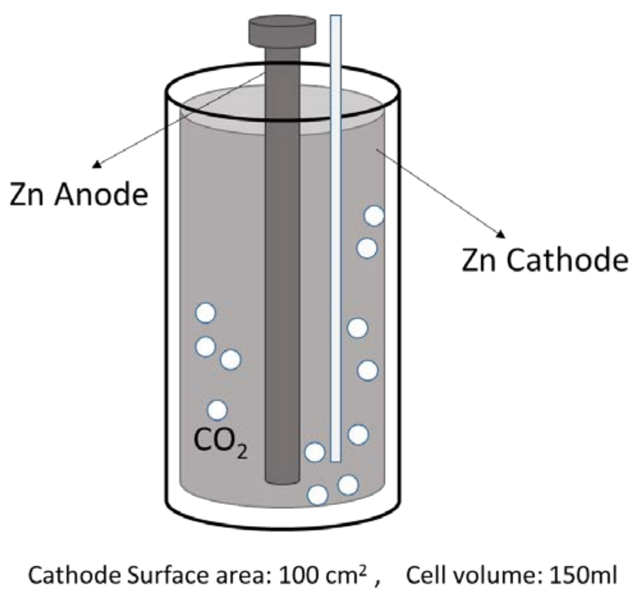

Figure 39: (a) Membrane Electrolysis cell for converting CO2 to Oxalate. (b) Modified cell

Modified electrode surface:

We have modified the cathode surface with lead coating for two purposes. 1) Lead has proven more selective for producing oxalic acid in an aprotic solvent. 2) The lead coating on the cathode surface is rough, which provides more active sites for CO_2 to adsorb and undergo further steps of reduction.

5.4.2 XRD Studies:

The solid precipitate sample was dried in a vacuum drying oven and hand ground for XRD analysis. X-ray Powder Diffraction was used to identify different phases in the solid precipitate sample collected from experiments. The XRD pattern of the solid sample was determined by using Scintag XDS2000 Powder Diffractometer in a 2Θ range of 10–45^o at a scanning rate of 2.4^o min^{-1}.

5.5 Results and discussions

Generation of Oxalate from CO_2 without the addition of a catalyst is thermodynamically unfavorable at 298K and atmospheric pressure, due to the high negative redox potential (E= -2.2V vs SCE). The addition of O-tolunitrile or other aromatic nitriles as a catalyst results in a highly selective reaction system. This should create sodium oxalate with 80%

or higher coulombic efficiency. Without it, the reaction is more favored towards carbon monoxide product.

The primary reaction is the electron addition to an aromatic nitrile catalyst $A + e^- \rightarrow A^{\cdot -}$, which is accompanied by electron transfer to CO_2 from anion radical $A^{\cdot -} + CO_2 \rightarrow A + CO_2^{\cdot -}$, which then dimerizes to oxalate $2CO_2^{\cdot -} \rightarrow C_2O_4^{2-}$. This was collected at the bottom of the cell as zinc oxalate solid precipitate. It was also found that the cation exchange membrane is not intended for use in strongly basic solutions. That was fixed by buffering the sodium hydroxide solution in the anolyte region to a lower pH with a weak acid.

5.5.1 Electrode selectivity:

Type of electrode and cell potential play a crucial role in electrochemical reduction of CO_2. Lead and steel can be mentioned as good examples of inert, “outersphere” electrode materials for CO_2 reduction. Lead, Zinc and steel electrodes with rough surface have shown promising results. We have tested a range of voltages and current densities. 6 to 11 volts and more than 25mA/cm^2 has given promising results as opposed to less than 3 volts and 25mA/cm^2. Figure 3 shows the XRD of oxalate sample produced at 11 volts. High intensity oxalate peaks were observed in case of 11 volts and 25mA/cm^2. We have tried lead, copper, Zinc, silver and steel as cathode materials. Zinc and steel have proven to be most efficient among others, due to alloying effect. Table 3 shows the weight percent of oxalate produced at different cathode materials and various voltages. When gases accumulate on the cathode surface over time, the reduction potential decreases. In this scenario, most of the energy provided is lost as heat. When this happens the reaction-rate slows down and eventually stops. To avoid this, the electrolyte was continuously stirred.

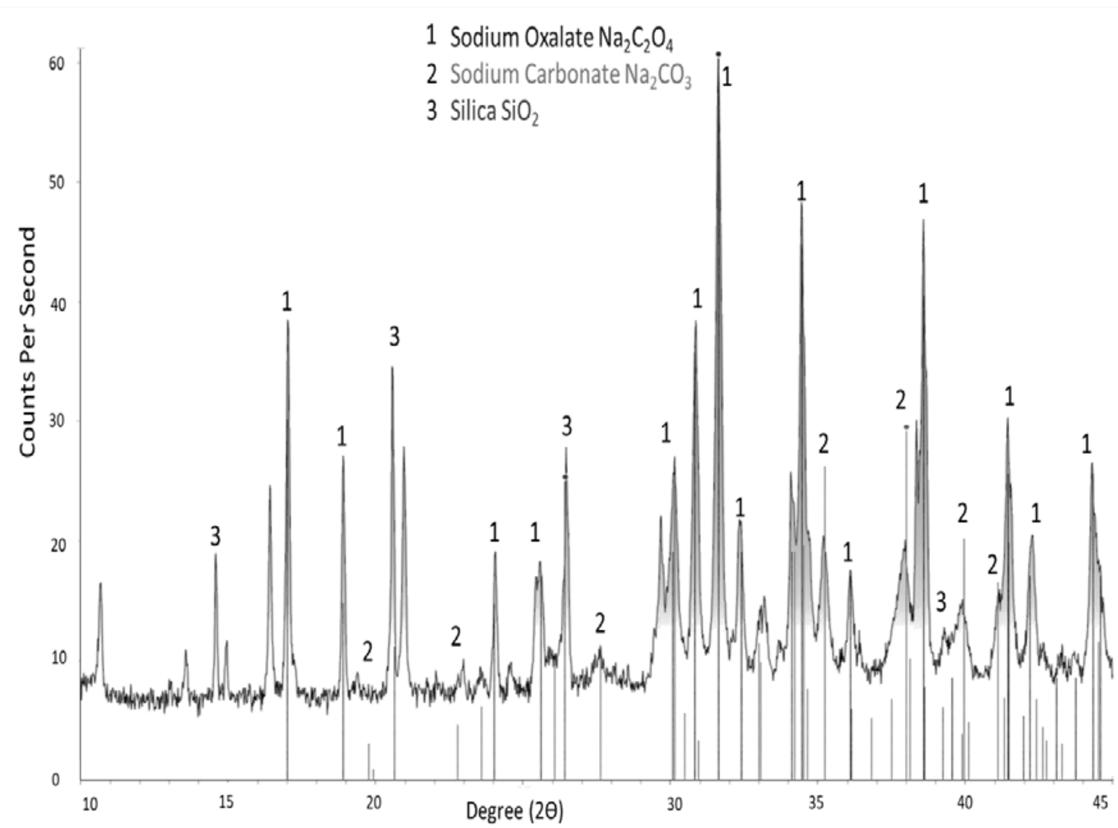

Figure 40: XRD analysis of Oxalate sample with high current densities.

Table 2 shows coulombic yield vs. current density observations for different cathode materials tested. As one can observe, lead, Zinc and steel have more catalytic activity for generating oxalate from CO_2. In addition, steel electrode coated with lead surface irregularities has shown very high (85.23%) coulombic yield. Surface irregularities result in more active surface sites available for effective charge transfer.

Coulombic yields were determined as follows:

Theoretical yield of Oxalate (grams) = $\frac{Number\ of\ coulombs \times mol,wt.of\ oxalate}{2 \times 96{,}500\ coulombs}$

Percent coulombic yield = $\frac{actual\ yield}{theoretical\ yield} \times 100$

$$= \frac{gm\ \ of\ oxalate\ salt}{theoretical\ \ yield\ \ of\ Oxalate\ (gm)} \times 100$$

Table 19: Current density vs coulombic yield observations.

Cathode	Current density (mA/cm^2)	%Coulombic yield*
Zinc	10	-
Steel	15	5.23
Silver	25	-
Steel	25	87.23
Zinc	25	95.01

Lead	27	60.10
Iron (Mild steel)	25	59.32
Copper	25	85.23

Table 20: Oxalate product obtained in weight percent at different cathode materials.

Cathode	**Cell Potential**	**Final product (Individual wt%)**
Zinc	3.5 V	Negligible solid precipitate
Steel	6 V	Oxalate (1.2%), rest zincite
Silver	11 V	Oxalate (5%), Zincite (ZnO) powder (50%)*, TEABR (25%)
Steel	11 V	Oxalate (91%), zincite (6), TEABR (3%)
Zinc	11 V	Oxalate (95%), formate (3%), TEABR (2%)
Lead	11 V	Oxalate (75%), formate (10%), zincite (10%)
Iron (Mild steel)	11V	Oxalate (45%), zincite (25%), TEABR (15%)

Copper	11 V	Oxalate (86%), formate (2%), zincite (10%)

5.5.2 Redox Catalysis:

In case of aromatic esters and nitrile catalysts, the reduction product is exclusively oxalate. When the standard potential of the catalytic pair is more positive, the catalytic efficiency decreases rapidly. These findings relate to a system of redox catalysis through which two CO_2 anion radicals would combine to produce oxalate after being generated by transferring an outer-sphere electron between CO_2 and the anion radical of nitrile or ester.

The reaction scheme involving aromatic nitrile catalyst 'A' is shown below. In step (3) the CO_2 anion radicals undergo dimerization to form oxalate anion. Step (3) is a fast reaction. In step (4) the addition product of carbon-oxygen formed from $CO_2^{\cdot -}$ and CO_2 is due to the base characteristic of $CO_2^{\cdot -}$ and lewis acid properties of CO_2. This intermediate step has been previously Investigated by Seveant, et. al. (1983), to explain the formation of CO in competition with oxalate at electrodes with low hydrogen overpotential. We have observed formation of sodium carbonate (shown in XRD image in figure 4) along with oxalate, which confirms the mechanism observed in step (5).

$$A + e^- \rightleftharpoons A^{\bullet -} \quad (1)$$

$$A^{\bullet -} + CO_2 \rightleftharpoons A + CO_2^{\bullet -} \quad (2)$$

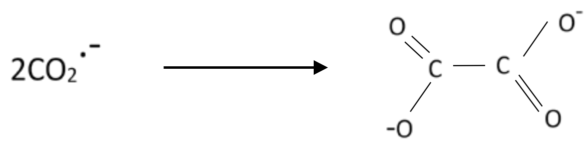

(3)

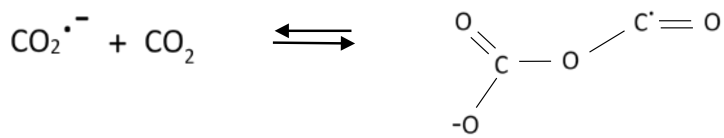

(4)

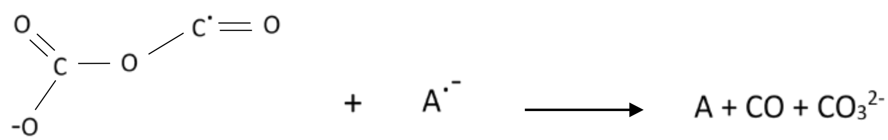

(5)

Table 21: Homogeneous Catalysts: Name, Standard Potentials, and Rate Constants of the Reaction with CO_2.

(Sevant et al., 1983).

Catalyst name	E°cat (V vs SCE)	log *k* (M^{-1} s^{-1})
dimethyl phthalate	-1.928	0.50
di-isobutyl phthalate	-1.948	0.82
dibutyl phthalate	-1.958	0.90
phenyl benzoate	-2.026	2.15
ethyl 3-fluorobenzoate	-2.043	2.43
methyl 3-phenoxybenzoate	-2.085	3.01
phenyl 4-methylbenzoate	-2.094	3.08
methyl benzoate	-2.202	4.19
ethyl benzoate	-2.221	4.21
methyl 3-methylbenzoate	-2.237	4.44
methyl 2-methylbenzoate	-2.276	4.74
methyl 4-methylbenzoate	-2.290	5.04
benzonitrile	-2.260	5.31
O-tolunitrile	-2.297	5.60

The reason for selecting O-tolunitrile as catalyst is that its log *k* value is the highest when compared to others from Table 4. It has been assumed that the reduction of carbon dioxide or the catalyst happens directly at the cathode. If this is correct, then the presence of the catalyst elsewhere in the system is inconsequential. The most obvious way of testing this is to limit the cathode's conductive surface without disrupting the overall electric field across the cell. If the field across the cell is all that is required, then the kinetics should remain unchanged. We tested different sizes for the surface of the cathode and found that the smaller the surface area available for reduction, the lesser the oxalate formation.

Since the aromatic nitrile catalyst is surface active, there is essentially no requirement for any internal volume beyond what is necessary to hold a few bubble-diameters of fluid and maintain conductivity between the cathode and the membrane. This would decrease the quantity of aprotic solvent required considerably, decreasing the overall cost of the process. Figure 4 below shows the further step of preparing oxalic acid from sodium oxalate precipitate.

Preparing Oxalic acid from sodium oxalate:

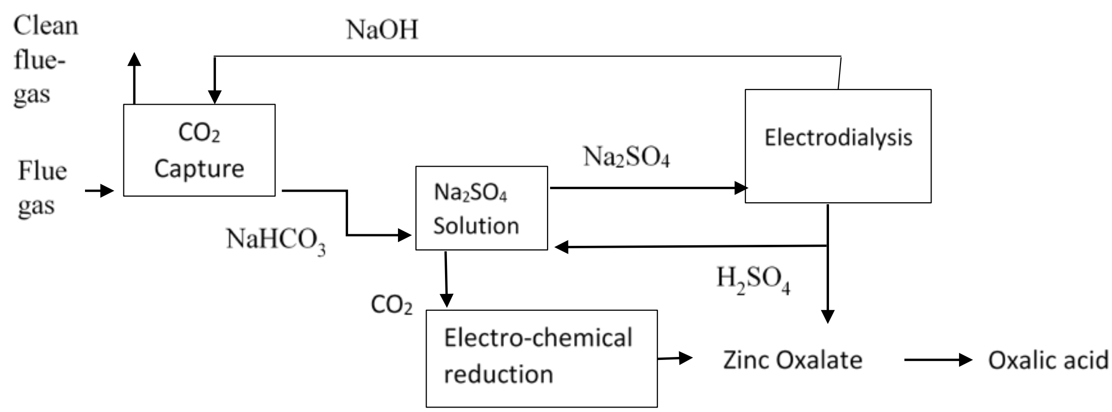

Figure 41: CO_2 capture and electrochemical reduction loop, to produce oxalic acid.

5.6 Conclusion and future objectives:

An Oxalate salt (Zinc Oxalate) from which Oxalic acid may be produced is prepared by reducing carbon dioxide at Zinc/lead cathode in an organic solvent, with an addition of aromatic nitrile catalyst. Current densities of 25mA/cm^2 and higher have proven effective in producing more oxalate in the solid precipitate product. The future scope of this study includes:

- Minimizing the side products like carbon monoxide and formic acid
- Scale up for pilot scale setup
- Cost estimation for retrofitting the cell to existing power plants
- Economic analysis for returns and profits

5.7 References

- Abbott, A.P. and Eardley, C.A., 2000. Electrochemical reduction of CO2 in a mixed supercritical fluid. *The Journal of Physical Chemistry B*, *104*(4), pp.775-779.
- Amatore, C. and Saveant, J.M., 1981. Mechanism and kinetic characteristics of the electrochemical reduction of carbon dioxide in media of low proton availability. *Journal of the American Chemical Society*, *103*(17), pp.5021-5023.
- Costentin, C., Robert, M. and Savéant, J.M., 2013. Catalysis of the electrochemical reduction of carbon dioxide. *Chemical Society Reviews*, *42*(6), pp.2423-2436.
- Eggins, B.R., Ennis, C., McConnell, R. and Spence, M., 1997. Improved yields of oxalate, glyoxylate and glycolate from the electrochemical reduction of carbon dioxide in methanol. *Journal of applied electrochemistry*, *27*(6), pp.706-712.
- Gennaro, A., Isse, A.A., Saveant, J.M., Severin, M.G. and Vianello, E., 1996. Homogeneous electron transfer catalysis of the electrochemical reduction of carbon dioxide. Do aromatic anion radicals react in an outer-sphere manner?. Journal of the American Chemical Society, 118(30), pp.7190-7196..
- Hori, Y., Wakebe, H., Tsukamoto, T. and Koga, O., 1994. Electrocatalytic process of CO selectivity in electrochemical reduction of CO2 at metal electrodes in aqueous media. *Electrochimica Acta*, *39*(11-12), pp.1833-1839.

- Kushi, Y., Nagao, H., Nishioka, T., Isobe, K. and Tanaka, K., 1994. Oxalate formation in electrochemical CO2 reduction catalyzed by rhodium-sulfur cluster. *Chemistry letters*, *23*(11), pp.2175-2178.
- Malik, K., Singh, S., Basu, S., & Verma, A. (2017). Electrochemical reduction of CO2 for synthesis of green fuel. *Wiley Interdisciplinary Reviews: Energy and Environment*, *6*(4), e244.
- Oloman, C., & Li, H. (2008). Electrochemical processing of carbon dioxide. *ChemSusChem: Chemistry & Sustainability Energy & Materials*, *1*(5), 385-391.
- Qiao, J., Liu, Y., Hong, F., & Zhang, J. (2014). A review of catalysts for the electroreduction of carbon dioxide to produce low-carbon fuels. *Chemical Society Reviews*, *43*(2), 631-675.
- Savéant, J. M. (2008). Molecular catalysis of electrochemical reactions. Mechanistic aspects. Chemical Reviews, 108(7), 2348-2378.
- Savéant, J.M., 1983. Kinetics and mechanisms of electrochemical dimerizations. *Acta Chem. Scand. B*, *37*(5).

6. Pilot plant experimental studies of post combustion CO_2 capture at Michigan Tech central energy plant: Case study

6.1 Abstract:

Carbon dioxide, a byproduct of combustion reactions, is a greenhouse gas linked to climate change. At Michigan Technological University, we have studied the capture of CO_2 using alkali absorbent solutions in a pilot scale packed bed counter-current scrubbing column. To do this, we have simulated flue gas by combining streams of CO_2 and compressed air. Real flue gas has impurities such as CO, SO_2, and NO_x, and has lower levels of O_2 than our simulated flue gas. In order to study CO_2 capture from a real flue gas, the Department of Chemical Engineering worked with the facilities department to install a pilot scale scrubbing column at the Michigan Tech steam plant. Experiments were conducted using a sample stream of the flue gas from the boiler exhaust in the steam plant. Data collected from these experiments were compared to the data collected from identical experiments conducted on simulated flue gas in the lab. The capture efficiency of the real flue gas is discussed in this section.

6.2 Background:

The most common equipment used to separate CO_2 from a flue gas stream is a counter-current packed-bed scrubbing column. The department of Chemical Engineering at Michigan Technological University has two such pilot scale columns. In order to study the effect of impurities found in real flue gas, one is installed in a controlled laboratory using a simulated flue gas created by mixing CO_2 and compressed air. This column was used to establish a baseline for percent capture analysis and is displayed by figure 1.

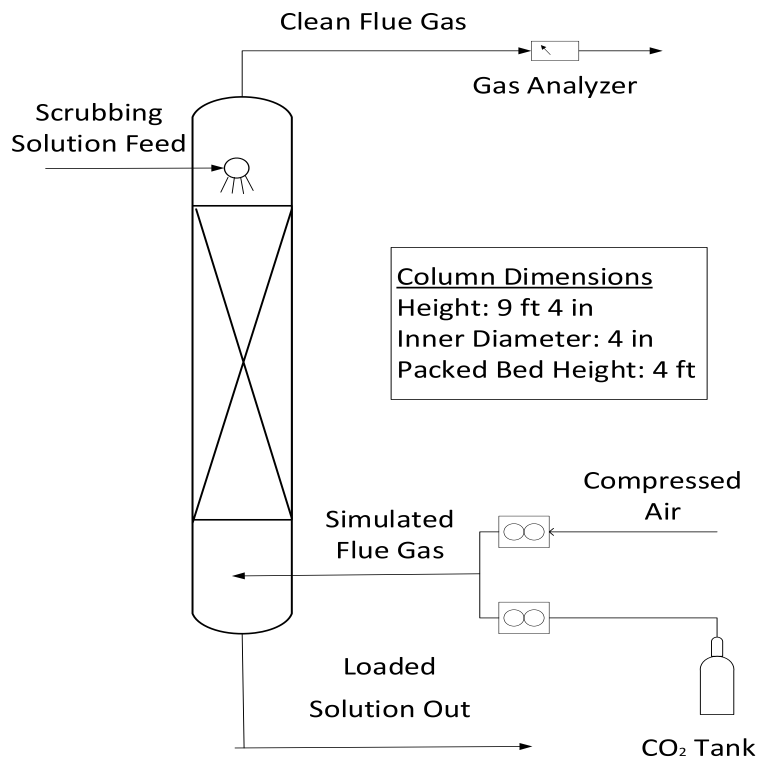

Figure 42: Pilot Scale Scrubbing Column in Laboratory

The second scrubbing column is identical to the first, and is installed in the Michigan Tech central energy plant. The plant produces up to 130,000 lb/hr of 80 psig steam to provide hot water and heat for campus buildings. A typical wintertime load burns around 25,000 SCFH of natural gas; this load releases 1.4 metric tons of CO_2 per hour. The flue gas that steam plant produces is roughly around 7.5% CO_2 by volume. In order to study CO_2 capture from this flue gas, a tap has been installed on the main exhaust duct which draws a sample of the flue gas into the pilot scale scrubbing column. Figure

2, a simplified diagram of the steam plant, shows the tap installed between the economizer and the stack condenser.

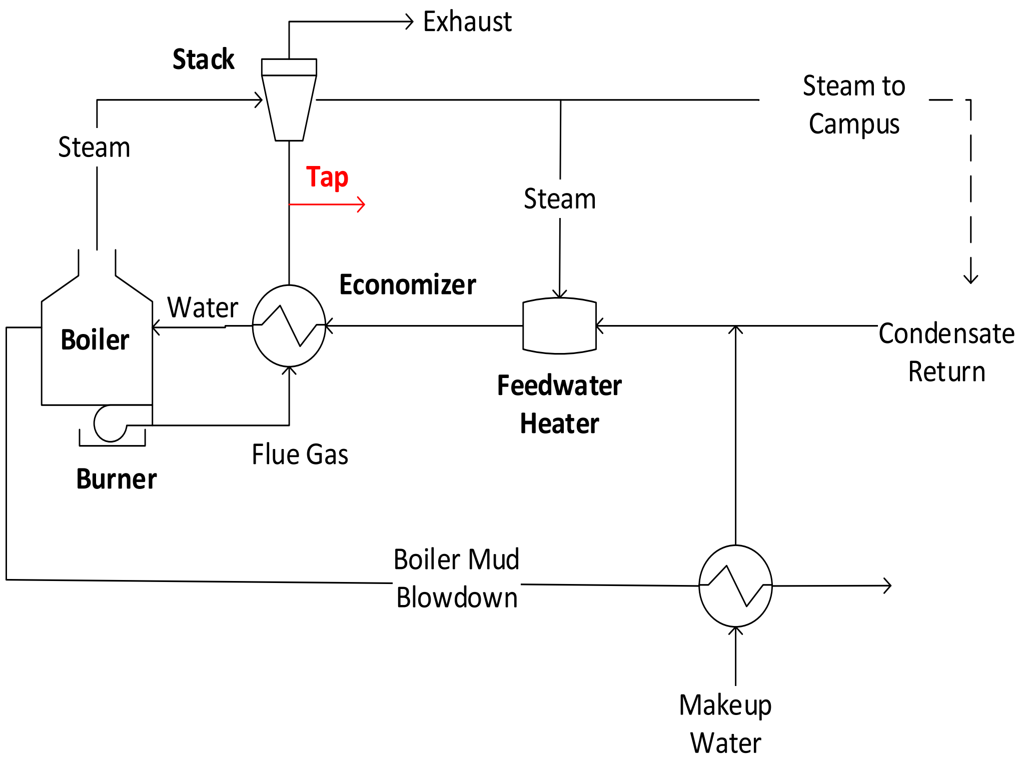

Figure 43: Simplified diagram of Michigan Tech Central Heating Plant.

The flue gas at the outlet of the economizer is 135°C. The vacuum pump used to draw the flue gas sample has a maximum operating temperature of 40°C. To cool the flue gas, it is passed through a heat exchanger that is submerged in water. The flue gas then passes through a filter canister in order to protect the vacuum pump from ash particulates, and any condensate that may form in the heat exchanger. The filter has a drain top to remove condensate. The scrubbed flue gas exits the top of the column and is blown out the window of the steam plant. An axial fan was installed on the exhaust line to improve ventilation.

6.3 Experimental:

Typically, when conducting scrubbing experiments in the lab, sodium carbonate is dissolved into distilled water for use as the scrubbing solution. There is no distilled water line in the plant, but there is access to both softened water and tap water. Water chemistry will have a great effect on CO_2 absorption, so this study will compare CO_2 capture by scrubbing solutions made from distilled water, softened water, and tap water, as well as from both simulated and real flue gas.

While operating the scrubbing column in the laboratory, 4.5 LPM of CO_2 enters the column from the bottom of the packed bed. The flowrate of compressed air is adjusted to yield a simulated flue gas with initial composition between 7% and 7.5% CO_2. The scrubbing solution is then pumped to the top of the column, and is distributed over the packed bed. The scrubbing solution is a 2% weight aqueous solution of sodium carbonate at a rate of 2 gpm. The composition of the flue gas exiting the top of the column is measured using a Quantek 906 CO_2 analyzer, and is recorded before the scrubbing solution pump is turned on and after the scrubbed gas reaches steady state. This procedure is followed for each of the three types of water being tested: distilled, softened, and tap water.

While operating the scrubbing column in the central heating plant, the sample flue gas enters the column from the bottom of the packed bed. The scrubbing solution is then pumped to the top of the column, and is distributed over the packed bed. The scrubbing solution is a 2% by weight aqueous solution of sodium carbonate. The composition of the flue gas exiting the top of the column is measured using a Quantek 906 CO_2 analyzer, and is recorded before the scrubbing solution pump is turned on and after the scrubbed flue gas reaches steady state. This procedure is followed for each of the three types of water being tested: distilled, softened, and tap water.

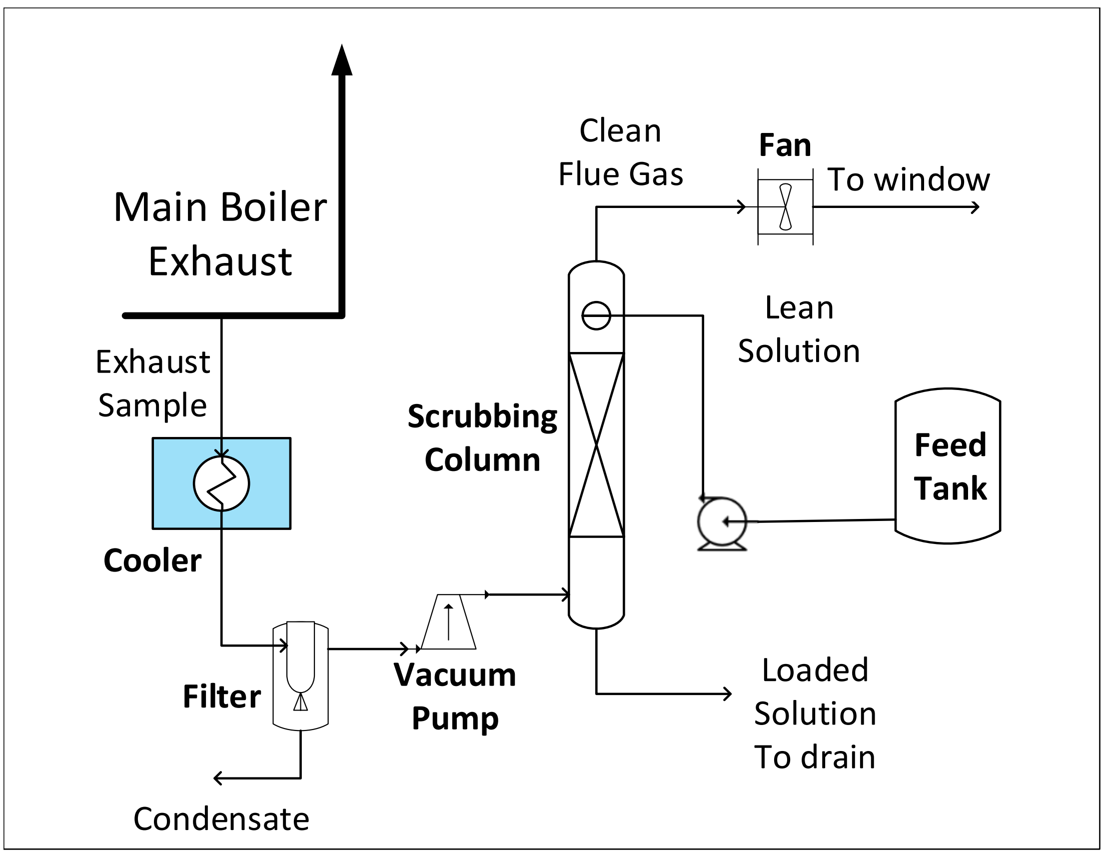

Figure 44: Pilot Scale Scrubbing Column installed in the Michigan Tech Central Energy Plant.

6.4 Results

As expected, scrubbing solutions prepared with distilled water performed the best, with tap water performing the worst. The performance of scrubbing solutions made with softened water showed an intermediate performance. In addition to this, identical scrubbing solutions performed better on simulated flue gas than real flue gas. This seems to be due to other impurities dissolved in the solution.

$$Capture\ Ratio = \frac{Moles\ of\ CO_2\ captured}{Moles\ of\ CO_3^{2-}\ used}$$

Figure 4 displays the data collected during the experiments discussed in the above section. The black bar corresponds to the left axis, and displays the volume percent of CO_2 in the gas stream after it passes through the scrubbing column. The white bar stacked on top of the black bar also corresponds to the left axis and is the amount of CO_2 captured by the scrubbing column. The top of the white box is therefore the volume percent of CO_2 in the gas before it enters the column. The gray bar corresponds to the right axis and is the capture ratio of CO_2 to CO_3^{2-} as defined by equation 1.

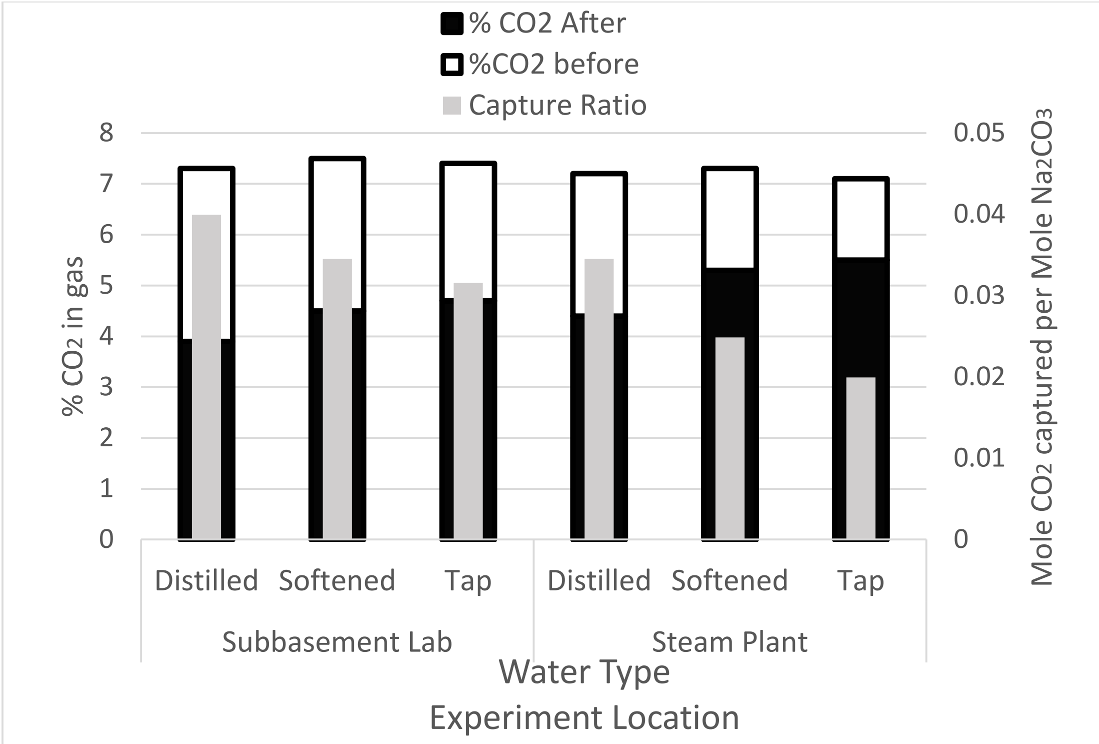

Figure 45: Comparing CO_2 capture in 2 locations, with 3 types of water used in the scrubbing solution

6.5 Conclusions:

Some of the challenges in real flue gas situation are: temperature and pressure conditions in a boiler exhaust will constantly vary compared to the lab conditions. We were able to capture the CO_2 successfully, but the only challenge for us was the varying CO_2 concentration and gas flow rate, which is pretty common in a real flue gas exhaust. This can be easily taken care of in the industry by optimizing the system with aspen plus custom modeler.

7. Conclusion and future work

This research provided a solution to reducing the CO_2 capture costs, which involves the use of low-cost alkali absorbent CO_2 capture solutions, combined with an electrochemical regeneration method (EDBM regeneration) that uses the least amount of energy available for capture and regeneration. This research has also further addressed the issue of how to deal with the captured CO_2. Several viable storage and utilization methods have been explored, as well as their technological readiness level. We were able to convert CO_2 to oxalic acid successfully, with 95% columbic efficiency.

As a summary, the following points can be noted:

- Improved absorption kinetics of the low cost sodium carbonate slurry with surfactants for post combustion CO_2 capture.
- Carbonate conversion to bicarbonate increased by 43.2% with the addition of surfactant.
- Total CO_2 Absorption increased from 50% to 97% after the addition of H_2O_2/ NaOCl.
- Maximum absorbance of 31% was reached for NO, due to slower kinetics in alkaline pH.
- SO_2 absorption reached 95% almost instantaneously, without the addition of oxidizer.
- H_2O_2 acted as better homogeneous catalyst than NaOCl.

- Using electrodialysis with bipolar membrane (EDBM) process for Reagent regeneration we were able to achieve reagent regeneration energies as low as 1.18MJ/Kg CO_2 captured.

- Conversion of CO_2 to oxalic acid with the help of electrochemical reduction was achieved at 95% columbic efficiency.

Figure 46 shows the overall research objective in a flow diagram, which includes CO_2 capture with EDBM separation and simultaneous utilization by conversion to oxalic acid.

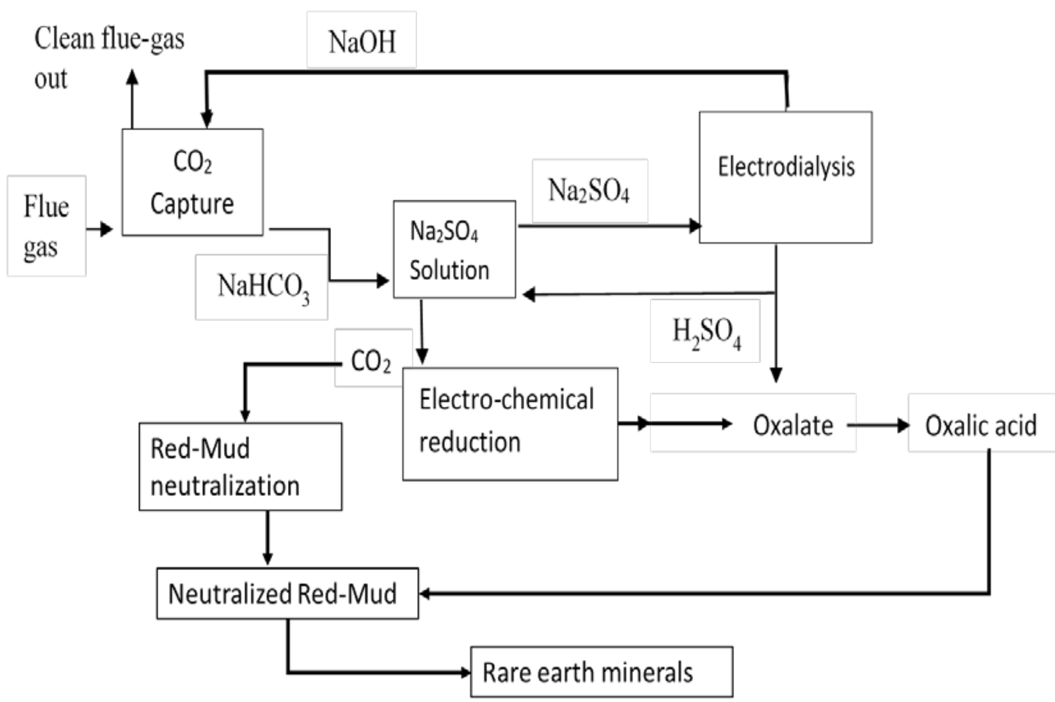

Figure 46:CO_2 capture with EDBM separation and simultaneous utilization by conversion to oxalic acid.

7.1 Future work

Finally, for someone who wants to continue this work, I suggest Using aspen custom modeler to optimize the CO_2 capture system which has variable input gas rate and concentration, since we have all the experimental data required for optimization. For modelling CO_2 absorption in sodium carbonate solution, I suggest using electrolyte NRTL (e-NRTL) model for vapor liquid equilibria which is available in aspen plus, and Radfrac distillation column design, generally used for amine capture system can be used for designing the packed column. And I also suggest a techno-economic analysis of the overall capture and utilization by capture with alkali solution and conversion to oxalic acid and other product.